Chapter 1 Introduction

1.1 Research background

The purpose of this research was to meet increased needs for quasi-distributed sensors capable of operating reliably in harsh environments or large extended structure. The multiplexing measurement of temperature and strain is quite important in many industrial areas such as electric power, bridge monitoring, oil exploration, and smart structures, as well as in the medical temperature profile applications. Strain or temperature measurement is also necessary in many other engineering fields, especially in severe environmental conditions, including high temperature and high pressure, toxicity, and high electromagnetic interference. Temperature distribution is required to obtain the entire field information and to compensate for temperature-induced variations in the strain measurement.

Fiber–optic Bragg grating sensors are very attractive candidates for the measurement of strain and temperature. They have many advantages over conventional sensors due to the sensitivity, immunity to electromagnetic interference, resistance to any corrosion, avoidance of ground loops, large bandwidth, and capability of remote operation as well as potent to sense micro

strain at high temperature. They can directly incorporate into many structures, e.g. embedded into concrete configurations to evaluate the material deformation. My dissertation research exploits the advantages of very low-reflectance fiber Bragg gratings (FBG) to develop a pc OTDR-based multiplexing scheme that has maximum sensor capacity up to a thousand and high resolution in temperature and strain measurements. This type of photon counting OTDR provides high sensitivity detection, at least to 10^{-17} J optical energy (10^{-5} reflectance) and thus can interrogate a large of multiplexed sensor. Meanwhile, the low reflectance and loss of the FBGs can also provide self-calibrating configuration to eliminate power variation in the whole system for reliability improvement.

1.2 Multiplexed fiber Bragg grating Sensor measurement technique

1.2.1 Review of multiplexed fiber Bragg grating sensors

Optical fiber sensors have been widely developed in a variety of applications, and deliver high accuracy measurements encompassing physical parameter (pressure and temperature etc.) as well as chemical measurements. Fiber Bragg gratings have been becoming widely recognized as very promising technology for optical communication systems, structural monitoring application from aerospace to bridge applications. FBGs can be photo-inscribed techniques into a single length of silica fiber core using a UV laser at 244 nm [1]~[6]. They are encoded by the Bragg reflection wavelength, therefore eliminating the problems of intensity variations that plague many other types of fiber optic sensors. In addition, the devices have an inherent self-referencing capability with an arbitrarily narrow bandwidth and they are also conveniently multiplexed in a serial fashion along a single length of fiber [8]~ [10]. Grating-based sensors appear to be useful for various types of applications. In particular the area of distributed

embedded sensing in materials for creating "smart structures" is of major interests in the last 10 years. Here fiber Bragg grating arrays have been embedded into the composite materials to allow monitoring and measurement of parameters such as load level, strain, temperature and vibration, from which the health of the structure can be assessed and tracked on a real time basis. Grating sensors may also prove to be useful as the optical sensor elements in acoustic sensing tests, chemical sensors, and grating–based pressure sensors. Applications of FBG have also been strongly demonstrated in the area of fiber communication and laser amplifiers.

1.2.2 Multiplexing Schemes for Fiber Bragg Grating Sensor

As mentioned in the introduction, the capability to multiplex a large number of grating elements is one of the key advantages in designing a fiber grating sensor system, as it is in the domain of distributed sensing. Therefore, by sharing the light source and processing electronics, the cost per sensor is drastically reduced with an increase in the number of multiplexed sensors, and improves the competitiveness of optical fiber based sensor against conventional electro-mechanical sensors. As a result of intensive research over the past few years, a number of multiplexing techniques have been proposed and developed for optical fiber sensors. The most commonly used multiplexing schemes are

1. Wavelength division multiplexing (WDM)[11]~[16]
2. Time division multiplexing [15] [17]~ [21]
3. Frequency division multiplexing (FDW)[22]~[26]
4. Spatial division multiplexing [27] and combined SDM/WDM/TDM [19][28]~[31]
5. CDMA multiplexing [32] and coherence domain multiplexing [33]

Any one of these techniques, however, is limited to a few tens of sensors due to various interferences, including detection speed, crosstalk, SNR, and the wavelength bandwidth. In general, the most popular formats for increasing sensor number combines time domain multiplexing with other techniques, since these combinations do not generally degrade system performance.

1.2.3 Wavelength Division Multiplexing (WDM)

Obviously, the Bragg reflection wavelength encodes the Bragg grating sensor, therefore, one of the advantages in using a fiber-grating array is that the grating element can be discriminated by wavelengths. The most popular technique for multiplexing FBG sensors is the wavelength division multiplexing technique [10][11], called WDM and shown in Fig 1.1. This is based on the assumption that the wavelength for each grating sensor is different from any other one in the array, and you have to know the position of each grating that corresponds to its wavelength. The maximum sensor number that can be multiplexed using this technology is determined by the ratio of the source spectral width over spacing between the Bragg wavelengths of the FBGs' array. The most commonly used de-multiplexing devices are the Optical Spectrum Analyzer (OSA) [11], matching grating pairs and wavelength tunable filters [16] operated in its scanning mode with each scanning period covering the wavelength range occupied by all gratings in the chain. Since the number of grating sensors that can be interrogated is principally determined by the bandwidth of light source and the spectral regions covered by the gratings, the sensor number is relatively limited in the multiplexing configuration. As a simple example, for an LED light source with a bandwidth of about 40 *nm*, a grating operating bandwidth of ±2.5 *nm*, and grating test range of about 3 *nm* for temperature testing to determine on one

sensor test bandwidth. Only seven sensors could be interrogated in a series. In order to increase the total number of sensing gratings, another multiplexing schemes must be in conjunction with the WDM scheme. A tunable Fabry-Perot filter or OSA can also be applied to the tensile measurements in a Bragg grating

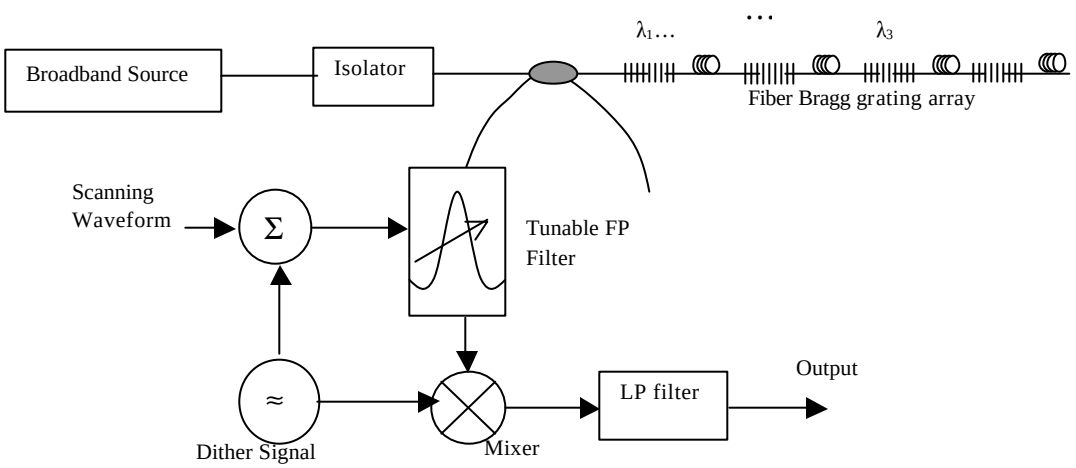

Fig1.1 Multiplexed FBG array with scanning FFP demodulation [16]

based laser system to decode the wavelength shift. But the strain sensor resolution is limited by the identification of peak position of each maximum signal intensity or minimum peak shift in filter scheme.

1.2.4 Time Division Multiplexing (TDM) [15]

It is highly important in the use of TDM to greatly increase the number of measurable grating sensor devices by reusing the spectrum source. By simultaneously employing an interferometric detection scheme, a high sensor resolution can still be maintained in such test.

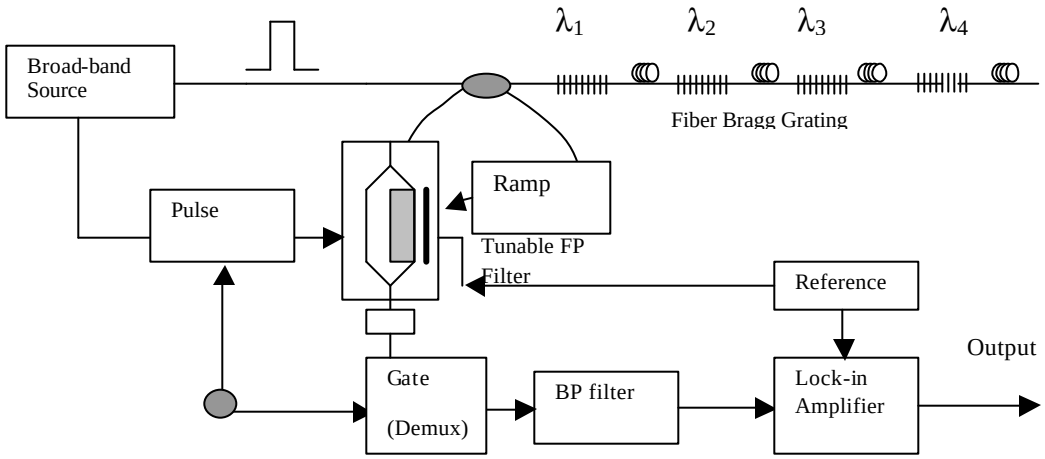

Fig1.2 TDM system employing an unbalanced M-Z interferometer

Figure 1.2 shows an example of such a multiplexing system combining the two techniques.

A single laser source in the multiplexing system offers highly pulsed power within a narrow spectral width, thus improving signal-to-noise (SNR) as well as allowing for a larger number of sensors for the same nominal Bragg grating. If the laser source is tunable within some range, through WDM detection, the sensor number might be further increased by using the combination of WDM and TDM multiplexing technique.[34] The different combinations of WDM and TDM in the serial configuration shown in Fig 1.3, several wavelength-stepped arrays are concatenated, each at a great distance along the fiber. By launching a short pulse of light from the laser source, the signal reflected from each successive FBG will return to the detector at successively a later time. The detection system is constructed to respond to the reflected signals only during a selected window of time after the pulse is emitted, so that a single WDM set of sensors is chosen for measuring.

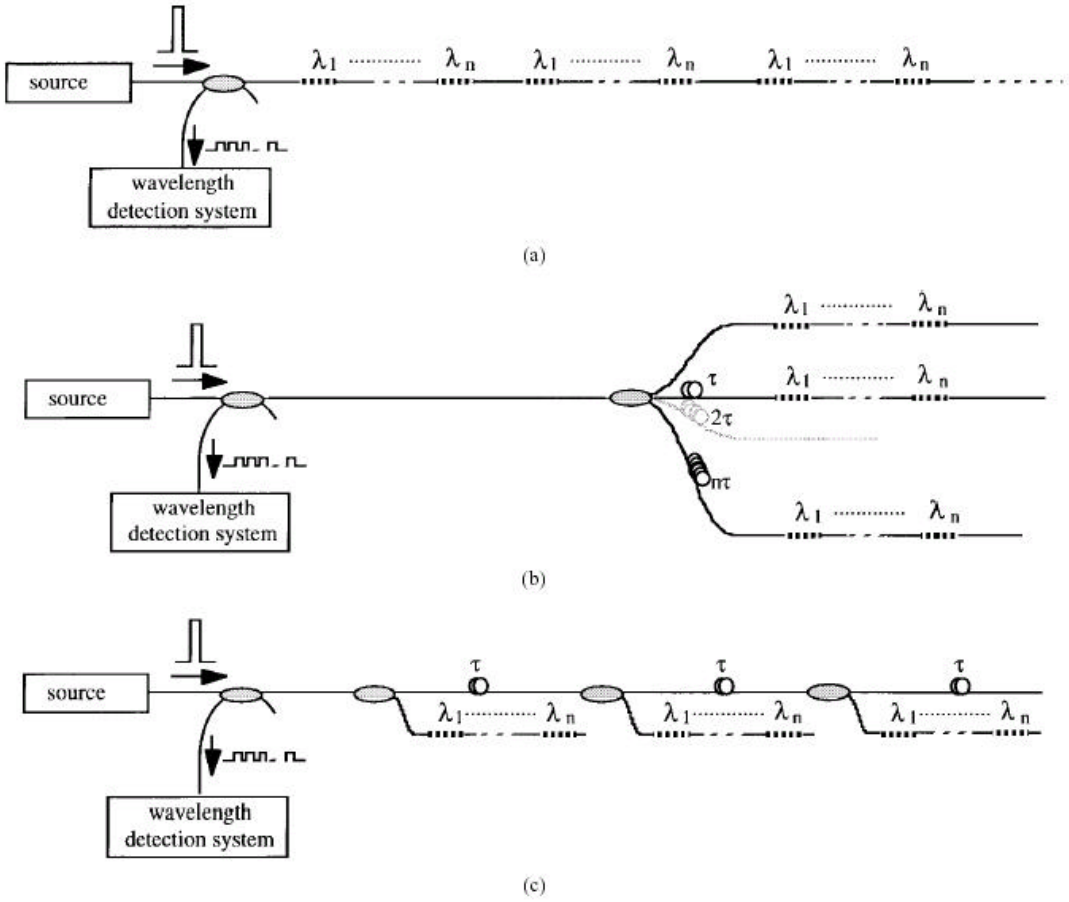

Fig. 1.3 WDM/TDM addressing topology for fiber grating array (a) serial system with low-reflectance, (b) branching network (c) parallel topology [34]

1.2.5 Code Division Multiple Access (CDMA)/ Frequency-modulated continuous wave (FMCW)

The TDM approach suffers from a spectral bandwidth limitation of the LED source and a reduced sensor optical output power. An alternative to TDMA is the code division multiple access (CDMA) scheme [32] which has been demonstrated in the ability to dense wavelength division multiplexing [32] over 100 FBGs by the combination of both WDM and CDMA

schemes. CDMA is based on a correlation technique for separating out an individual sensor. The CDMA process has a high duty cycle or continuous in time and therefore can deliver more sensor signal power than the TDM technique. For the same the source power level, the sensor number limited by the input power level in the CDMA configuration could be significantly larger than that of the TDM. The CDMA approach also allows a large reduction in the wavelength separation between FBGs by 10 times without the formation of the Fabry-Perot cavity. The sensor number and channel isolation are proportional to the sequence lengths of the code. Currently, only a two-sensor system has been experimentally demonstrated with a cross-talk level of about 20 dB. [33]

The FMCW technique has been developed for multiplexing intensity-based [22][24] and interferometric fiber optic sensors [35] [25]. The idea is to address an array of FBG sensors that have approximately the same Bragg wavelength. The high duty cycle available using the FMCW technique provides larger average power at the photodetector and thus a SNR improvement. The basic theory of the FMCW technique has been described by Hymans *et al*. and Manafza *et al*. [36] Here some of the pertinent techniques for multiplexing sensors will be simply outlined. A time difference between a triangular chirped reference waveform and a delayed signal produce a difference frequency (beat frequency f_{beat}) proportional to the rate of frequency excursion and the time difference between the two waves τ. The resultant output is a line spectrum at intervals of f_s ($f_s = 1/T_s$ frequency chirping period). Figure 1.4 shows as these two waves. The position of the peak in the envelop of the line spectrum gives the beat frequency f_{beat}. Figure 1.5 shows a serial FBG sensor array that is addressed by the FMCW technique.

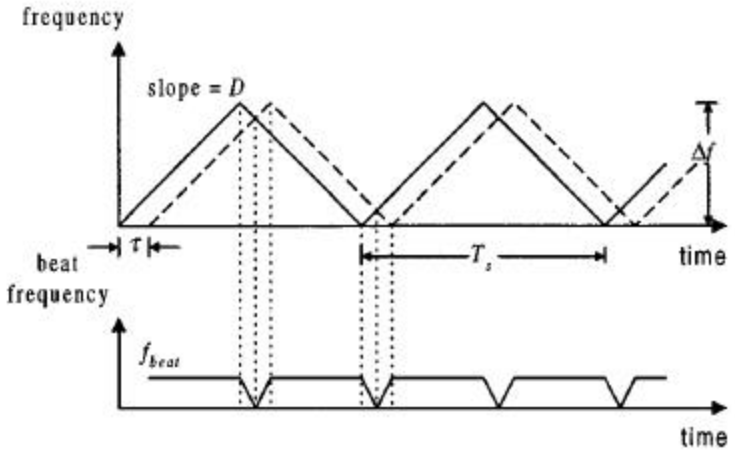

Fig. 1.4 Production of beat note

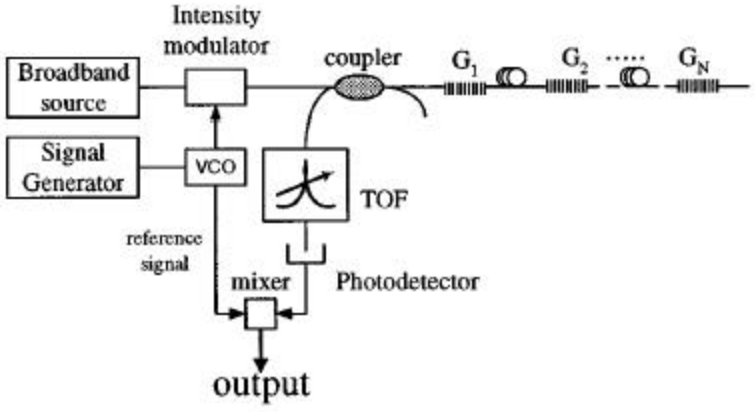

Fig 1.5 Schematic diagram of an FMCW multiplexed FBG sensor array in serial topology

The FBGs in the chain may have either identical or different Bragg wavelengths. The light from the broadband source is modulated with a saw-tooth or triangle chirped frequency carrier generated by a voltage-controlled oscillator (VCO) and launched into the FBG sensor array. The reflected signals from the FBGs are guided back to a tunable optical filter and then to the detector and are subsequently combined with a reference signal from the VCO subsequently. The system output will consist of a number of beat notes with beat frequencies determined by the time delay difference t between the signal returned from individual FBGs and the reference

signal. If the t is selected properly, the beat note signal may be separated in the frequency domain and can be viewed using an ESA or using FFT analysis of time domain signal. The sensor signal has an amplitude proportion to the convolution of the spectral response of the TOF and that of the specific FBG sensor. The wavelength can be interrogated by scanning the TOF and recording the control voltage of the TOF that corresponds to the peaks of the different frequency components. In theory, using this approach it is possible to multiplex a few tens of Bragg gratings of the same nominal Bragg wavelength with crosstalk between any two sensors below –32 dB. The array size could reach a hundred if the FMCW and WDM are mixed up, not considering the FBG loss. The available source power level may limit the maximum sensor number that can be multiplexed using this technique. A serial multiplexing structure requires considering a low-reflectivity FBGs to satisfy the cross-talk requirement. An optical amplifier usually may be applied to overcome the source power problem.

1.3 The Opto-electronic millimeter resolution OTDR system

In this section, the optical time-domain reflectometry (OTDR) system performance and operating principle will be introduced. OTDR is a well-known method for investigating the attenuation characteristics of an optical fiber. In a basic OTDR measurement, a laser transmitter emits a short optical pulse into the fiber at a time determined by an internal delay generator. The OTDR detects the backscattered light after a time delay n* t associated with the time that the pulse was launched into the fiber. The relative time delay between emission and detection is determined by an internal delay generator. Normally, it is assumed that the optical path differences between adjacent reflection points are the same, and t is correspondingly the time-delay difference between FBGs. Assuming the repetitive period T_p and width T_w of the

incident optical pulsed amplitude modulation satisfy the conditions, $t \geq T_w \quad T_p \geq N \times t$, where *N* is total sensor number, then the pulses from FBGs can be distinguished in the time domain as they arrive at the photon-counting detector and can be separated by electronic switching after detection. The time-delay is unique addressing information related to a specific location along the fiber, and the temporal profile of the light intensity returned from the fiber each time delay is also measured and analyzed. This technique was demonstrated for the first time by Barnoski and Jensen [51]. They coupled light from a pulsed injection laser into an optical fiber, and obtained its attenuation characteristics by analyzing the time dependence of the detected Rayleigh backscattered light. Fresnel reflected light intensity caused by any discrete element in the optical fiber is much greater than Rayleigh backscattered light by about 3 or 4 orders of magnitude, so when pulsed light is injected from fiber end face to obtain the Rayleigh backscattering light, Fresnel reflected light at both fiber endfaces saturates the detector sensitivity. Consequently, any weaker backscattered light that follows Fresnel reflected light cannot be measured for a while, and the fiber attenuation features within the region cannot be evaluated. This region is defined a "dead zone". It is important to suppress Fresnel reflection at discrete elements in high spatial resolution optical fiber measurement. However, most of the discrete reflecting devices in the optical transmission line under test, such as connector and circulator or coupler, obviously, lead in dead zone, which it is unavoidable without gating function are used. Personick [52] used a gated photomultiplier receiver, operating in the 0.8-μm-wavelength region. This gating feature eliminated saturation caused by the strong Fresnel reflection.

Gate-detected technology that has been developed in longer wavelength areas demonstrates its potential for the research of optical network, multiplexing sensor application, particularly an

innovative photon counting technique, in which the backscattered light photons are digitally detected. An APD can be used to count photons if biased slightly above its break down voltage. Healey [53][54][55] developed this technique and it has become an important application in high-resolution fiber measurements.

The high-resolution photon counting OTDR [56] [57] actually consists of pulsed semiconductor laser transmitters, a matched optical receiver with photon counting function and electronic signal processing, as well as display assembly, as shown in Fig.1.6. The transmitter launches optical pulses with widths less than one centimeter. The photodetector is a 50-ohm electronic photon-counting system, and the processor is designed to detect the reflected signal feature that is able to measure both insertion loss and returned loss without deadzone limitation. In principle, the photon counter is a single photon avalanche photodiode (SAPD [58]). The SAPD

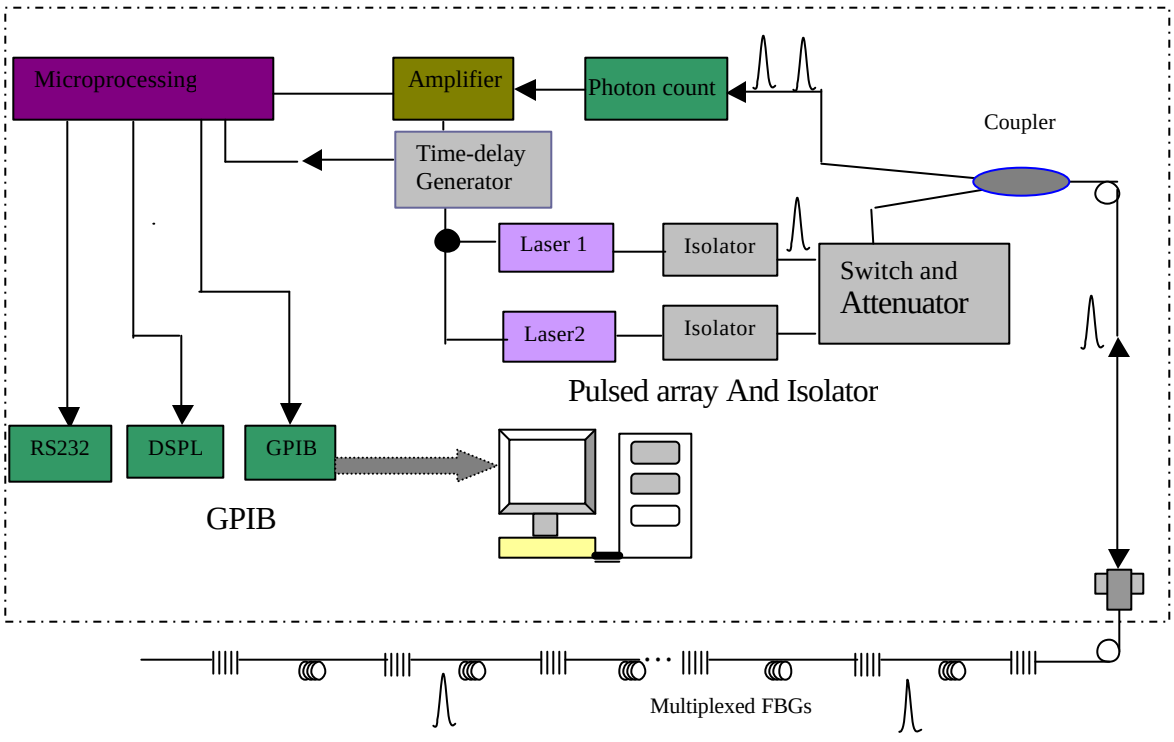

Fig. 1.6 Schematic of the optical components and electrical connections in the OFM

is activated by increasing the bias voltage above its natural breakdown value. If operated just above the breakdown voltage it may take as long as a few milliseconds to breakdown. Well above the breakdown voltage, the SAPD will breakdown in perhaps 1 to 2 ns. We find it to be reasonably stable for about 800 *ps*. If the light (a photon) arrives during this activation time the SAPD avalanches causing a large electrical pulse, which can be recorded. If light arrives at other times, the SAPD will conduct and cause a normal multiplication type current that can be ignored. The optical pulse is sent into the fiber, and then the detector (SAPD) is gated on (activated) at a predetermined delayed time. Thus for each optical pulse generated, there is a time interval where there is either light returned or no light returned. That time interval corresponds to a particular position along the fiber. We are not really measuring the amount of light returned but are measuring the probability of a single photon being returned, where the probability is 1 saturation occurs.

This is a substantial difference from the conventional OTDR. Regular OTDRs are usually designed to measure Rayleigh backscattered signal from a longer optical fiber with great sensitivities, however, it suffers from large deadzone (tens meters long) caused by the Fresnel reflection signals, resulting in low spatial resolution measurement. Because of the high detector gain and low noise required by the detection of the Rayleigh backscatter signal, the detector must be kept at high impedance for conventional OTDR, which forces a lower limit on the optical pulsewidth at around the 100-centimeter mark.

1.4 The Research description

The research described in this dissertation, entitled " Multiplexed Broadband Bragg Grating Sensors for Self-referencing pc- OTDR-Based Interrogation" is focused on the following issues.

1) Fabricating a type of Bragg grating sensor with low-reflectivity (less than 10^{-4}) and broad bandwidth (about 1 *nm*) that could be interrogated by the high sensitivity pc-OTDR using a low-power phase mask and UV laser system.
2) Designing a high capacity FBG sensor for multiplexing scheme, to include in the thousand sensors based on the reflectance or power budget, which is able to monitor the material deformation in a large range structure.
3) Investigating the referencing-calibration configuration that can reduce system drifts or noises caused by the source and fiber bending etc.
4) Evaluating sensor performance in the multiplexing structure and sensor to-sensor crosstalk simulation to determine multiplexing interference performance for temperature and strain measurements.

More detailed descriptions of the relevant researches will be presented in the following chapters. Chapter 2 illustrates the principle for the fabrication of broadband fiber Bragg gratings to achieve a linear output in OTDR spectral detection. Chapter 3 describes some theoretical analysis and required conditions for multiplexing a large number of FBGs in an array. Chapter 4, the core of the dissertation, analyzes grating interrogation approaches and some implementation results. Chapter 5 presents results from the performance evaluation of the FBG sensor and system performance. Chapter 6 outlines the system noise analysis and Chapter 7 will describe some future areas of researches.

Chapter 2 Broad Bandwidth Fiber Bragg Grating Sensor Fabrication

The multiplexed grating system is composed of the photon counting OTDR and a number of the grating sensors with specific wavelengths. The pc-OTDR is a unique type of instrument designed to operate in the long wavelength region (1300 nm) with very high sensitivity and resolution. The dynamic range of the pc-OTDR using high powered optical pulses, which approaches 85 dB range for returned loss measurements in the Fresnel mode, made it possible to detect very weak FBG reflection signals. Therefore, it was also possible to measure an array of fiber Bragg gratings with very low-reflectivity (up to 10^{-5}) along a single length of optical fiber. The high spacing resolution allows FBG components to be separated by as little as ten centimeters and millimeter for single point resolution. The pc-OTDR could thus demodulate numerous weak-reflectance sensors within a short haul if the insertion loss of each sensor is significantly low. On the other hand, since the pc-OTDR source is characterized as multi-longitudinal mode semiconductor laser with each single spectral bandwidth approximately 0.4 nm and total enveloping spectral bandwidth 10 nm, in order to achieve a linear response for pc-OTDR spectrum-based interrogation, the FBGs must be fabricated with a broadband [37][38][39] larger than 0.8 nm to smooth the enveloping ripples.

2.1 Special requirements for fiber Bragg gratings

1) The FBG wavelength must be positioned on the most sensitive interrogation region of the OTDR spectrum, which implies that FBG wavelength should be in the steep regions from 1290 to 1305 nm or 1310 to 1316 nm, so that the FBG sensor is subjected to the largest wavelength shift under applying on any physical field.
2) Since the phase mask technique was only capable of fabricating narrow bandwidth FBGs ($\Delta\lambda$ = 0.05~0.3 nm), [37] a fabrication setup with adjustable angle and position between the photosensitive fiber and phase mask is necessary to realize fiber Bragg gratings with broad bandwidths (0.8-1.2 nm).
3) To obtain the objective of multiplexing a large number of gratings, a low reflectance (about 0.1 % or less) by each grating is desired.

2.2 Fiber Bragg grating fabricating techniques by Phase Mask [40]

Fiber Bragg gratings were first fabricated using the internal writing [41] and holographic techniques [42]. Both these approaches have been largely superseded by the phase mask technique in recent years [43], [44], illustrated in Fig 2.1. The phase mask technique has the advantage of greatly simplifying the manufacturing process for Bragg gratings over other techniques, yet yielding gratings with high performance and similar characteristics. The phase mask is made from a slab of silica glass, which is transparent to ultraviolet light. On one of the flat at surfaces, a one-dimensional periodic surface relief structure is etched using photolithographic techniques. The shape of the periodic pattern approximates a

square wave in profile. Photosensitivity optical fiber is placed almost in contact with the corrugations of the phase mask as shown in Fig 2.1. Ultraviolet light that is incident

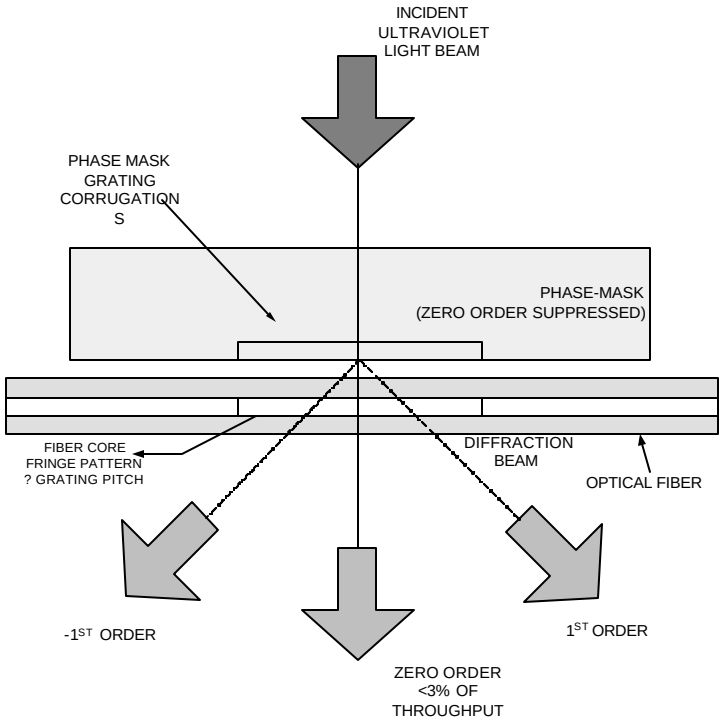

Fig. 2.1 Bragg grating fabrication apparatus based on a zero-order diffraction phase mask.

normal to the phase mask passes through and is diffracted by the periodic corrugations of the phase mask. Normally, most of the diffracted light is contained in the zero, 1, and -1 diffracting orders. However, the phase mask is designed to suppress the diffraction into the zeroth-order by controlling the depth of the corrugations in the phase mask. In practice the amount of light in the zeroth-order can be reduced to 5% or less with approximately 40% of the total light intensity divided equally in the $\pm$ 1 orders. The two ± 1 diffraction order beams interfere to produce a periodic pattern that can photo-inscribe a corresponding grating on the core of optical fiber. If the period of the phase mask grating is Λ_m, the period of the photoimprinted index grating is $\Lambda_m/2$. Note that this period is independent of the wavelength of ultraviolet light irradiating the phase mask; however,

the corrugation depth required to obtain reduced zeroth-order light is a function of the wavelength and the optical dispersion of the silica. In comparison to the holographic technique, the phase mask technique offers easier alignment of the fiber for imprinting, reduced stability requirements on the photo-imprinted apparatus and lower coherence requirements on the ultraviolet laser beam, thereby permitting the use a cheaper ultraviolet laser source. Though phase masking just provides a single central Bragg wavelength determined by the basic equation $l_B = 2n_{eff}\Lambda$, in some cases, several techniques have been demonstrated to allow tuning of operational wavelength and bandwidths of fiber Bragg gratings through adjusting photo-imprinting system parameters.

Furthermore, there is the possibility of manufacturing several gratings at once in a single exposure by irradiating parallel fibers through the phase mask. The capability to manufacture high-performance gratings on a large scale at a low per unit grating cost is critical for the economic viability of using gratings in multiplexing applications.

The phase mask technique not only yields high performance devices but also is very flexible in that it can be used to fabricate gratings with controlled spectral response characteristics, such as the fabrication of chirped or aperiodic fiber gratings by tilting technology. Chirping means varying the grating period along the length of the grating in order to broaden its spectral response.

2.3 Tuning Technique for Inscribing Bragg Grating

In practice, it is often important to tune Bragg grating wavelengths to desired values. This is particularly true for our OTDR spectrum-based interrogation method. Its optical spectrum is approximately a typical Gaussian shape, so that there is a limited wavelength range available to obtain a high sensitivity output on the both of the sloping sides. A. Othonos [39] has done some works on techniques for tuning the Bragg wavelength within a few nanometers. In this final report, we had completed a tuning technique based on parallel motion or tilt angle in the phase mask setup (Fig2.2) was used to adjust the Bragg grating wavelength up to 25 nm. The focus length of second cylindered lens must also be tuned so that the fringe spacing can be adjusted through the beam spot size change. The adjustable phase mask (APM) technique has been shown a precisely to be controllable approach for fabricating FBG wavelengths in some required ranges. It produces a stable spatial modulation and diffracts the UV light to form an interference pattern immune to the outside influence that induces a periodic refractive index change in the fiber core. A fiber Bragg grating holder is placed on the optical platform three-dimension adjustment function. Interference with low coherence requires the fiber to be placed in sufficiently close contact to the grating corrugation on the phase mask (PM) in order to create the maximum modulation in the index of refraction. Obviously, the separations of the fiber from the phase mask and focus lengths are critical parameters in determining grating performance.

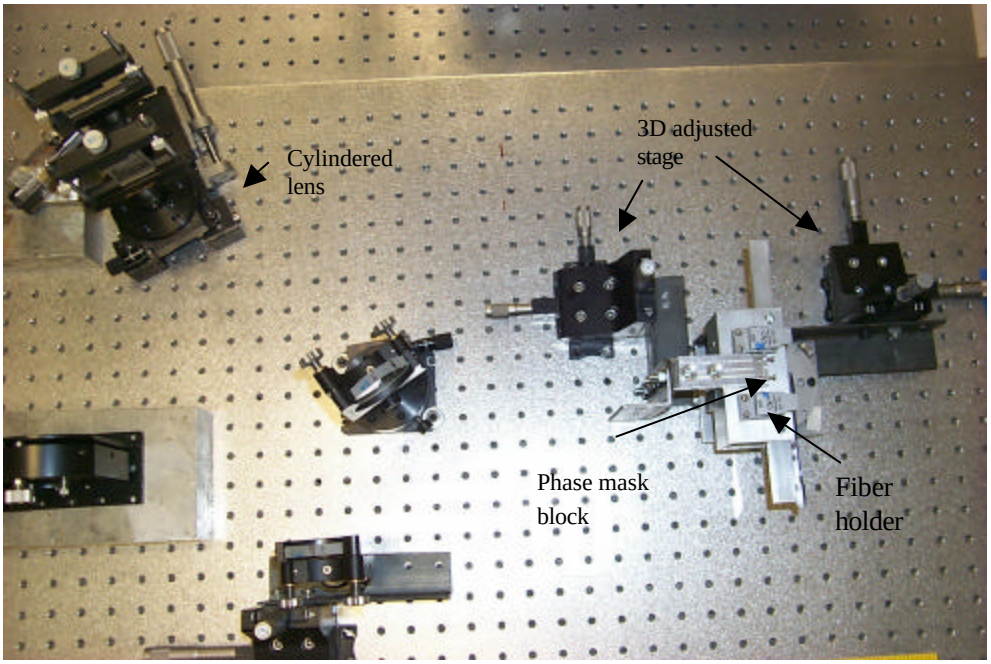

Fig 2.2 Fiber Bragg grating fabrication setup on the optical table

Through tilting and parallel movement of the fiber, it is possible to demonstrate the large tunable range of Bragg grating wavelengths. This can be achieved simply by placing the fiber at an angle with regard to the facet of the phase Mask (PM), and aligning the two

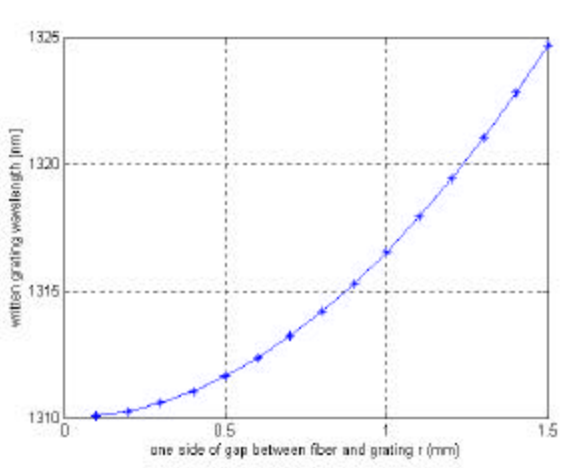

Fig. 2.3 Bragg grating central wavelength tuning as a function of distance r

cylindrical lenses and shifting the fiber relative to the PM a small distance (about 2 mm).

In other words, for the tilt angle technique, one end of the exposed fiber is positioned right against the PM, and the other end is set at a different distance (0~1,500 μm) from PM. As the angle between them is varied, the Bragg grating central wavelength changes.

Therefore, in theory, the Bragg grating resonated wavelength is determined by vertical axis change in Fig 2.3. If the distance deviation is about 1.2 mm at one end of fiber, the central wavelength will shift approximate10 nm. Experimentally, a frequency-doubled Argon Ion laser at 244 nm was used as the radiating source, and its output power was about 80 mW. Two orthogonal cylindrical lenses with a focal length of 700 mm, UV reflective mirrors, and a phase mask with a periodicity of 906.5nm are major optical components in the experimental setup. The simple geometrical configuration for tuning grating fabrication is shown in Fig 2.4. Based on the specific position of the phase mask, the required grating wavelength can be achieved.

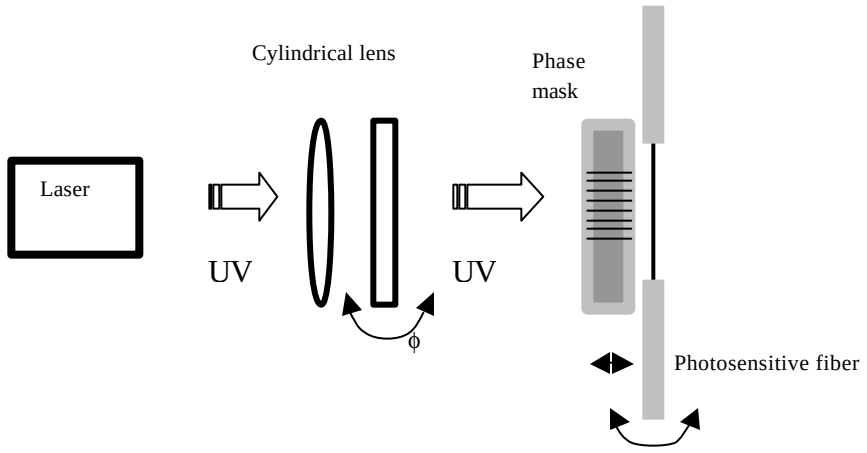

Fig. 2.4 Schematic of the FBG Fabrication

.

A general expression for the tunability of the Bragg grating central wavelength is given by,[39]

$$l_B = 2n\Lambda\sqrt{1+\frac{r^2}{l^2}} \tag{2.1}$$

where Λ is the fiber grating period, r is is the distance from one end of the exposed fiber section to the phase mask, and l is the effective length of the phase mask. Therefore, for a fixed phase mask period 2Λ, the change in system parameters will be given by introducing a rotation angle between the fiber and phase mask, in order to form chirped-like gratings.

Figure 2.5 shows the tested Bragg grating with several reflection peaks induced by titling the PM angle. The tilt angles of 1°, 2°and 4° produce several reflected peaks causing a maximum wavelength shift of about 5.5nm. Note that the last peak intensity is attenuated a great deal because of the UV laser loses its coherence. When one fiber end is separated far from the phase mask (PM), the interference of diffracted beams will produce a weakened refractive index modulation. Obviously, the technique allows us to finely adjust the Bragg wavelength to the position we desire in the OTDR interrogation, since the PM does not always provide exactly the required wavelengths. The optimum approach for tuning the Bragg wavelength is to always keep the fiber and PM parallel in order to obtain maximum interference. This implies that the fiber has no angle with the PM surface in all directions. In this case, the light coherence will be the same along the entire writing section of photosensitive-fiber. Consequently, the interference fringe on the fiber core as being close to each other will become smaller, leading to a shorter grating period.

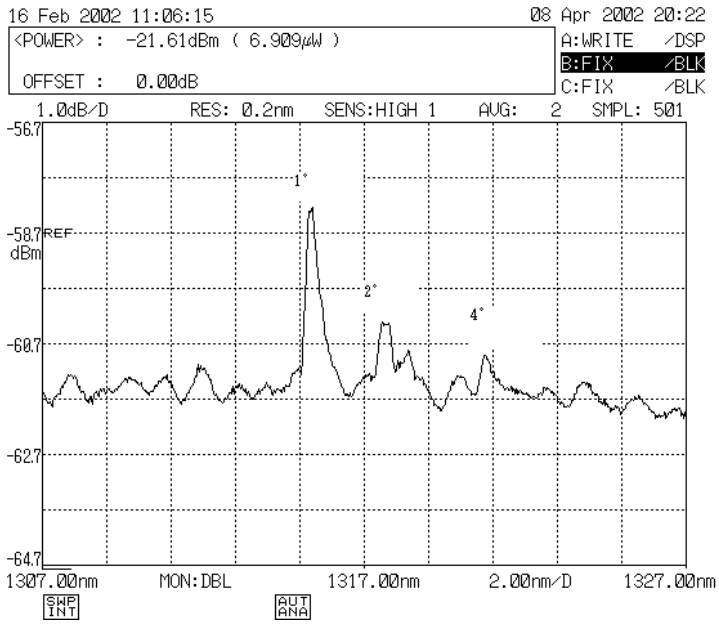

Fig. 2.5 Multiple FBG Bragg peaks produced by the change in angle between the PM and the fiber

2.4 Tuning broadband FBG through parallel adjusting method

To modifying the Bragg wavelength, we can just simply shift the photosensitivity fiber farther away from the PM or closer to the PM in a parallel fashion so that the wavelength can change in either direction relative to the original wavelength. Precisely adjustable wavelength offers the potential to control Bragg grating performance in a multiplexing sensor array. A 40 nm (1295 to 1335 nm) wavelength shift can be achieved by tilting the second cylindrical lens* duo to the change in the focal point position relative to the PM. The experimental results shown in Fig 2.6 describe one direct angle change of the cylindrical lens.

* Two cylindrical lenses are required to form UV light line spot on the photosensitive fiber, Tilting the 2nd lens can adjust its focus length so change interference

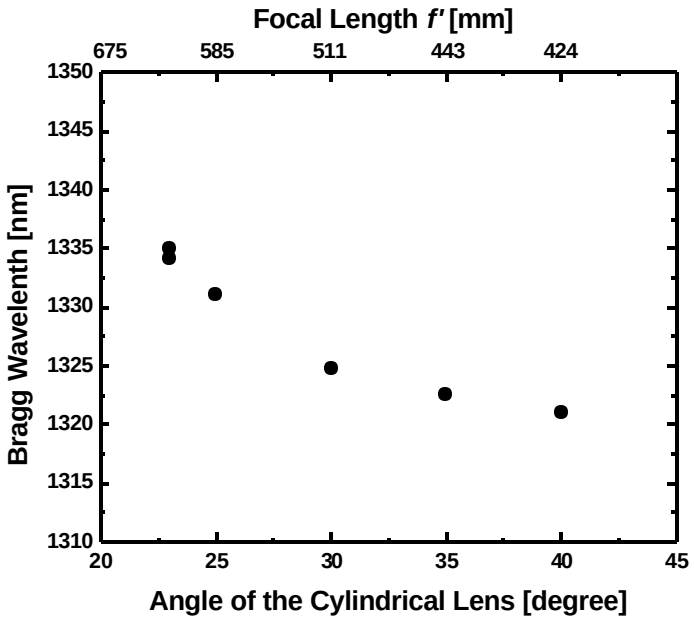

Fig.2.6 Wavelength shifts by changing angle of the cylindrical lens

For a large wavelength shift in FBG writing, the reflectance of FBG could be reduced a great deal for the same incident UV light power. That is probably appropriate for controlling the FBGs in multiplexed system. Meanwhile, the technology makes it possible to broaden the bandwidths of FBGs to satisfy the OTDR low noise detection, by repeatedly writing a grating on the same fiber position after tuning a small gap between the fiber and PM or focus length. In order to achieve optimum FBGs, the UV laser system must have better spatial coherence by adjusting the UV lens, and the phase mask should be placed on the ultra laser focal point to obtain maximum effective interference.

Chapter 3 Theoretical Analysis of a Large Number of Multiplexed Bragg Grating Sensors

3.1 Introduction

A densely multiplexed FBG sensor system is able to perform in distributed measurement of temperature and strain in large structures or in the down-hole environment. The basic system requirement for the densely multiplexed FBGs is that it must connect a few hundred FBG sensors in a length of optical fiber less than a hundred meters. Each FBG sensor can either monitor environmental temperature or strain variations with a resolution of about 0.5 ºC and a few μstrain, respectively. Some basic analyses will be presented in the following to evaluate the system feasibility.

In the multiplexed system the fraction of input optical power coupled into the bus fiber is distributed over the FBG serial array via many splices, connectors, and fiber couplers. Thus, it is necessary to consider the attenuation associated with the multiplexed system, including the loss of the FBG themselves, as well as any reflections, all of which will determine the number of multiplexable sensors. The pc-OTDR dynamic range and receiver noise floor also significantly limit the sensor measurement range. Based on those parameters, a multiplexing

configuration can be simply modeled neglecting multiple reflections or interferences between the sensors (See discussion in Chapter 6) since the sensor spacing is much broader than the light-wave coherence length. In addition, the pc-OTDR is based on photon counting detection, which measures the Poisson probability of reflected photons, which cause a slight nonlinear effect (saturation) at probability amplitudes close to 1 that will be described in detail in Chapter 4. In most cases, however, we can still adopt the intensity point of view to analyze multiplexing performance because the OTDR usually operates in its linear region.

Let's clarify factors affected by the reflected intensity of specific FBG. The output of signal I reflected from the down-stream sensor, which is exponentially related to detected photon probabilities P ($P = 1 - \exp(-hI/hu) \approx -hI/hu$, as I is very small), depends on the fiber optic transmission loss, FBG excess losses, and coupling ratios of up-stream sensors, and the source input power I_o at the Bragg wavelength. As we know, the reflected signal for a test sensor not only carries information of physical measurands, but also, exhibits some crosstalk with previous FBGs in the array under the condition of the same wavelength in multiplexing system. Therefore, very low-reflectance (below 0.1 %) is vital to satisfy FBG multiplexing requirements to reduce crosstalk. Thus we need to account for the balance of multiplexing signal intensities corresponding to crosstalk acting as a noise source.

In general, a multiplexing configuration can be modeled by two approaches to evaluate relationship of reflected intensities versus the sensor capacity n and reflectivity R. One method is the equal reflectivity scheme for each sensor but detecting a pc-OTDR minimum measurable intensity for the last sensor; and the other is using distributed FBG reflectivity starting out with a small value of reflectance and increasing it to 100% to achieve similar average receiving power for each sensor. Obviously, the down-stream gratings are subject to higher loss due to

the transmission light passing through more sensors in a round trip, Therefore for a multiplexed system with identical reflected power, the reflectivity will increase with an increase in grating sensors being put in, and after on reaching the reflectance limitation (100 %), the sensor array has to be broken. We can realize very low-reflectance FBG sensors based on the fiber Bragg grating writing system, which utilizes low photosensitive fiber and weak illuminant laser power of a few millwatts.

3.2 Description of OTDR system specifications

The OFM 130 Optical Fiber Monitor is a short haul, photon counting OTDR with a high resolution designed to operate in both Fresnel and Rayleigh modes. Operating in the Fresnel mode, it can measure insertion loss, and detect very weak returned strength such as low reflection FBGs or Fresnel reflectors induced by intrinsic refractive-index variations. This is a fundamental point in our measurement. The dynamic range that approaches 85 dB (+25 dB to -60 dB) for measuring returned strength in the Fresnel mode is made possible for the high sensitivity detector combined with a high powered optical source. Input optical pulse consists of about 10^8 photons and is sent at a 1 MHz repetition rate. The pulse width is normally less than 0.8 ns (~8 cm width). This generates measurement ambiguities when features are less than 8 cm apart. For the multiplexed sensor measured, the window size will usually be set at 0.5~2 m over a hundred meters. The high spatial resolution that is different from conventional OTDR allows measurements to be made on components separated by as little as 5 mm and 10 cm for one and two-point distance apart, respectively. The measurement range (sensitivity) of the OTDR versus its input power is shown in Table 1: OTDR power range

OTDR Input Power I_0 (dBm)	-61.94	-59.62	-56.24	-51.89	-41.09	-31.31	-21.01	-11.66
OTDR Sensitivity S dB	-6.02	-9.99	-15.08	-20.15	-30.34	-40.02	-50.19	-60

3.3 Analysis of intensity based multiplexing scheme with identical FBG reflectivity

3.3.1 Multiplexing reflection equation

As mentioned before, the several parameters will determine the multiplexed FBG number *n*. Simply saying, if the FBG is considered as a sort of Fresnel reflector with a peak reflectivity *R* at the Bragg wavelengths λ_B, the intensity at the n^{th} position should be a function of *R*, demodulation system sensitivity *S* (input power I_o = - 0.95862**S*-69.6199) and various loss coefficients. It is convenient to consider that all multiplexed sensors have an identical reflectivity *R* and connection loss coefficient a with approximately the same Bragg wavelength λ_B (single wavelength case). Obviously, a multiplexed system with multiple Bragg wavelengths allows the many more gratings to be multiplexed. Meanwhile, for the weak reflectivity (less than 0.1%) in the chain the details of the grating spectral profile can be neglected. Hence, returned powers can be written as $I_1 = I_o R$ for the first sensor and for the 2nd sensor

$$I_2 = I_o R(1-R)^2 b_1^2 a_1^2 \tag{3.1}$$

where I_2 is the 2nd sensor reflected intensity, b_1 the optical fiber transmission coefficient between adjacent gratings, a_1 the previous grating coupling coefficient, and I_o the incident power at Bragg reflecting wavelength. (Separately denote FBG loss a and fiber loss b)

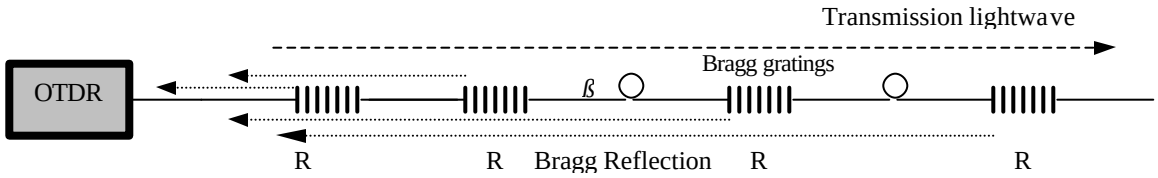

Fig 3.1. Schematic diagram of multiplexing sensor system

The schematic is shown in Fig 3.1. Thus, similarly, the n^{th} sensor reflected intensity could be given as follows.

$$I_n = I_o R \prod_{i=1}^{n-1}[(1-R_i)^2 b_i^{\,2}] \prod_{i=1}^{n-1} a_i^{\,2};$$
$$R_i = R(i = 1,2,3,...,n) \tag{3.2}$$

Here, all of reflectances equal to a constant *R*. Compared to the first sensor, the returned power of down-stream sensors decreases due to the backscattering caused by up-stream sensors so that we has to enhance the detection sensitivity to achieve an acceptable level of *SNR*.

After taking the ratio of the power equation (3.2) and the first sensor power to compute the intensity difference, we obtain the ratio expression in decibels:

$$h = I_n/I_1 \text{ (dB)} = 2\sum_{i=1}^{n} b_{i(dB)} + 2\sum_{i=1}^{n} a_{i(dB)} + 20(\text{n-1}) \log_{10}(\text{1-R}) \tag{3.3}$$

where a_i is the i^{th} FBG coupling coefficient and $b_{i(dB)}$ is the fiber optical transmission coefficient in adjacent FBGs in decibels. This is a basic multiplexing equation used for evaluation of system capacity. In general, fiber optic loss is very small (about 0.00022dB/m). For the low-reflectivity sensor, FBG insertion loss can be narrowed in the range of 0.01dB to 0.001dB. n represents the total number of multiplexed sensors. η indicates the system dynamic range is the ratio of the first and last sensor power in multiplexing. Therefore, we can evaluate the power attenuation between the 1st and last grating (the 1000th sensor) by changing these two parameters, the grating loss coefficient and average reflectance *R*, as shown in Fig 3.2. Given an example of 1000 sensors, the multiplexing attenuation rate becomes large as sensors increase and the maximum total loss between the first and the last sensor will be –28.5dB or -31 dB, respectively for these two cases for constant R and a. The OTDR can still operate in this range.

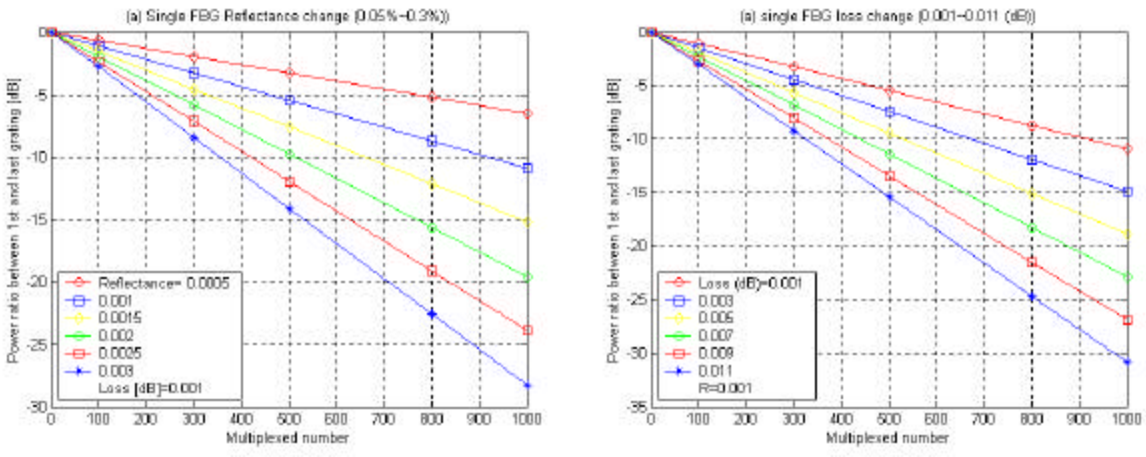

Fig. 3.2. The power attenuation between the first and the last sensor determined by (a) unchanging insertion loss 0.001 dB and (b) fixing the grating reflectance 0.1 %

3.3.2 Multiplexed FBG system evaluation

How to assess the maximum number of multiplexed sensors is a fundamental problem in setting up a required system. Assuming a sensor array with the number *n*, the reflected photon probability (power) for single FBG can change about total 8 dB in the OTDR test at a certain sensitivity level. In downward tracking OTDR amplitude, the initial OTDR trace has to be set at the full-scale state. Obviously, for the identical reflectance case each sensor will produce a different reflection power due to reflections from the previous sensors. However, similar OTDR traces should eventually be obtained for all gratings in the OTDR operations by adjusting their trace to maximum scale. This implies that reflected peak of the grating at the specific scale on the OTDR trace should be the same; just the OTDR incident power is changed. In other words, the OTDR sensitivity determines the input source power. Therefore, identical gratings actually achieve an identical reflected power by controlling the incident power during each testing. Equation (3.1) and (3.3), in fact, indicate an identical reflected

power with different input power I_{io}. Thus, the reflected power from the first to the last sensor can be given by a new equation,

$$\begin{aligned} &I_n = I_{n-1} = I_{n-2} = \ldots = I_1 \\ &\textit{then, } I_{1o} R = I_{no} R(1-R)^{2(n-1)} (ab)^{2(n-1)} \end{aligned} \tag{3.4}$$

where a and b are average coupling coefficients and n is the number of sensors multiplexed. Note that the incident power is different for different FBGs. Hence an alternative equation is written as

$$\begin{aligned} &Dr = \frac{I_{1o}}{I_{no}} = (1-R)^{2(n-1)} (ab)^{2(n-1)} \\ &So, n = 1 + \frac{5 \times \log_{10} Dr}{10 \times \log_{10}(1-R) + a_{dB} + b_{dB}} \end{aligned} \quad , \tag{3.5}$$

where Dr can be definited as the OTDR dynamic range. According to measured results from Table 1, the incident power can have a maximum value of –11.66 dBm. In an experiment using a free fiber endface reflection and the combined detection using the OTDR and an OSA, we could calibrate the reflected intensity with respect to its incident signal that has a power of 61.94 dBm in an OSA measurement at the OTDR's output saturation state (~4 div, or 120 full scale). As long as all grating peaks are placed on the 4 div on the OTDR screen, their reflected powers will be I_1 =-79.44 dBm (-61.94 dBm-17.5 dB, 17.5 dBm is included a free end Fresnel reflectance, 4% (-14 dB) plus 50 % coupling ratio and coupler returned loss 0.5 dB). We are currently able to evaluate system capacity *n*. Assuming the reflectance of grating *R* is about 0.1 % (-30 dB), and the last sensor measurement has to be operated at –60 dB sensitivity for a multiplexed system. The first sensor incident power will be $I_{1o} = I_1/R$ = -49.44 dBm (-79.44 dB+30 dB). The incident power of the last sensor n is I_{no} = –11.66 dBm at –60dB sensitivity based on Table 1. Hence, multiplexing dynamic range *Dr* is 49.44-11.66=37.78 dB. Assuming

that a grating loss of 0.01 dB is reasonable, Equation (3.5) determines a multiplexing number of 1320.

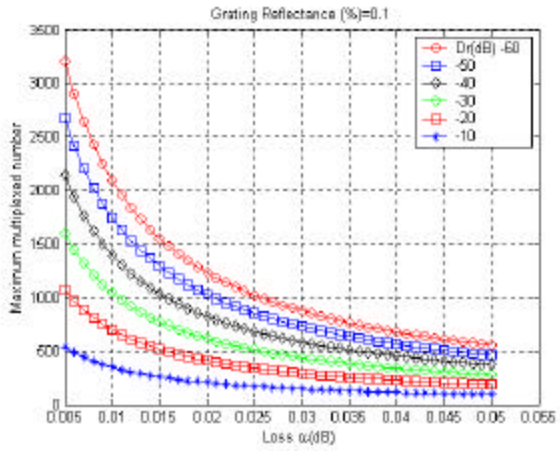

a

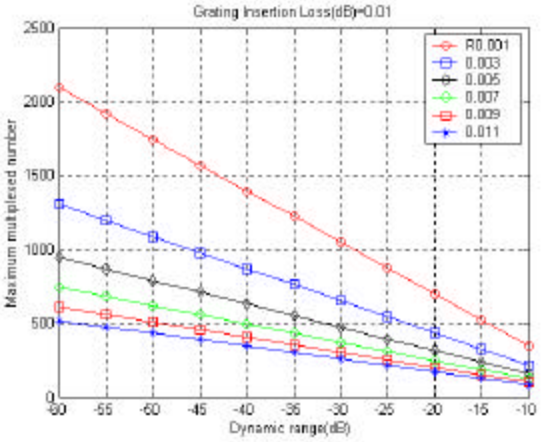

b

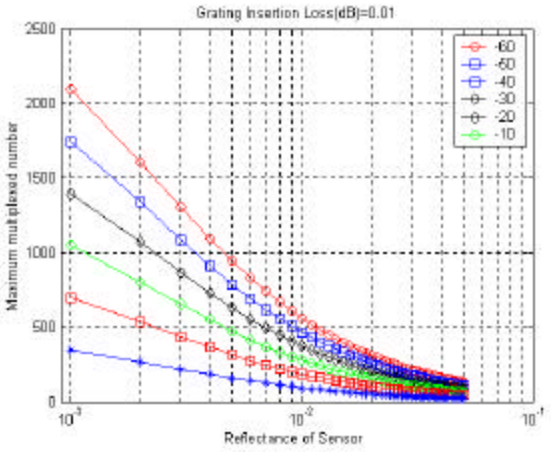

c

Fig.3.3 Multiplexed number changes with all three parameters: a) Multiplexed number versus coupling coefficient; b) Multiplexed number versus dynamic range; c) Multiplexed number versus reflectance of sensors

The system dynamic range *Dr* is a variable with the sensor reflectance *R*. As we mentioned before, $Dr=I_{10}/I_{n0}$. To measure the minimum detectable reflective signal in the FBG array (I_{n0} is -11.66 dBm), the maximum incident power I_{n0} should radiate on the FBGs to achieve minimum reflected measurement, whereas I_{10} (the first incident power) is inversely proportional to the reflectance *R*,

$I_{10(dB)} = -10log_{10}R + I_{1(dB)}$, $I_{1(dBm)}$ is the first sensor returned power, approximately –78 dBm in the OTDR measurement. Hence,

$$Dr\ (\text{dB}) = -10logR + I_{1(dBm)} - I_{n0(dBm)} = -66.34 - 10log_{10}R \tag{3.6}$$

Thus, substituting (3.6) into the multiplexed number (3.5), yield,

$$n = 1 + \frac{0.5 \times (-66.34 - 10\log_{10}(R))}{10 \times \log_{10}(1-R) + a_{dB} + b_{dB}} \quad . \tag{3.7}$$

The multiplexed number is only a function of the reflectance R and coupling coefficient a .

3.3.3 Best reflectance for maximum multiplexing reflected power

If the coupling coefficients remain unchanged, Equation (3.2) is a binomial equation having only one variable R, and the optimized reflectance R to achieve maximum reflected power for the n'th FBG can be computed by simply using the extremum-finding method in the equation. Let's take a simple transformation of Equation. (3.2) as following:

$$\begin{aligned} &\frac{I_n}{I_{no}\prod_{i=1}^{n-1} b_i^{\,2} a_i^{\,2}} = R\prod_{i=1}^{n-1}[(1-R_i)^2]; \\ &R_i = R\ (i = 1,2,3,....,n) \end{aligned} \tag{3.8}$$

After taking the derivative from both sides of the equation, the optimum reflectance can be determined as follows:

$$R = \frac{1}{2n-1} \quad , \tag{3.9}$$

where n is the maximum number of multiplexed grating sensors. Figure 3.4 (a) shows, only considering R variation, that in a 100-FBGs system the power of the n^{th} sensor changes with reflectance and that maximum returned power is obtained for a reflectance of 0.5 %. Figure 3.4

(b) plots a distribution of optimum reflectance for numbers of multiplexed sensors from 2 to 2002. The reflectance *R* can reach values as small as 0.025 % at a multiplexed number of 2000.

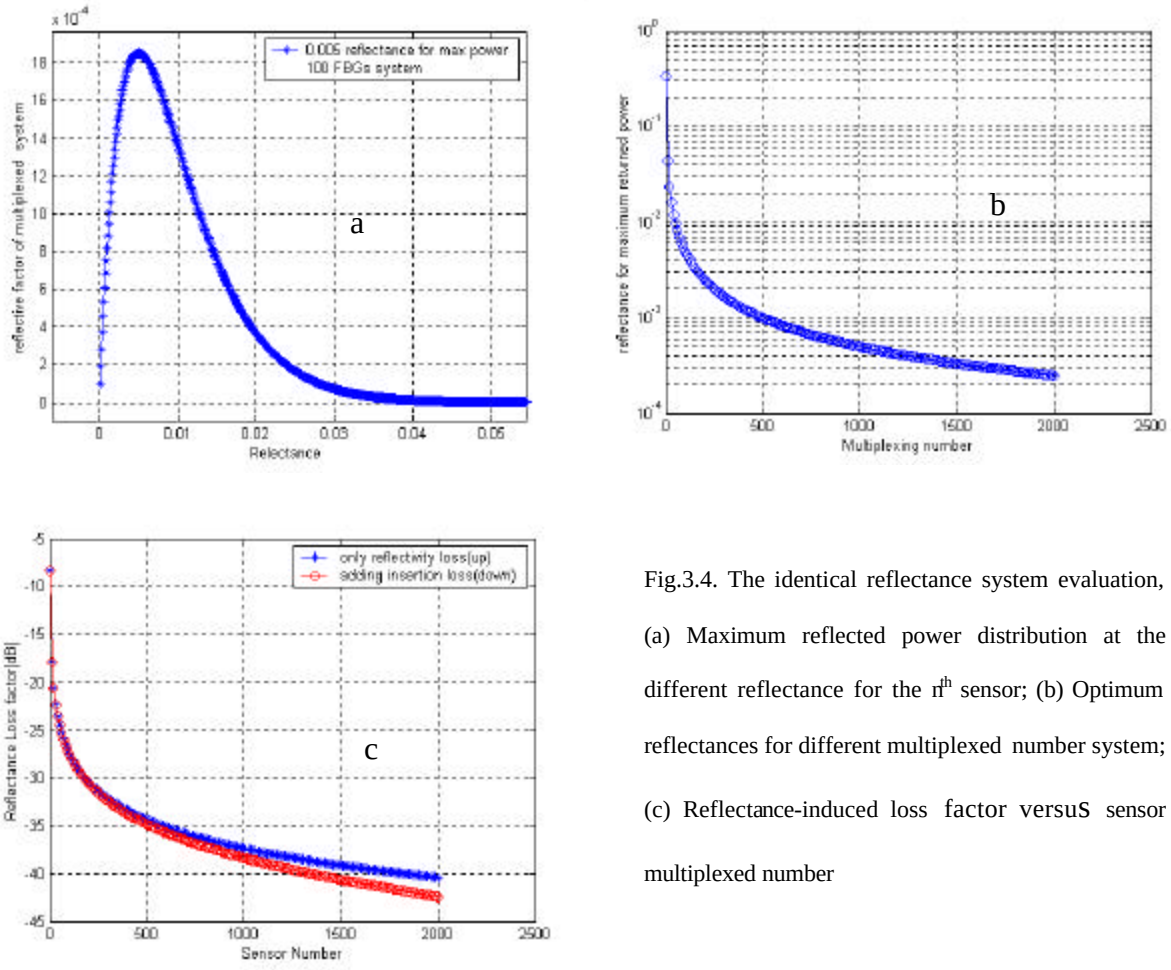

Fig.3.4. The identical reflectance system evaluation, (a) Maximum reflected power distribution at the different reflectance for the nth sensor; (b) Optimum reflectances for different multiplexed number system; (c) Reflectance-induced loss factor versuS sensor multiplexed number

Figure 3.4c indicates the reflectance-induced power loss of the n^{th} grating with and without insertion loss.

3.3.4 Best reflectance from the analysis of multiplexed number versus *R*

Based on Equation (3.7), Figure 3.5 shows a typical relationship between multiplexed number *n* and their *R* for a given FBG-related coupling coefficient of a= -0.015dB. As we can see, the maximum multiplexing number at a reflectance of 0.05% can be obtained by finding extremum

in Equation (3.7) (i.e. $\alpha = 66.34 + 10 \times (\log_{10} R) \frac{R}{1-R} + 10 \log_{10}(1-R)$ (3.9.1)) so that n has the same relation as Equation (3.9), $R = \frac{1}{2n-1}$, for a insertion loss α given. The sensor multiplexing number will drastically drop when the reflectance is smaller than 0.0005.

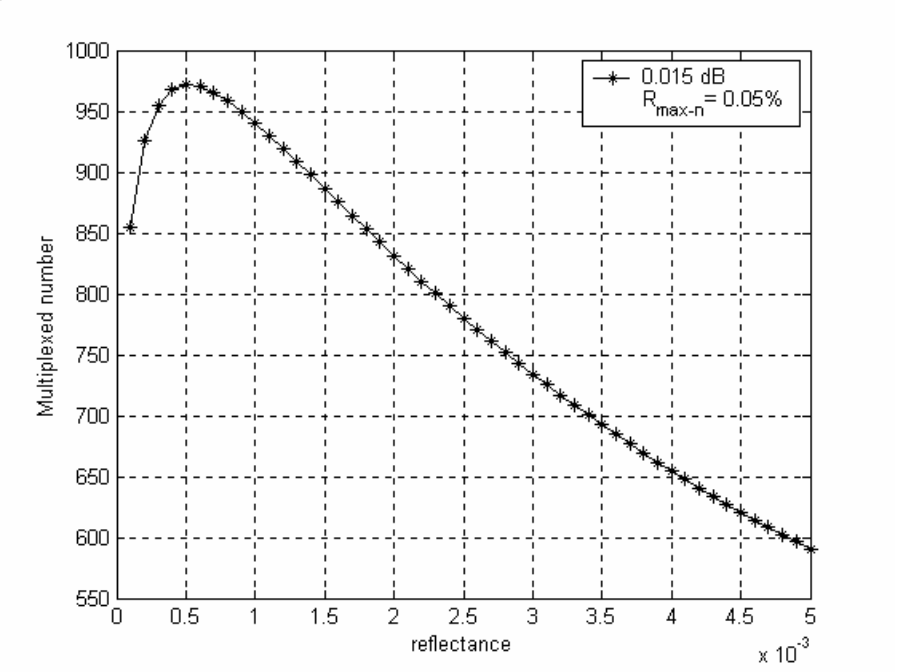

Fig.3.5 Multiplexable sensor number n versus reflectance *R* in equal-reflectance scheme

This is because a larger incident power is demanded to maintain a high resolution when the sensor has a very small reflectance and thus it results in multiplexed dynamic range decrease. On the other hand, if the reflectance *R* increases to 0.08%, the total multiplexed number of gratings starts to decrease approximately linearly. This is because the increase of reflectance results in a decrease in power arriving at downstream sensors. Thus the system needs more input power to meet the large capacity detection requirement. Obviously, in order to achieve a thousand-sensor system, the average fabricated grating reflectance has to be around 0.05% if the coupled coefficient is less than α_{dB}= 0.015dB. Let us consider an extreme example for a

super low loss multiplexed system that has a coupling coefficient to 0.001dB (0.9998). Nearly ten thousand sensors can be multiplexed in a single fiber when the sensor reflectance is 0.0001 as shown in Fig 3.6. This is almost a sort of ultimate case. In fact, the additional limitations for evaluating maximum multiplexable number from TDM or OTDR multiplexing are the pulse duration t_d = 0.8 ns, the pulse period T = 1 us, and the i^{th} FBG delay time t_i,

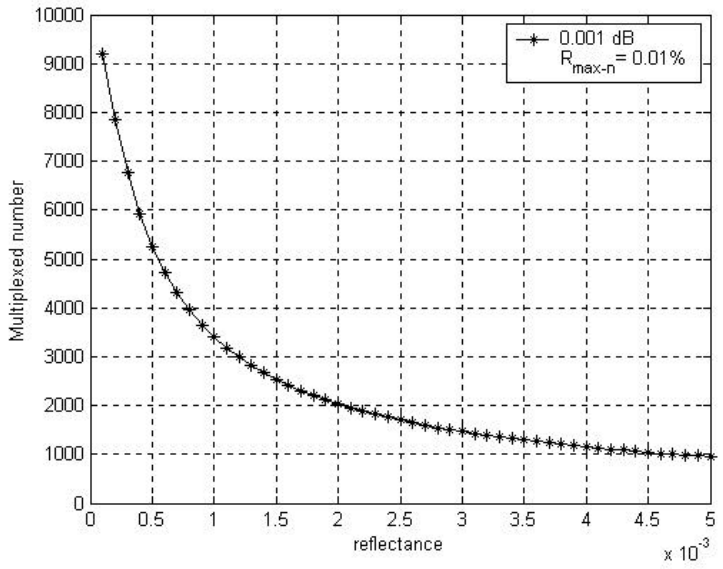

Fig 3.6 Super low loss (0.001 dB) system analysis that the number of multiplexed sensors can reach ten thousands, also the number multiplexable sensor *n* versus different reflectance *R* in equal-reflectance scheme

N sensor signals can only be separated from each other if $t_d < t_i$ for all values of *i* and $\sum_{i=1}^{N} t_i < T$ as described in Chapter 1. Consequently, the maximum FBG number should be approximately $10^{-6}/(0.8\times10^{-9}) = 1250$ in the pc-OTDR measurement.

If the light experiences a higher loss caused by the splicing connection between the regular and photosensitive fibers, the graph would be largely changed. The average coupling coefficient will significantly determine the optimum average reflectance *R* (i.e. Eq (3.9.1)). The maximum

number of multiplexed gratings can thus be obtained by Equation (3.9). In Fig 3.7, the maximum sensor number reduces to 339 for a large coupling coefficient close to 0.05dB.

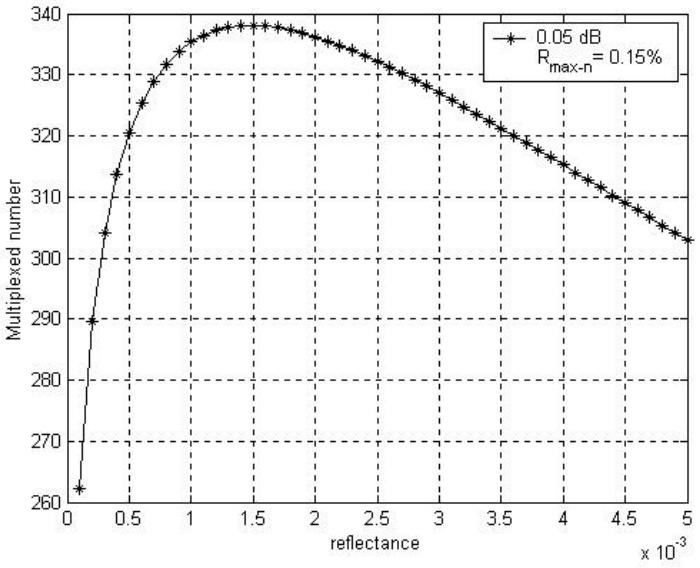

Fig. 3.7 Big loss in multiplexing system (0.05 dB loss)

Also multiplexable sensor number n versus different reflectance *R* in equal-reflectance scheme

In fact, the splicing loss would be considered a big deal for the evaluation of system capacity. Usually, an average loss of 0.01dB in adjacent grating sensors is an acceptable value if all grating sensors are printed on a single low-loss photosensitive fiber without a regular fiber connection. Thus, 1350-FBG sensors can be multiplexed in an array. The loss coefficient α (~0.05dB) is vital factor in determining the total number of gratings in the system. Figure 3.8 shows an overall picture of the optimum (reflectance) multiplexing system for an analysis with different loss coefficients. Obviously, the multiplexing number increases exponentially with the decrease of FBG insertion loss, so does the optimum reflectance.

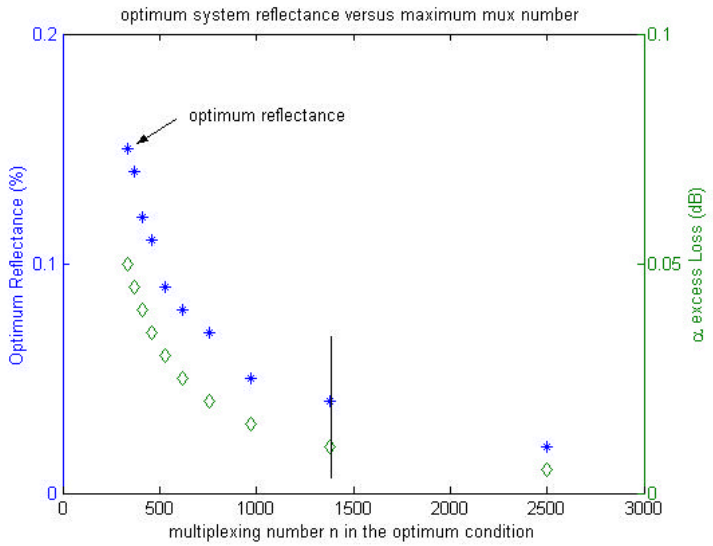

Fig. 3.8 The multiplexed numbers of grating array for different grating loss coefficients under the condition of optimum reflectance

3.4 Analysis for Reflected Power Budget—Identical Reflected Power Analysis

From the above analysis, we know that it is relatively easy to fabricate identical property grating using the UV laser inscribing system to form the FBG chain. But in the OTDR measurement system, each Bragg grating at a different distance could be monitored by the time-division reflected signal on the OTDR. It is implied that *an equal reflected* power for each sensor could be achieved by real-time control of the reflected intensity observed by the OTDR as gratings are fabricated so that all of the FBGs may be balanced at the same energy level. Therefore, an analysis, i.e. a kind of distributive grating reflectance $R(i)$ approach for the identical reflected power scheme, will help to improve the problem at the cost of increased reflectivity. For the serial grating array shown in Fig. 3.1, the reflected light from different FBGs will not only depend on the peak reflectivity, but also on their relative Bragg wavelength. If all gratings have different wavelengths over entire operating range, the returned power from

different gratings could be balanced if all reflections are the same. But in fact, it is impossible to multiplex a few hundred gratings over tens of nanometer range, and each sensor has a 2 nm as sensing range without any overlapping effect. So the same Bragg wavelength among sensors is a basic prerequisite condition for multiplexing a large number of FBGs sensors. In this case, we actually cannot balance the power from different sensors because the reflected power from the i^{th} fiber grating sensor depends upon the Bragg wavelength of downstream sensors from the first to $(i-1)^{th}$ sensor. That implies that the change in any previous sensor caused by the measured parameter would affect the i^{th} sensor power level. Therefore, low reflectivity of each grating in the array is necessary to decrease the interacting influence of up-steam sensors.

To obtain the same reflecting power for all grating sensors, each grating sensor must increase its reflectance slightly compared to the previous one. Let's analyze the system capacity in this situation. An optimum mode of reflectance change can be achieved by evaluating identical multiplexed sensor reflection power, and a maximum grating number N can be computed based on the following equations, similar to Equation. (3.1) and (3.3)

Hence, the returned optical power of the n^{th} sensor: $$I_n = \alpha_{n-1}^{\ 2} I_o R_n \prod_{i=1}^{n-1} (1-R_i)^2 \qquad (3.9)$$

where R_i (i=1,2, …,n) denotes the peak reflectivity of the i^{th} grating, and α_i is the coupling coefficient or power transmission coefficient of the connecting fiber between adjacent gratings. Based on the expression for the n^{th} sensor intensity (3.9), and assuming all the sensors have the same reflected peak power, that is, $I_{i-1}=I_i\ (i=1\ldots n)$, by neglecting the multiple-reflection effect, we can write a recursive formula from Equation (3.9):

$$R_n = \frac{R_{n-1}}{\alpha_{n-1}^{\ 2}(1-R_{n-1})^2} \quad . \qquad (3.10)$$

From the simple mathematical relationship, the later sensor reflectivity is inversely proportional to square of the transmission rate of the previous one. After setting the first sensor reflectance, we can obtain maximum multiplexed sensor number *n* when the final reflectivity is close to 100%. After solving Equation (3.10) the new form can be written as

$$R_{i-1} = \frac{2a^2 R_i + 1 - \sqrt{4a^2 R_i + 1}}{2a^2 R_i} \quad . \tag{3.11}$$

Through Equation (3.11), provided that the reflectivity of the last grating sensor in the array is given, the reflectance of the previous sensors and corresponding reflected power at the OTDR detector can be computed from Equation, (3.10) and (3.11), respectively. It was concluded that the sensor reflectance would continually increase to make the reflected power constant. The FBG transmitted power drastically decreases for the last a few sensors since their reflectance will rapidly increase based on the relationship (3.10). Figure 3.9 shows the relationship between grating number and corresponding reflectivities based on Equation (3.10). The formula can easily evaluate the maximum multiplexable number N_{max} using Matlab to obtain the last grating reflectance if its reflectance is close to 100%, i.e, $R_N < 1$ or $R_{N+1} > 1$, N_{max} is the system capacity number and the whole map shows a monotonic increase with the sensor number. Based on Equation (3.12), Figure (3.10) plots the maximum number of grating versus the first grating reflectivity in the grating array. Therefore, we could theoretically multiplex a few thousand Bragg grating as long as they have very low reflectivity and insertion loss. Figure 3.11 shows the distribution of the reflectivity (0.005% for the first reflectance) in an array with 3740 FBGs. Note that the maximum number of FBG is located near 10 % reflectivity without considering the OTDR source pulse repetition rate limitation. Meanwhile, we also observe that the reflectivity sharply grows at the end in Fig 3.9.

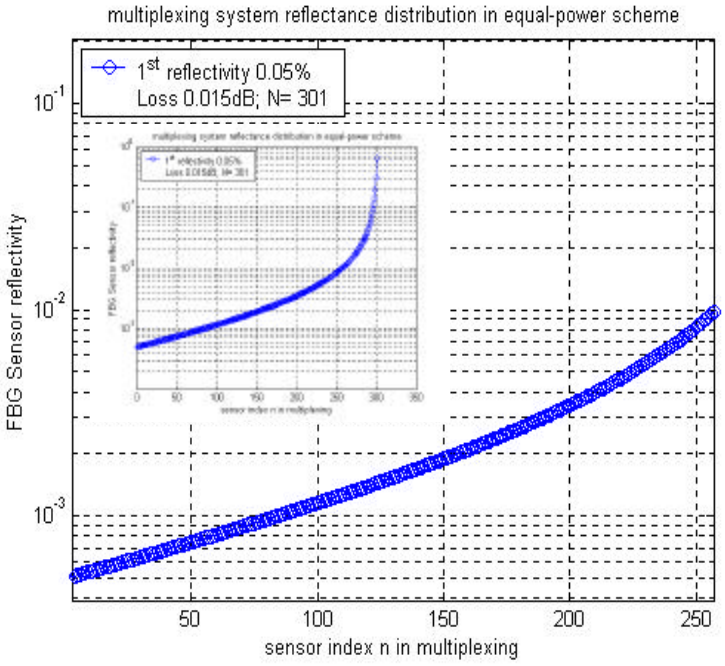

Fig.3.9 Reflectance distribution versus FBG index ID, until the reflectance R_n~1, (R_1 = 0.05%; 0.015dB)

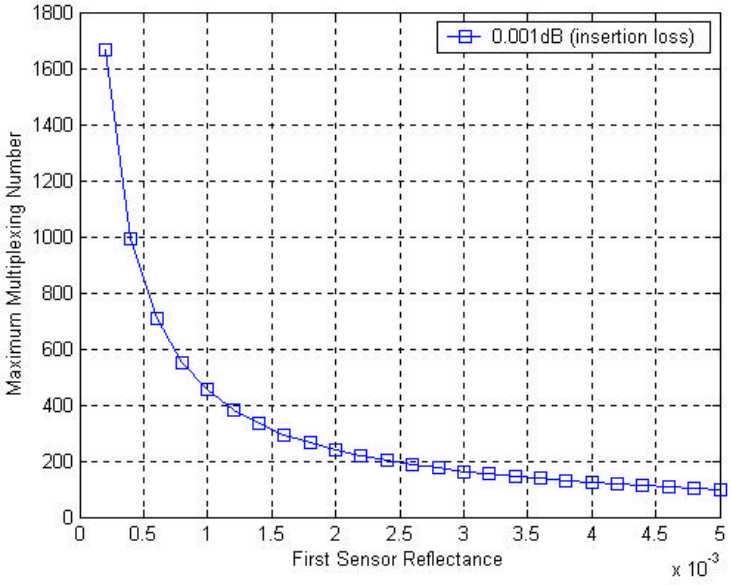

Fig.3.10 The first sensor reflectance versus maximum multiplexed number

According to the recursive equation (3.12), it is evident that the reflectance of a downstream sensor is inversely proportional to the square of the previous FBG transmission coefficient (1-

R_{i-1}), and proportional to its reflection coefficient R_{i-1}. Hence, with an increase of the reflectance in the array, the recursive reflectance will exponentially increase up to 100% within only a few sensors.

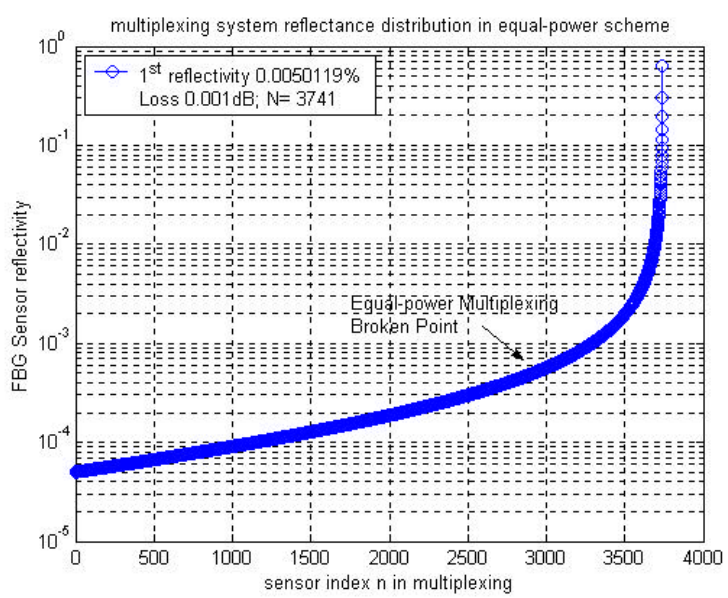

Fig. 3.11 plot a possible 3700 multiplexed gratings, assuming a higher repetition of OTDR pulse

For high-reflectance multiplexing, many multiple reflections will occur to obscure all useful reflected signals. This is not allowed in a multiplexed system. In order to avoid this situation, a hybrid of the two multiplexing schemes described above was adopted to limit a low-reflectance in multiplexing. The multiplexed array will thus be divided into two parts: the first is equal-reflectance multiplexing based on the adjustment of the OTDR dynamic range; and the second is equal-power FBG multiplexing based on the constant OTDR sensitivity (incident power, low dynamic change). Therefore, in the example of Fig 3.5, which described the optimum reflectance R_{max_n} (at the maximum multiplexing number) in the equal-reflectivity scheme that has a 0.015dB-loss, the optimum reflectance of 5×10^{-4} can lead to a multiplexing number of 971 occupying a 33 dB dynamic range. We continue with the equal-power multiplexing

scheme. According to Fig. 3.9, a first reflectance of 5×10^{-4} can generate about 250-multiplexed FBGs without occupation of the dynamic range and high-reflectance section cut in the OTDR detection. By taking advantage of the large dynamic range of the OTDR and variable FBG reflectance, we can obtain a densely multiplexed FBG array (eg. total 1221 FBGs) and weaken the multiple reflections caused by the high-reflectance section.

Chapter 4 OTDR Theory to Interrogate Low-Reflectance Bragg Grating Sensors

4.1 Rayleigh and Fresnel reflections in the OTDR

In general, the simplest characterization of the grating spectra can be obtained by the use of an Optical Spectrum Analyzer (OSA) with broadband light sources and tunable filter, or multimode laser demodulation. All of these approaches can potentially track fiber Bragg grating wavelength variations, which respond to changes in environmental parameters. If the demodulating method is combined with a low-coherence Michelson interferometer [46], the location and coupling coefficients of Bragg gratings can be determined. However, due to the very low insertion loss and low reflectance for the gratings (loss about 0.001~0.01dB per 2 mm sensor grating length and 0.1% or less reflectance), their applications to in-line sensor networks are more attractive. [45] The photon-counting-OTDR based technique seems to be a simple and reliable technique for the interrogation of very low-reflectivity multiplexed gratings in large numbers. In fact, the OTDR transmitter with a central wavelength of 1305 nm actually outputs a light pulse with pulsewidths of less than 10^{-10} s (100 ps) for peak power of about tens of milliwatts.

It produces two types of returned light: one is the backscattering from the microscopic density fluctuation, called Rayleigh backscattering, and the other is reflection from abrupt macroscopic discontinuities in the fiber index of refraction called Fresnel reflection. Rayleigh backscattering is a very small portion of the reflected pulse energy that is randomly distributed from every point and fairly uniform along the length of the fiber. It has been popularly used in the conventional measurement of fiber attenuation. It is not suitable for a sensor reflective measurement in a very short length. However, Fresnel backscattered light, caused by the local indices periodic modulation such as a FBG or IFPR (Intrinsic Fabry-Perot reflector), has a larger reflective power (3~4 order of magnitude larger than Rayleigh), and may be easily detected and can eventually be considered as a series of Fresnel reflected facets. Although each of them reflects a very small amount of power due to the refractive indices variation ($\sim 10^{-4}$), a grating consists of a few hundred periods of refractive index variations, which all will reflect the incident light in the same direction. The grating will therefore introduce interference intensification for the returned light power. It can be observed as an obvious reflected peak at the OTDR's APD detector within a very narrow spatial region with a zero-deadzone. This is based on the principle of the detection of the probability of received photons from reflective features. Therefore, the measurement based on Fresnel reflection allows us detecting each FBG's reflection with a very high spatial resolution and leads to an effective approach to detect dense Bragg grating arrays in a short length of fiber. As mentioned previously, in this system the minimum spatial separation for adjacent fiber gratings is about ten centimeters. The OTDR contains a broadband light source. According to the Bragg spectral reflection principle (Fresnel), reflected signals are a

function of the Bragg grating central wavelength, reflectivity and incident optical spectrums. Thus, the Fresnel backscattering allows [47] [48] the direct evaluation of the reflection ratio R associated with the reflected power of each grating. Owing to the spectro-temporal multiplexing possibility for Bragg gratings continuously inscribing on a length of the fiber, the *photon counting* OTDR methodology therefore appears to have a potential advantage in the interrogation of economical, high-density sensors networks. A theoretical analysis in reflectance measurement is described below.

4.2 Theoretical analysis of low-reflectance measurement based on photon counting

4.2.1 Statistics for photon counting

The photodetector of the photon counting OTDR is a single photon avalanche photodiode with a very high sensitivity, which will be described in detail in Chapter 6. In principle, we are not really measuring the amount of light returned but are measuring the probability of a single photon being returned, when the probability is 1 saturation occurs. In fact, this is a kind of counting statistics processing in photon measurement. A simple Poisson probability distribution P can depict k photon radiations from the source with a constant optical power P_o and possibility being registered in the time interval T in which the photons are detected.

$$P(k,T)=\frac{(nT)^k e^{-nT}}{k!} \tag{4.1.1}$$

where n is the average number of radiated photons per time unit, and k is the number of registered photons. In the OTDR detection, the relationship between the received light field and the number of released electrons in the detector is governed by the interaction between the radiation field and the electrons of the photosensitive material. In the purely

quantum treatment, the field is quantized into photons, and each field photon usually gives rise to an electron with some probability. The electrons released are, thus, a statistical processing of the photon occupancy in the field and electron counting is often called photon or photoelectron counting. One defined Fermi rule for the probability per second *P* for a state transition over a differential area ? **r** located at point **r** on the detector surface. The probability rate can be satisfied by the equation

$$\frac{dP}{dt} = a\, I_r(t,r)\Delta r \tag{4.1.2}$$

where *P* is interpreted as the probability of an electron emission from ? **r** at t. a is a proportionality constant that may be a quantum coefficient or backscattering parameter, and I_r is the field intensity (reflection) at time *t* and point *r* on the surface. The primary consequence of the Fermi rule implies a proportional relationship between the probability P_t of ejecting an electron and the incident light strength over ? **r** and ? t. That is, $P = a\, I_r(t,r)\Delta r\Delta t$.

The derivative form of the probability of k emissions of photoelectron over ? $\mathbf{r}^3$ is also a Poisson distribution

$$P(k,T) = \frac{(m)^k e^{-m}}{k!} \tag{4.1.3}$$

where $m = a\int_0^t \int_{A_d} I_r(t,r)\,dr dt$ and

$a\, I_r(t,r)$, as said above, represents the probability density of photon occurrence in the measured the OTDR waveform at time *t* and ? **r.** The parameter ***m*** is also a mean value of the count during pulse duration T. For single photon absorption processing, a is ?/h?,

where *h?* is one-photon energy. Thus, (4.1.3) becomes $P(k) = \frac{(hn_p)^k e^{-hn_p}}{k!}$ where n_p is the number of photons arrived at the detector within one a light pulse (sensor reflected signal).

4.2.2. Fresnel reflection in the evaluation of the reflectivity

The shape of OTDR Fresnel signal is shown in Fig. 4.1

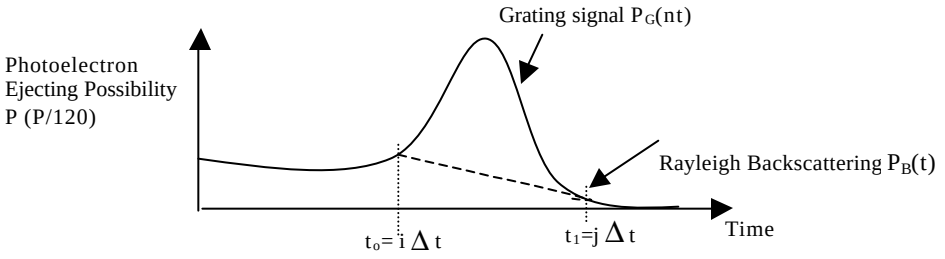

Fig 4.1. Schematic of the pc-OTDR trace (horizontal axis quantized 256 sections)

The Fresnel backscattering waveform resulting from a light pulse includes average photon n_o. The normalized vertical axis in Figure 4.1 denotes the probability of photoelectron emission, and the horizontal axis is quantized into 256 time sections for an OTDR window. It allows estimation of the sensor reflectivity *R* through the relationship between the power P_r reflected by the grating and the incident power using the equation normalized in real time at t_o.[45][52] The detection probability is, the possibility of emission a photoelectron and the complement of the non-detection probability, can be expressed as

$$P_n = P_{Ampl}/120 = 1 - e^{-hn_p} \tag{4.2}$$

where P_{Ampl} is the measured value of OTDR output. By solving this equation for photon number n_p, the mean number of photons obtained per pulse can be computed as

$$n_p = \frac{1}{h}\ln(1 - P_n) \tag{4.2.1}$$

Thus the average power for reflected photons is $P_r = hn\, n_p b$ (4.2.2)

where P_r is the power reflected by the fiber Bragg grating and b is an attenuating factor of the OTDR, The peak reflectance R_{peak} of the grating can be obtained from the analog reflecting spectra of the Bragg grating and the OTDR emission laser spectrum $S(\lambda)$. Therefore, the power of the fiber backscattering signal P(nt) applied as a reference to evaluate R_{peak}, is proportional to the overall incident power over the spectrum. A Bragg grating sensor with a narrow spectral bandwidth will reflect a limited wavelength range of the incident spectrum and thus only a small amount of input power is reflected. Actually, the reflection characteristic of a Bragg grating can be described by a coupled-mode equation, in which the reflectivity dependence on the wavelength is a complex function, and it is quite difficult to process analytically. To simplify the numerical process, it can be idealized as a Gaussian model curve when the reflectivity index is not very high. The normalized reflection-spectrum may then be calculated as

$$G_n(l - l_B) = \exp(-4\ln 2 * (\frac{l - l_B}{\Delta l_B})^2) \tag{4.3}$$

where l_B and Δl_B are the central Bragg wavelength and the bandwidth of a grating, respectively. Much work has proven that the Gaussian spectrum mode fit well with the exact coupling-mode spectrum, especially in the low reflectance case. At this time, it is

reasonable to assume that (4.2.2) and (4.3) are equal, so we could calculate peak reflected power as,

$$P_r = \int_{-\infty}^{\infty} S(l - l_o) G_n(l - l_B) R_B \, dl \tag{4.5}$$

Here, in the case of lower reflectance, that is, |k*L|<<1, where L is the length of the Bragg grating and k is the coupling coefficient of the grating, and according to the coupling theory the reflectance $G(\lambda)$ can be written approximately as

$$G(\lambda)=R_B * G_n(\lambda-\lambda_B) \tag{4.6}$$

and $G_n(\lambda-\lambda_B)$ is characterized as a normalized Gaussian profile. Hence, the reflecting peak intensity in Bragg wavelength can be written as,

$$R_B = \frac{P_r}{\int_{-\infty}^{\infty} S(l - l_o) G_n(l - l_B) \, dl} \quad . \tag{4.7}$$

4.3 Implementation of multiplexed Bragg grating array

4.3.1 Demodulation for a single FBG

According to Equation (4.4), the reflected intensity for each Bragg grating sensor is partially determined by the OTDR spectrum. The principle of interrogation, as illustrated in the previous section, is based on using a section of the pc-OTDR edge spectrum that has an approximately linear relationship between wavelength and the output intensity. Therefore, if the grating central wavelength corresponds to a certain position in the OTDR source spectral region with a larger slope rate, high sensitivity would be achieved when grating central wavelength has shifts induced by temperature or strain. The returned

signal power is mathematically a form of overlapping integral from the OTDR (S) and FBG (G) spectral function.

$$P(l_B) = \int_0^\infty S(l - l_o)G(l - l_B)dl \tag{4.8}$$

where l_o and l_B are, respectively, the central wavelength of the OTDR source and FBG. The reflected spectral envelope of the pc-OTDR source can be directly measured by an OSA at a resolution of 0.2-nm from 1273 to1325 nm, as shown in Fig 4.2.1.

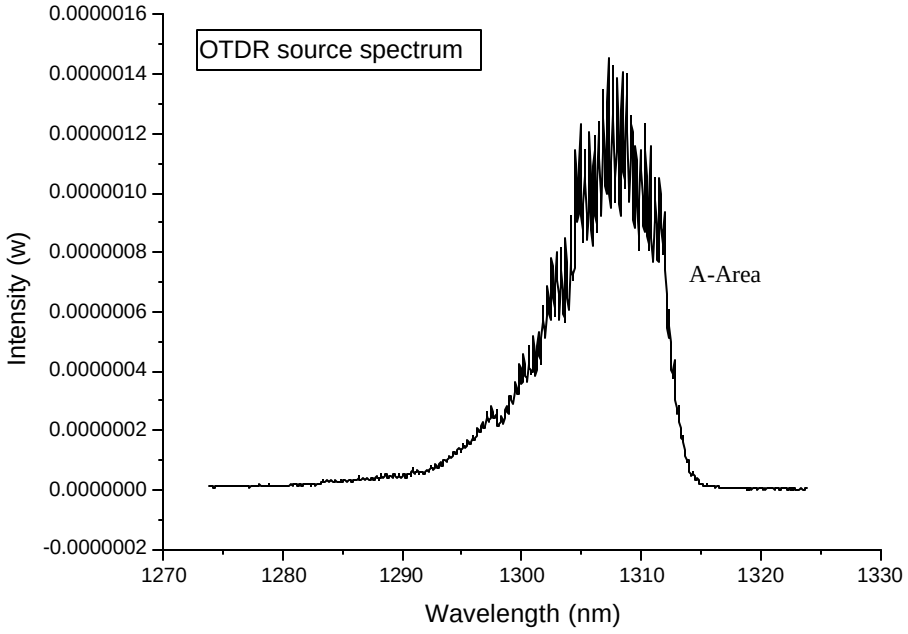

Fig 4.2.1 Typical OTDR light source spectrum (linear scale)

From the source spectrum, it is seen that the highest slope rate is located in the range 1310 to 1315 nm. So if the FBG wavelength is positioned in this area, called A-area, we can obtain the highest sensor sensitivity approximately 10 dB/nm. But A-area is a quite limited range. Therefore, an alternative option for the grating detection sensitive region is

1290 ~ 1305 nm range that has positive sensitivity coefficient and still has a good slope rate with a small amplitude oscillation than A-area, which is not smooth envelope due to varied peaks of the multi-longitude modes of the source semiconductor laser pulse, as shown in detail in Fig 4.2.2. Note that there is about a 0.39 nm gap in spectral mode over the overall spectral range.

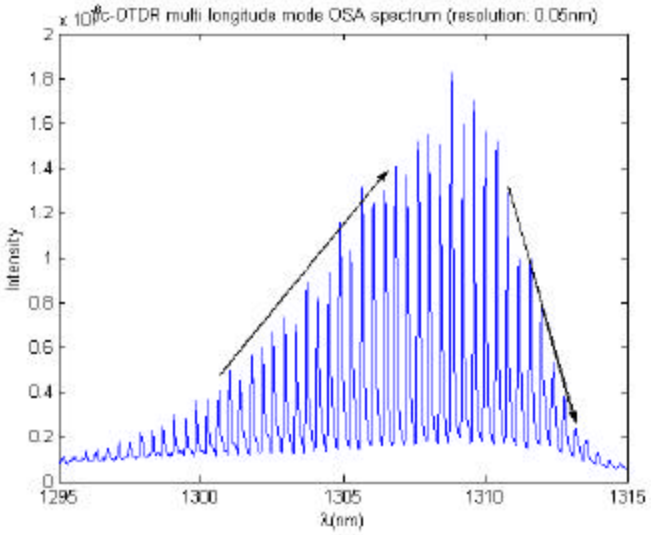

Fig 4.2.2 Average optical spectrum of a multi-longitude mode laser of OTDR with a central wavelength of 1309nm and a mod spacing of 0.39nm. It is directly modulated into pulse trains with a pulse width of ~1ns, repetition cycle of 1us, and is measured using OSA with a resolution bandwidth of 0.05nm and shows a Gaussian distribution with FWHM of 5nm.

Assuming that both the source and FBG reflection spectra are characteristic Gaussian distributions such as Eq.(4.3), Eq.(4.8) can be determined as an exponential relationship written as the following.

$$P(l_B) = S_o \frac{R_B\sqrt{p}}{\sqrt{4\ln 2}} \left\{ \frac{\Delta l_B \Delta l_o}{(\Delta l_B^2 + \Delta l_o^2)^{1/2}} \exp\left[-4\ln 2 \frac{(l_B - l_o)^2}{\Delta l_B^2 + \Delta l_o^2} \right] \right\} \tag{4.9}$$

where S_o is the peak power injected into the fiber by optical source, and R_B is the FBG peak reflectance.

4.3.2 Multiplexed FBG demodulation

Let's consider a multiplexed FBG system with identical peak reflectance R and a nominal wavelength l_B for each grating sensor. The reflection power of the nth multiplexed sensor detected by the photodetector is determined by the coupling coefficients of the previous sensors and their reflectance. So the intensity of the ith reflection, as in (3.3), can be calculated as

$$\begin{aligned} I_{mux\_n^{th}} &= \int_l G(l - l_B)(1 - G(l - l_B))^{2(n-1)} S(l - l_o) dl \\ &= \sum_{k=0}^{2(n-1)} C_{2(n-1)}^k (-1)^k R^{k+1} \int_l G_n (l - l_B)^{k+1} S(l - l_o) dl \end{aligned} \tag{4.10}$$

where $G(l - l_B)$ and $S(l - l_o)$ are the Bragg reflection and the OTDR source spectrum envelope, respectively. The above equation could be simplified by expanding the 2(n-1)th-order binomial. Assuming the source spectrum has an approximately Gaussian profile, given by

$$S(l - l_o) = S_o \exp(-4\ln 2 \frac{(l - l_o)^2}{\Delta l_o^2}), \tag{4.11}$$

after substituting Eq. (4.3) and (4.11) into Eq (4.10), the integral result of Eq.(4.10) can be given by

$$\begin{aligned} P_{mux\_n}(l_B) &= \int_l G(l - l_B)(1 - G(l - l_B))^{2(n-1)} S(l - l_o) dl \\ &= \sum_{k=0}^{2(n-1)} C_{2(n-1)}^k (-1)^k R^{k+1} S_o \int_l \exp(-4\ln 2 \frac{(l - l_o)^2}{\Delta l_o^2}) \exp(-4(k+1)\ln 2 \frac{(l - l_B)^2}{\Delta l_B^2} dl \end{aligned} \tag{4.12}$$

If we set $\Delta l_B' = \Delta l_B / \sqrt{k+1}$, after integral calculating, we can simply get a new equation. For the nth sensor, the reflected power is written as

$$P_{mux\_n} \approx S_o \frac{\sqrt{p}}{\sqrt{4\ln 2}} \sum_{k=0}^{2(n-1)} C_{2(n-1)}^{k} (-1)^k R^{k+1} \left\{ \frac{\Delta l_B / \sqrt{k+1}\Delta l_o}{(\Delta l_B^2/(k+1) + \Delta l_o^2)^{1/2}} \exp\left[-4\ln 2 \frac{(l_B - l_o)^2}{\Delta l_B^2/(k+1) + \Delta l_o^2} \right] \right\} \tag{4.13}$$

Since $\Delta l_o^2 >> \Delta l_B^2/(k+1)$ in most cases, the intensity can thus be simplified to

$$\begin{aligned} P_{mux\_n} &\approx \frac{P_o}{\Delta l_o} \sum_{k=0}^{2(n-1)} C_{2(n-1)}^{k} (-1)^k R^{k+1} \left\{ \Delta l_B / \sqrt{k+1} \exp\left[-4\ln 2 \frac{(l_B - l_o)^2}{\Delta l_o^2} \right] \right\} \\ &= \frac{P_o \Delta l_B}{\Delta l_o} R \exp\left[-4\ln 2 \frac{(l_B - l_o)^2}{\Delta l_o^2} \right] \sum_{k=0}^{2(n-1)} C_{2(n-1)}^{k} (-1)^k R^k / \sqrt{k+1} \end{aligned} \tag{4.14}$$

where P_o is the total power injected into the fiber by the OTDR optical source. From Eq (4.14) we know that the intensity at the far-end sensor, after passing many previously multiplexed FBGs, not only depends upon its performance, but also upon the multiplexed attenuation factor $A(n) = \sum_{k=0}^{2(n-1)} C_{2(n-1)}^{k} (-1)^k R^k / \sqrt{k+1}$. Figure 4.3 shows that A(n) is a function of the number of multiplexed sensors n.

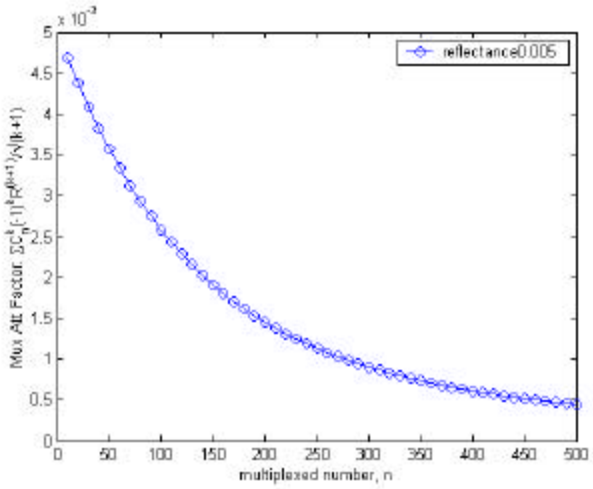

Fig. 4.3 multiplexing attenuation factor versus to sensor number

From the diagram, 500 sensors can be multiplexed in an array with approximately 10 dB of attenuation. Hence, the OTDR has sufficient dynamic range to cover the detection of

FBG arrays. If we consider the details of the source spectrum, the output would be affected by spectral ripples arising from the multiple-mode spectral peaks. The basic problem is how to achieve the proper grating wavelength in the most sensitive range and how to control the detecting noise caused by the source spectrum and the overall multiplexing system.

4.4 Simulating the overlap integral

The OTDR spectrum in Fig 4.4 was measured at the highest resolution of 0.05 nm (high II sensitivity mode). The dense source spectral lines characterized as the multi-longitude modes are focused on the major range of 1300 ~ 1310 nm, which look like a significant spectral noise (max 4.5 dB) at the top with a 0.39 nm of the adjacent spectral line gap.

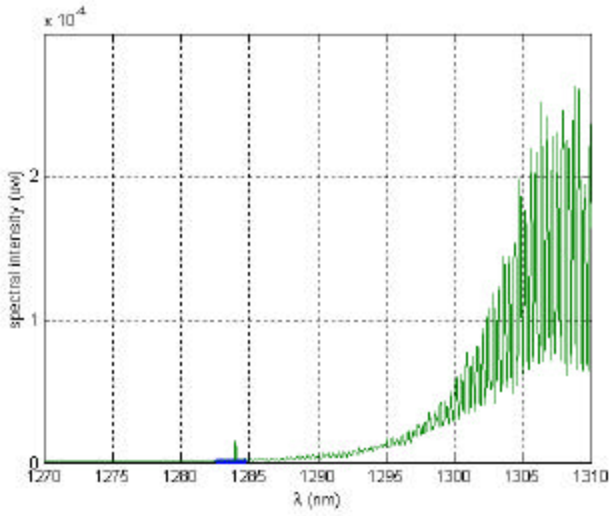

Fig 4.4. OTDR spectrum measured 0.1 nm resolutions at high II sensitivity

Obviously, if the wavelength of the Bragg grating sensor falls near 1306 nm, shifts of the Bragg grating wavelength induced by strain or temperature would cause a severe oscillation in the OTDR output. But the total signal returned has only a variation of 0.795 dB for a 2 nm wavelength shift. A simulation result is shown in Fig 4.4.1. In this case, the

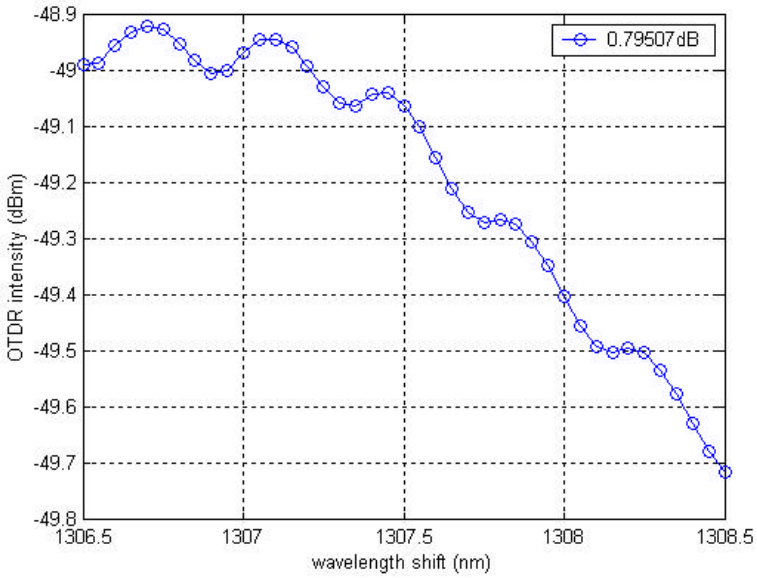

Fig 4.4.1 Simulated reflected signal output as FBG wavelength shifts near 1306nm

Bragg gratings cannot be used as a sensor for two reasons: low dynamic range and rapid fluctuation even using sufficient broad bandwidth of grating. Figure 4.4.2 presents a group of the OTDR source spectra for determining a desirable FBG bandwidth. The figure shows that for high-resolution (0.1 nm) OSA measurement the spectrum exhibits an obvious periodic variation with a period of 0.39 nm. Therefore, if the grating device has a line-width of 0.1 nm, obviously, the output will exhibit a similar fluctuation change pattern. But for a lower resolution (2 nm) measurement, the spectrum shows a much smoother curve with a slope rate that could be used as an intensity-based grating (2 nm bandwidth) measurement. After careful investigation of the OTDR spectra, it is believed that the useful spectra region is from 1311 nm to 1316 nm under the lower resolution condition. Hence, a simple way to eliminate the oscillations and to achieve a linear output is to broaden the fiber Bragg grating bandwidth to larger than 1nm and write the grating

wavelength in the approximately the linear region of the source spectrum so that we could smooth the fluctuation caused by source ripples.

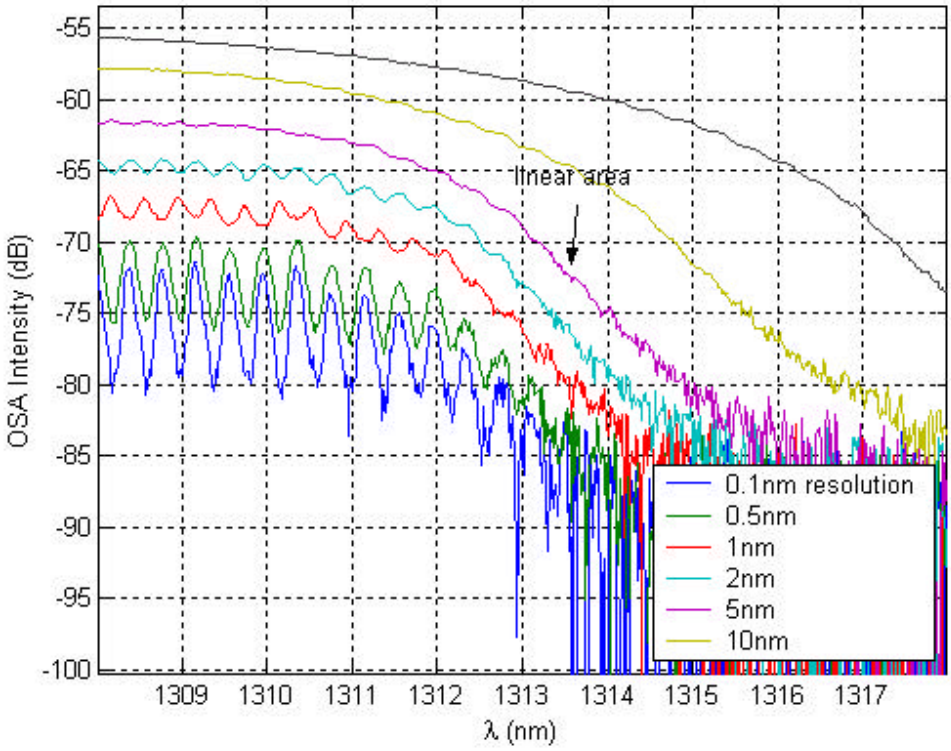

Fig4.4.2 OTDR source spectrum data for different resolution detection

Figure 4.5 shows the simulation results of FBG output with several FBG bandwidths. As its peak wavelength shifts in the overall spectrum, the OTDR linear output in the shadowing range on both sides can be gradually obtained with an increase in FBG bandwidths. Thus in this situation, the OTDR intensity-based output can be used to measure physical parameters that affect the Bragg wavelength. Obviously, for a grating bandwidth of 0.3 nm (a very normal FBG), the OTDR output is nonlinear due to the

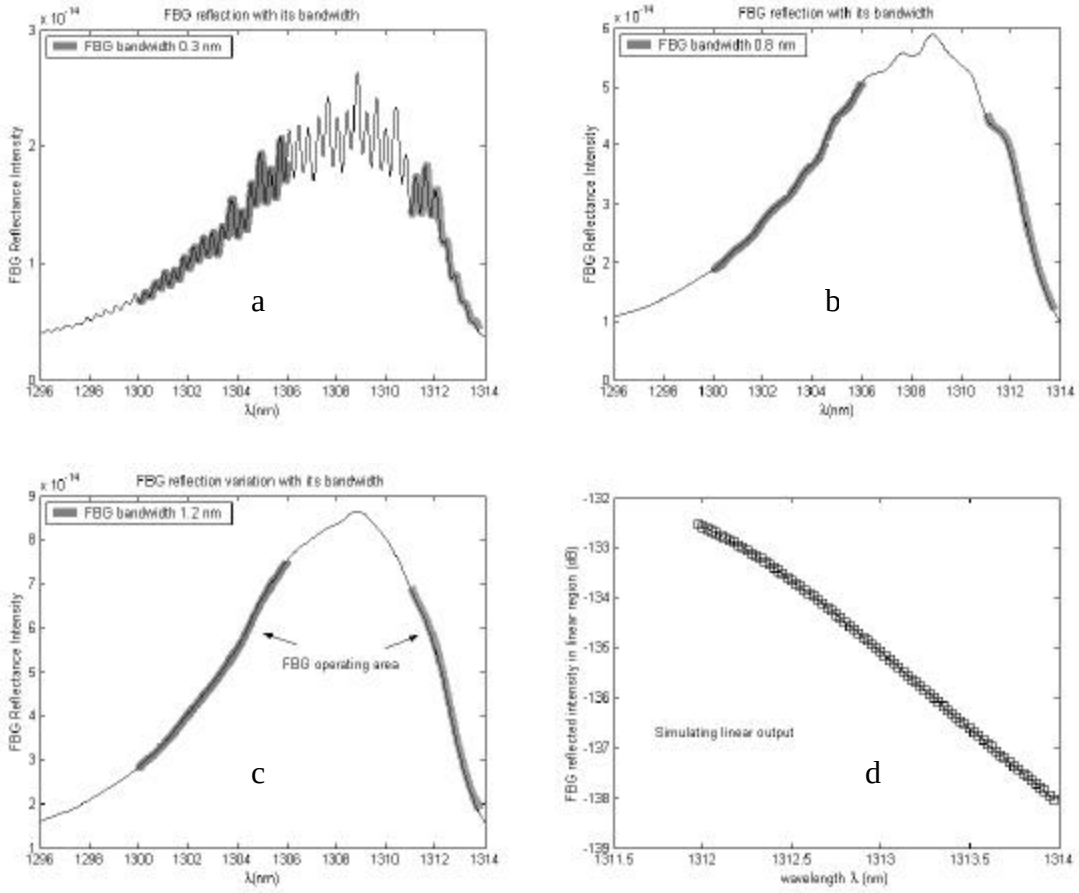

Fig 4.5 Simulation change of grating reflected intensity with the wavelength-shift, and FBG bandwidth a) 0.3 nm; b) 0.8 nm; c) 1.2 nm; d) linear output as 1.2 nm bandwidth

rapid oscillations of the light source's envelope. In fact, the narrow-bandwidth grating seems like a narrow movable filter that could clearly respond to any variation associated with the source spectrum when we take overlapping integral calculation. Therefore, for a grating sensor using the OTDR detection, it is essential to have a broader grating bandwidth to average the oscillated output.

In general, using a phase mask method, grating bandwidths to 0.2nm can be easily reached. But if employing a tilt angle method between the phase mask facet and the

photosensitive fiber, or bringing in small controllable vibrations during inscribing grating, the bandwidth of the Bragg grating could be effectively extended to 0.8 ~ 1.2 nm, which is exactly what is required for the pc-OTDR based grating sensors.

4.5. Duel-wavelength Bragg grating-based reference for intensity compensation

4.5.1 Referencing FBG selections

In general, the intensity signal from a grating sensor is also affected by the OTDR incident power variations and fiber bending, which are often misled as a measurand change. A real-time self-calibration to compensate for those unwanted changes is imperative before intensity-based multiplexed grating sensor can be

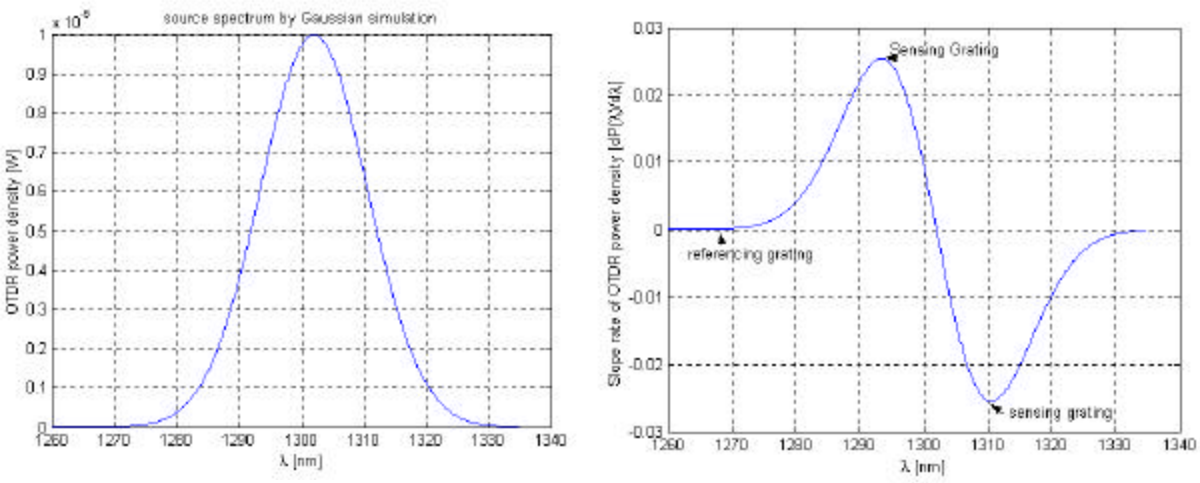

Fig.4.6 Comparison of Gaussian spectrum slope rate, a) source Gaussian spectrum; b) detecting slope rate change

applied in practice. For the self-referencing purpose, the multiplexed sensor array actually consists of two types of gratings with different resonant wavelengths. One Bragg wavelength operates at the most sensitive position of the source spectrum with a high

slope rate, whereas the other reference wavelength is placed on a flat spectral area that induces no power change only acting as a power reflector. Figure 4.6 describes a guideline for choosing the reference and sensing grating wavelengths. The left graph plots the OTDR source spectrum with an approximately Gaussian profile, and the diagram on the right shows the relationship between the slope rates (intensity variation with λ) with wavelength. When a sensor wavelength is less than 1270 nm, its slope rate is close to zero, which is appropriate for a referencing grating, and 1293 nm and 1310 nm are the two points between which can be obtained the highest slope rates. This range is good for a sensing grating wavelength. Note both the reference and sensing gratings are proportional to the incident power.

Since the reference-grating signal is reflected by the FBG near the sensing grating, though it still may sense a wavelength shift caused by the measurand, the reflection intensity will be constant, since the reference-grating convolution with the source spectrum is unchanged. Consequently, the sensing grating reflected light travels along the same optical path in the fiber as the reference grating has; it thus carries the same information about undesired attenuation and power variation. The ratio of both reflection signals is, therefore, immune to unwanted variations, which results in a measurement improvement. The reference grating has almost no loss and small intensity changes (0.11 dB at 1500 μstrain in experiment) even with applied strain or temperature due to its wavelength being far from the sensitive spectra area. Let us see the result of taking an intensity ratio. The sensing grating intensity at the detector is proportional to the overlap integral of $S(\lambda-\lambda_o)$ and $G(\lambda-\lambda_B)$ representing the spectral characteristics of the OTDR and the fiber Bragg grating, as shown in Eq. (4.3) and Eq. (4.7) respectively. According to

According to Eq.(4.9), the intensity of the signal at detector, for referencing grating 1, can thus be written as

$$I_{out1}(l_{B1}) = \int_0^\infty S(l-l_o)G_1(l-l_{B1})\,dl = S_o \frac{R_{B1}\sqrt{p}}{\sqrt{4\ln 2}}\left\{\frac{\Delta l_{B1}\Delta l_o}{(\Delta l_{B1}^2+\Delta l_o^2)^{1/2}}\exp\left[-4\ln 2\frac{(l_{B1}-l_o)^2}{\Delta l_{B1}^2+\Delta l_o^2}\right]\right\} \tag{4.15.1}$$

Similarly, the second sensor has the same form of output at the detector written as

$$I_{out2}(l_{B1}) = \int_0^\infty S(l-l_o)G_2(l-l_{B2})\,dl = S_o \frac{R_{B2}\sqrt{p}}{\sqrt{4\ln 2}}\left\{\frac{\Delta l_{B2}\Delta l_o}{(\Delta l_{B2}^2+\Delta l_o^2)^{1/2}}\exp\left[-4\ln 2\frac{(l_{B2}-l_o)^2}{\Delta l_{B2}^2+\Delta l_o^2}\right]\right\}, \tag{4.15.2}$$

ignoring the overlap of the sensing and reference spectra. In general, the bandwidth of the OTDR source is much larger than the bandwidth of the Bragg grating $\Delta l_o >> \Delta l_B$ and $\Delta l_{B2} \approx \Delta l_{B1} = \Delta l_B$. Since l_{B1} is far from the central wavelength of the OTDR, the l_{B1} shift will cause little variation in the reflected signal. This implies that the first grating equation (4.15.1) signal can be a constant and can serve as a reference. The ratio of Equations (4.15.2) to (4.15.1) is given as

$$I_{Ratio} \approx \frac{R_{B2}}{R_{B1}k}\exp\left(-4\ln 2\left(\frac{(l_{B2}-l_{B1})(l_{B2}+l_{B1}-2l_o)}{\Delta l_B^2+\Delta l_o^2}\right)\right) \tag{4.16.1}$$

where k is a constant, and R_{B1} and R_{B2} are the reflectance. As seen in (4.16.1), S_o, the source influence, has been eliminated; $l_{B2}-l_{B1}$ is unchanged in multiplexing and the ratio is only dependent on the reflectance ratio of the Bragg gratings and the wavelength shift

$$\Delta l = l_{B2} + l_{B1} - 2l_o \text{. Also note } I_{Ratio} = \frac{\ln(1-P_s/120)}{\ln(1-P_r/120)} \qquad (4.16.2)$$

where P_s and P_r are the sum probabilities of sensor and reference grating OTDR photon counting in 120 repeated measurements during the light pulse repetition, according to Equation (4.2.1).

In fact, there are also other ways to fabricate in-line fiber reflectors as a signal references In addition to grating as a reference, one can make a reflector by using the excimer laser to directly photo-imprint a photosensitive fiber to form a controllable F-B reflection, which requires a F-B cavity length in excess of the optical coherence length. Another approach is to splice a core-etched fiber to regular fiber to produce a power reflection. The etched fiber is dipped into mixture of NH_4 and HF acid for couple's minutes and is then spliced to single-mode fiber. In general, this method induces a slightly large uncontrollable excess loss of 0.5 dB ~1 dB.

4.5.2 The referencing reflection tests:

Figure 4.7.1 shows the results of a strain test for a reference grating with a wavelength of 1229 nm that should have low strain sensitivity. Various amounts of dead weights were applied to the FBG to create different strains. The maximum intensity variation is 0.11 dB over 1500 μ strain change. This provides a good method for fabricating reference sensors to decrease light power oscillation. Core-etched fiber reflectors also can be used as an intensity reference because they have low temperature sensitivity as shown in Fig. 4.7.2. The temperature was applied to 450 ℃ but the photon-counting output is only change by the standard deviation 0.323.

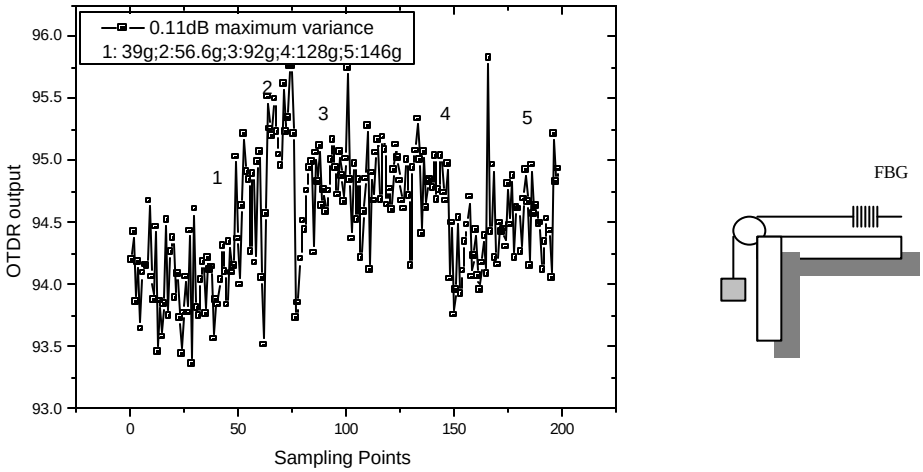

Fig 4.7.1 Reference sensor strain test for the evaluation of strain sensitivity

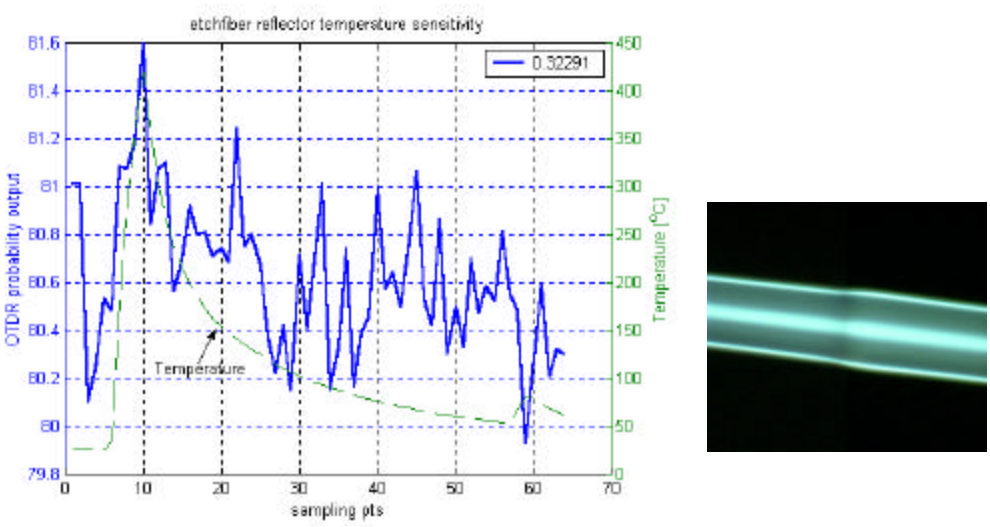

Fig.4.7.2 Temperature sensitivity for a core-etched fiber reflector with 0.7 dB excess loss

4.5.3 Dual Bragg grating spectrum

The dual-grating configuration offers several advantages due to their largely different resonant wavelengths. One is that there is no interaction between the two gratings, since the first grating spectral reflection will have nothing to do with the second grating in

power transmission. Moreover, they have an advantage for the sensor multiplexing because of their different reflected signal groups in wavelength. Both of the gratings have a similar sensitivity to sense fiber bending and source fluctuation at the same time in multiplexing that is a basic referencing requirement. After taking a ratio, therefore, they will eliminate the environments disturbance except for the wavelength shift created by the strain or temperature. Dual-wavelength Bragg gratings are fabricated in the same way as a general FBG system. Two kinds of phase mask elements with different periods (1284 nm and 1312 nm) have to be used to inscribe the Bragg grating pairs, and the two reflected signals can be distinguished as long as the separation of the two gratings spacing is enough larger than the OTDR spatial resolution. Figure 4.8 shows the Bragg grating spectrum overlap with the OTDR spectrum. It is evident that the dual wavelength WDM OTDR based multiplexing system efficiently reduces the light intensity noise.

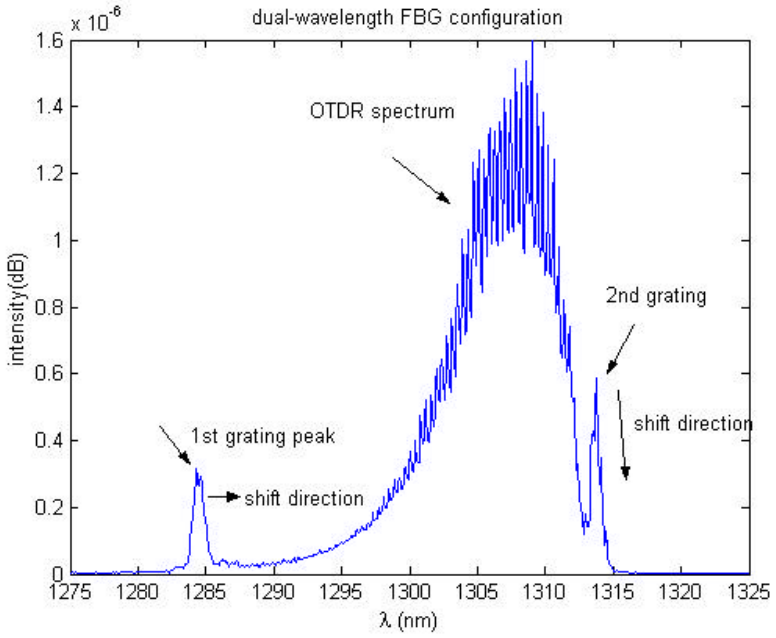

Fig 4.8 Spectral profile for a Bragg grating pair with different wavelengths added on the OTDR source spectrum

There is no optical crosstalk presented by these two types of gratings due to the absence of spectral overlap. Only a small amount of power attenuation is introduced to the multiplexed FBG due to additional insertion losses. We are able to multiplex a large number of Bragg gratings without obviously decreasing the multiplexed number. Figure 4.9 shows an experimental example by using dual Bragg gratings, and demonstrates the perturbation can be effectively eliminated by the self-referencing operation.

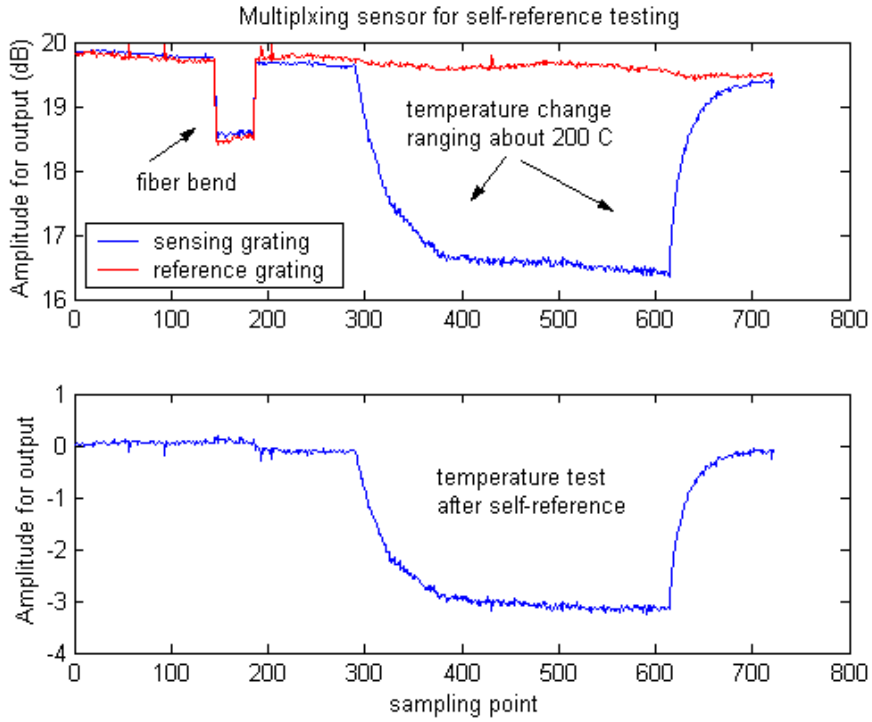

Fig. 4.9 Experimental results based on the dual gratings based self-referencing scheme

Both of the gratings, one sensing grating and the other a reference grating, were placed into a tube furnace at 200 °C. The fiber was bent before the grating pair undergoing the temperature test. As shown in Figure 4.9, after taking a ratio of the reference sensor output and the sensing sensor output, the fiber bending effect can be completely eliminated by the self-reference operation.

Chapter 5 Multiplexing Sensors Calibration and Performance Evaluation

The fiber Bragg grating can be directly measured by a regular optical spectrum analyzer (OSA), since the Bragg peak wavelength ?$_B$ shift has a simple linear relationship with temperature or strain variations, characterized as $\Delta l_B = a \times \Delta T + e \times \Delta L$. Hence, the wavelength shift is always a linear function of temperature or strain, regardless of the peak Bragg grating wavelength location. In the dissertation research, multiplexed fiber Bragg gratings are needed to evaluate their performance in the pc-OTDR based sensor system. The system in nature is the intensity-based detection so it requires knowing the characteristics of calibration curves, the grating peak wavelengths and relation with the source spectra. Moreover, the multiplexed system consists of a large number of low-reflectance Bragg gratings in a serial array, which produces a more complicated multiplexing spectrum. Therefore, each FBG sensor with different Bragg wavelength will produce various results in intensity-based measurements. The work described in this

chapter includes the temperature calibration, strain measurement and test for a large number of multiplexed gratings.

5.1 FBG wavelength shift measurement and fundamental properties

5.1.1 Basic measurement

A fundamental system for optical spectrum testing of a Bragg grating sensor is depicted in Fig. 5.1.

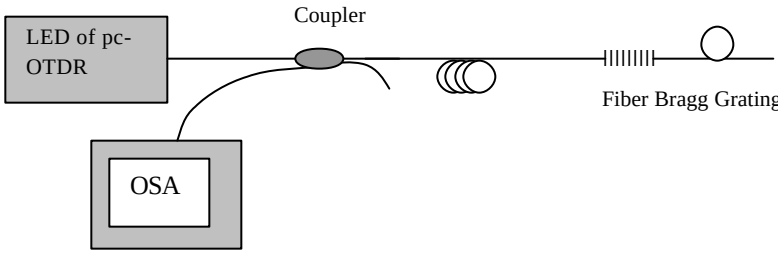

Fig. 5.1 Schematic for a single FBG measurement

The strain or temperature applied on a grating will cause a shift of the Bragg wavelength. A wavelength detector can directly measure the wavelength shift by detecting the reflected peak movement. The magnitude of the wavelength shift is a proportional function of the measured strain or temperature. In order to obtain certain grating wavelength shift regions, a broadband optical source is needed, and the system can function in a transmission or reflection mode. Measurement in the reflection way can offer a more sensitive and high signal-to-noise ratio detection. However, for a very low reflectance FBG (lower than 0.1 %), it is usually hard to observe the FBG spectral profile to determine wavelength shift. Consequently, signals returned from a weak Bragg grating reflection can be observed by the OTDR or optical fiber monitor, which is eventually intensity based detection tool for a millionth reflection.

5.1.2 Basic theory of fiber Bragg grating properties

Let's come back the topic of the Bragg grating wavelength equation. The basic theory of Bragg grating wavelength dependence on both strain and temperature has been well published in the past [50]. Strain directly elongates of the fiber, and thus, changes the grating period spacing. It also causes a refractive index change associated with a Poison's effect (photo-elasticity) due to dimensional variations in the radial direction. Temperature effects may produce thermal expansions that elongate the grating pitch, and also change the fiber refractive index. The Bragg center wavelength, λ_B is given by the Bragg phase-matching condition:

$$l_B = 2\, n_{eff}\, \Lambda, \tag{5.1}$$

where Λ is the fringe spacing of the grating and n_{eff} is the effective refractive index of the LP_{01} mode. By a Taylor expansion on the characteristic Bragg relation, Equation (5.1) can be rewritten as a fractional change in Bragg wavelength with temperature

$$\frac{\Delta l_B(T)}{l_B} = (a + x)\Delta T, \tag{5.2}$$

where a is the thermal expansion coefficient ($\sim 5\times 10^{-7}$ /K) and ? is the thermo-optic ($\sim 7\times 10^{-6}$ /K) coefficient ($x = \frac{\partial n}{n\partial T}$) of the fiber silica material. Since the thermo-optics effect is about one order of magnitude greater than that of the thermal expansion effect, this effect is the dominant cause for changes in the Bragg grating wavelength with temperature changes. For the silica fiber, the normalized thermal responsivity is

$$\frac{\Delta l_B}{l_B \Delta T} = 6.67\times 10^{-6}/^{o}C.$$

At a wavelength of 1300 nm, a temperature change of 1°C approximately results in a Bragg wavelength shift $\Delta l_B(T)$ of 0.01 nm. Similarly, the effect of strain on the reflected wavelength can also be evaluated. The analysis will be complicated by the fact that strain is a three-dimensional tensor field. From this analysis it can be shown that for an applied strain $e = \Delta\Lambda / \Lambda$, the fractional change in Bragg wavelength with strain can be written as:

$$\frac{\Delta l_B(e)}{l_B} = (1 - p_e)\Delta e \tag{5.3}$$

where $p_e = \frac{n^2}{2}(p_{11} - n(p_{11} + p_{12}))$, p_e is the effective photo-elastic coefficient, p_{11}(~0.113) and p_{12} are photoelectric components of the strain-optic tensor. For silica fiber operating at 1550 nm, a typical value for the change in Bragg wavelength with strain is 1.15 pm /μ e. With p_e ~0.24 (silica fiber), or p_e ~0.22 (germanosilicate fiber), the fractional wavelength change is only about 75% of the corresponding strain change. Since temperature and strain effects can be considered as mutually exclusive effects, when simultaneously acting on a fiber grating sensor, their effects are additive. Therefore, the total change in wavelength l_B for reflected Bragg grating signal associated with both strain and temperature perturbations is given by

$$\frac{\Delta l_B(T,e)}{l_B} = (a + x)\Delta T + (1 - p_e)\Delta e \ . \tag{5.4}$$

At room temperature, the experimental relative change in the Bragg center wavelength is usually then

$$\frac{\Delta l_g}{l_g} = 0.78 e_{axis} + 7.5 \times 10^{-6} \Delta T(K) . \tag{5.5}$$

At a wavelength of 1310 nm, the temperature-to-wavelength coefficient is approximately 0.1 K/pm, and the strain-to-wavelength coefficient is approximately 1 *me* /pm (1 *me* strain = 10^{-6}). Therefore a change in temperature of 0.1 K induces the same wavelength shift as that induced by 1 *me* strain.

5.2 Fiber grating sensor spectra and reflectance evaluation using the pc-OTDR

In the pc-OTDR photodetection with a zero deadzone for Fresnel reflection, we expected the gratings to maintain their high sensitivity to temperature variations using intensity detection. Based on the source spectrum characteristic, the best wavelength region is 1311 nm -1315 nm for achieving a 10-dB measurement range. However, at the top or the bottom on both sides of the Gaussian mode source spectrum, the measurement could suffer from the sensitivity reduction, a large laser multimode effect that appears as an intensity oscillation. Figure 5.2 shows the spectra of a Bragg grating with low reflectance less than 0.5 dB intensity gain. Figure 5.2a indicates the photosensitive single-mode fiber spectrum before photo-printing a Bragg grating, in which ripples in the spectrum are caused by the multimode effect of incident LED source, and Figure 5.2b exhibits the growth of a very weak FBG that peaks at 1312.6 nm. Though the ripple of the monitoring source spectrum obscures the FBG peak, we are still able to observe the growth of the peak to judge if it is a Bragg grating. For weak reflection, there are two methods to find the FBG low-reflectance that we will describe in the following.

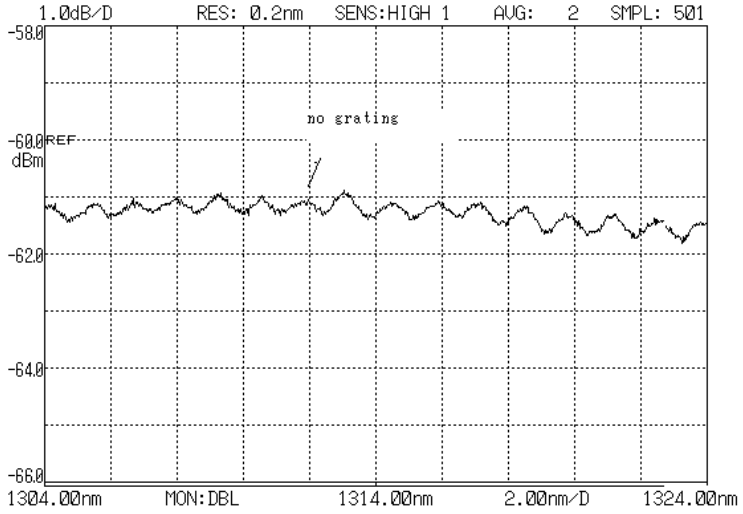

Fig 5.2 a

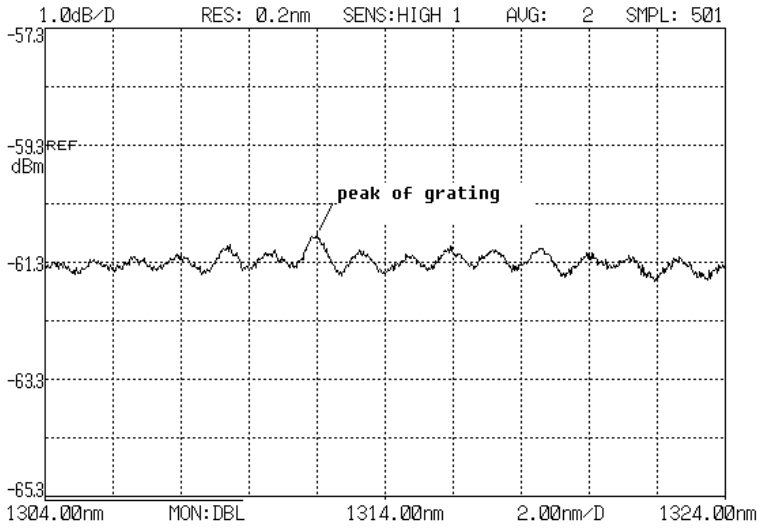

Fig. 5.2 b

Fig. 5.2 One Bragg grating peak with low reflectance, a) before inscribing grating b) after inscribing grating

a) ***Evaluation of Grating Reflectance by OSA***

Because of the spectral ripple feature from the LED spectrum, the reflectance of a weak grating will be difficult to assess precisely. But an empirical formula can be developed as

follows. The grating reflectance can be evaluated at less than 0.5 % based on the increase in grating reflective peak ΔG (dB) in the spectra calculated in appendix.

$$10^{\Delta G/10} = \frac{(1+(1-R)^2+\frac{R}{0.04})}{2}, \tag{5.6}$$

where *DG* (dB) is the Bragg reflected power gain, and *R* is a FBG reflectance value.

b) ***Evaluation of Peak Reflectance using the combination of OTDR and OSA***:

In the previous section, we described a fundamental theoretical analysis for very low reflectance case. Here we describe another practical measurement approach to evaluate grating reflectance less than 0.05 %, which is difficulty to eventually observe its reflected spectrum from an OSA so the reflectance cannot be calculated based on Equation (5.6). However, the FBG reflectance can still be properly evaluated by using a combination of the photon-counting OTDR reflected signal (*R* as low as 10^{-6}) and the OSA as a power meter. Both can be connected to the FBGs shared by a coupler. The OTDR output represented the photon counting *Poisson* probability P_r as described in the previous chapter, corresponds to the reflected photon energy from features. The OSA can measure the reflection power of an ideal fiber endface, so one can identify a monotony relationship between the OTDR vertical level P_r and the reflection power I_r as shown in Fig.5.3. After the OTDR calibration we can obtain a relationship I_r (dB) = -69.62 – 0.958**S (dB)*+*R (dB)*+ a, (chapter 3) where *S* (dB) is the OTDR sensitivity parameter given, -69.62 –0.958**S (dB)*+*R (dB)*+ a is the incident power, a is the excess loss and *R* is the unknown reflectance. Based on the OTDR detection principle, the reflection intensity at the photodetector is

$$I_r = -\frac{hn}{ht}\ln(1-Pr/120)\,, \tag{5.8.1}$$

where h? is a photon energy, ? is the OTDR quantum efficiency and t is the duration of the OTDR pulsed light. The reflectance can be written as a function of S and measured Pr

$$R_{(dB)} = 69.62 + 0.958S + 10\log_{10}(-\frac{hn}{ht}\ln(1-Pr/120)) - a \tag{5.8.2}$$

A simulated result for obtaining R is shown in Fig. 5.3 (a), assuming l =1.305μm; h is 10%, a = 1dB system insertion loss and t =1 μs.

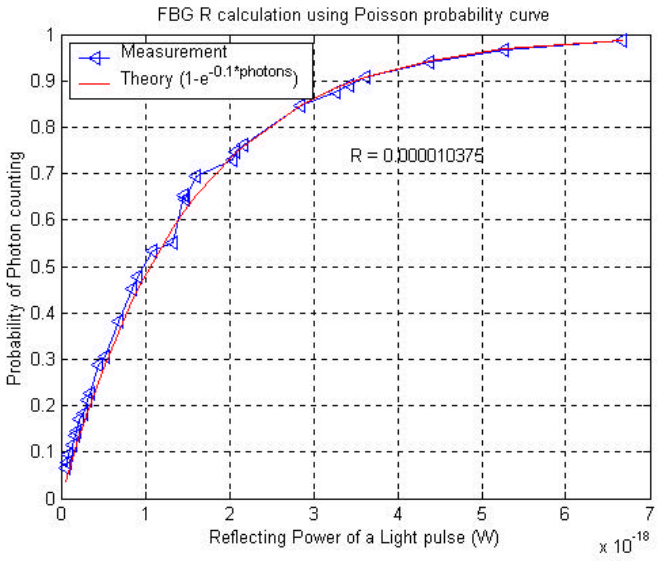

Fig 5.3 (a) FBG reflectance calculation based on the photon counting theoretical analysis

Therefore, we obtained a FBG reflectance of 0.001037% with respect to the total incident power. A test system was set up as shown in Fig. 5.3 (b). The OTDR is used as both the light source and detector. The OTDR unit is placed at one input end of the coupler, and the OSA (ANDO 6315A) is placed at the other input end of the coupler. The OTDR SAPD detector has the ability to interrogate all gratings along a length of fiber.

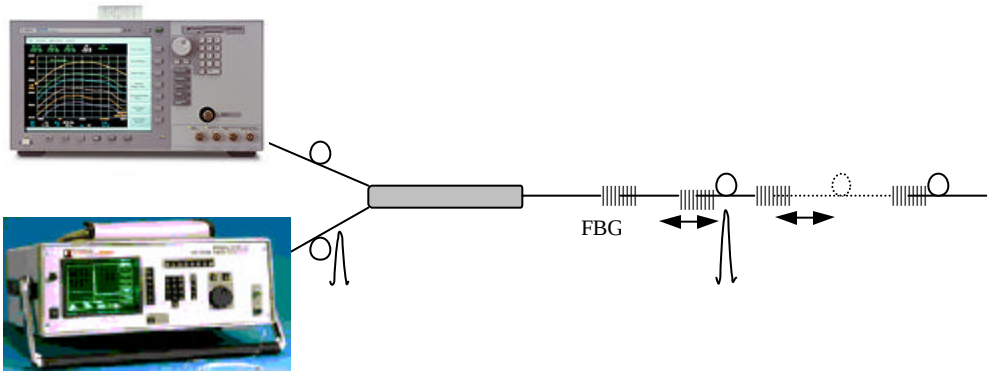

Fig 5.3 (b) a Fresnel pc-OTDR test system for detecting multiplexed Bragg grating array with OSA spectral monitoring

5.3 Single fiber Bragg Grating sensor OTDR calibration

Before the FBG sensors are multiplexed, it is first necessary to take temperature or strain calibrations. The sensor calibration is normally conducted by applying known temperatures or strains within the FBG operating range.

A FBG sensor at a wavelength of 1312.44 nm with a 0.032 % reflectance, made from a piece of photosensitive optical fiber, was calibrated by the pc-OTDR system. The Bragg grating was placed into a tube furnace monitored by a thermocouple and a transformer was used for manually controlling temperature variations. A PC computer connected to the pc-OTDR through a GBIP interface was used to save output data from the FBG reflected signal.

A temperature curve is shown in Fig 5.4.1 as the furnace cooled down. The FBG signal was operated at its maximum value by adjusting the OTDR sensitivity. With an increase in temperature the signal strength is reduced at a given sensitivity. Note that the vertical

scale indicates the Poisson probability sum of 120-repetition reflection measurements within the OTDR pulse repetition interval.

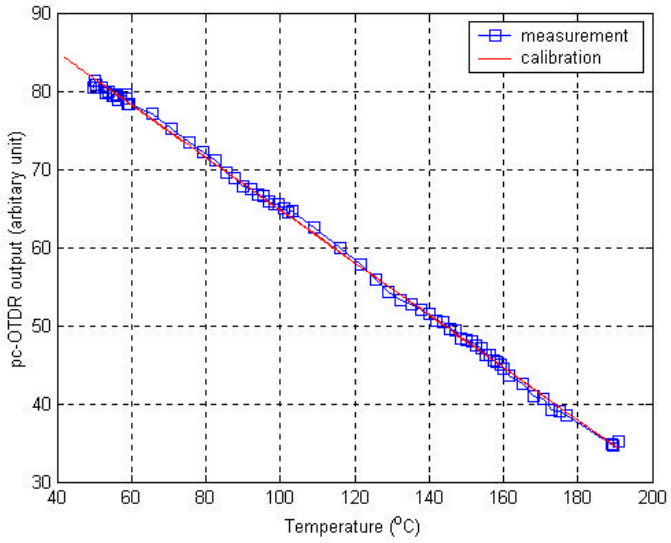

Fig 5.4.1 Fiber Bragg grating temperature curve measured by the pc-OTDR

The point-to-point relationship between the applied temperature and the FBG output was then used to determine the calibration equation through polynomial fitting. Usually, the calibration curve was achieved by taking the average of several consecutive calibrations to ensure the accuracy of the calibration. The FBG bandwidth and central wavelength determine the calibration curve shape and smoothness. Figure 5.4.2 shows four different calibration curves. As described in Chapter 4, a fluctuation of the curve in Fig 5.4.2 (a) is caused by the smaller FBG bandwidth not being able to smooth the OTDR spectral ripples; the temperature curve in Fig 5.4.2 (b) is of Gaussian shape due to the FBG central wavelength being placed on the nonlinear region of the source spectrum. Hence when the FBG wavelength

shifts a little, the output will exhibit a Gaussian-like curve. Figure 5.4.2 (d) is much better for a proper FBG sensor measurement. Therefore, the FBG spectral characteristic is a key factor in the fabrication of a good sensor.

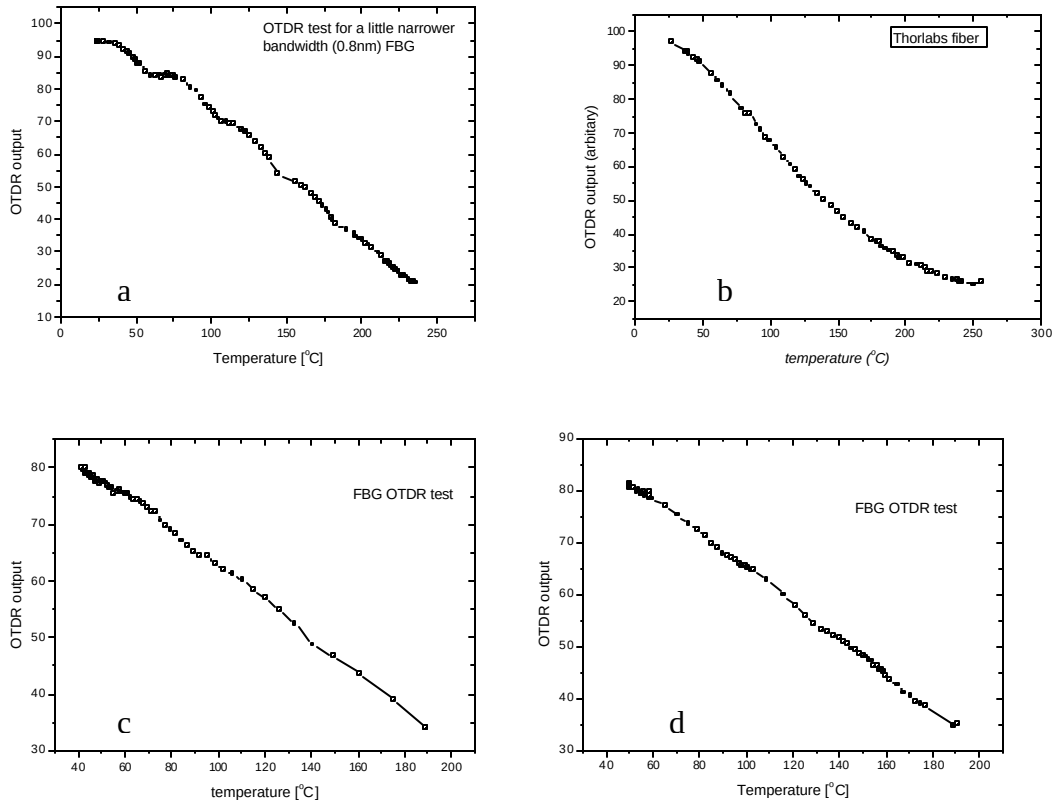

Fig. 5.4.2 various temperature curves in multiplexed sensors

Experimental results showed that a maximum dynamic range of about 6 dB with a resolution of 0.33% in a 220 °C test range could be obtained. Fig 5.4.2 shows a linear calibration curve of another Bragg grating fabricated using a H_2 loaded fiber.

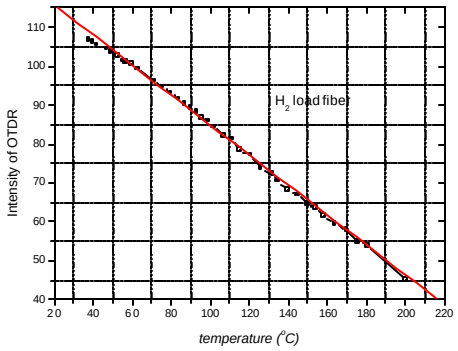

Fig5.4.3 Temperature calibration curve H_2 loading Bragg grating at 1311.98 nm

A Bragg wavelength of 1312.11 nm seems to be better in term of linear FBG output characteristics and it implies that that the value of wavelength falls into the linear spectral region of the source.

5.4 PC-OTDR system stability test

The system stability can be evaluated by measuring the FBG sensor reflection variation at room temperature. The fiber endface reflection with a low reflectance is not appropriate for the stability measurement for two reasons. One is that it belongs to the overall spectrum reflection, and does not take into account system performance at the FBG wavelength; the other reason is that this reflection is usually affected by the interference summation of a section of fiber inducing random change that does not explain the performance of the OTDR system. The FBG sensor was placed in the room temperature environment without any stress on it over night. The data acquisition system was programmed to sample the sensor output each minute. The test result is shown in Fig 5.5 (a) and (b); the standard deviation based on the scale-factor of thermal coefficient and calibrated strain was thus 0.142 % and 0.5 % of full dynamic range corresponding to 0.4℃ and 3.2 μstrain of standard deviation,

respectively. The test result shows that the system has a low one-directional drift in a long-term test that is primarily caused by the OTDR LED environmental temperature effects.

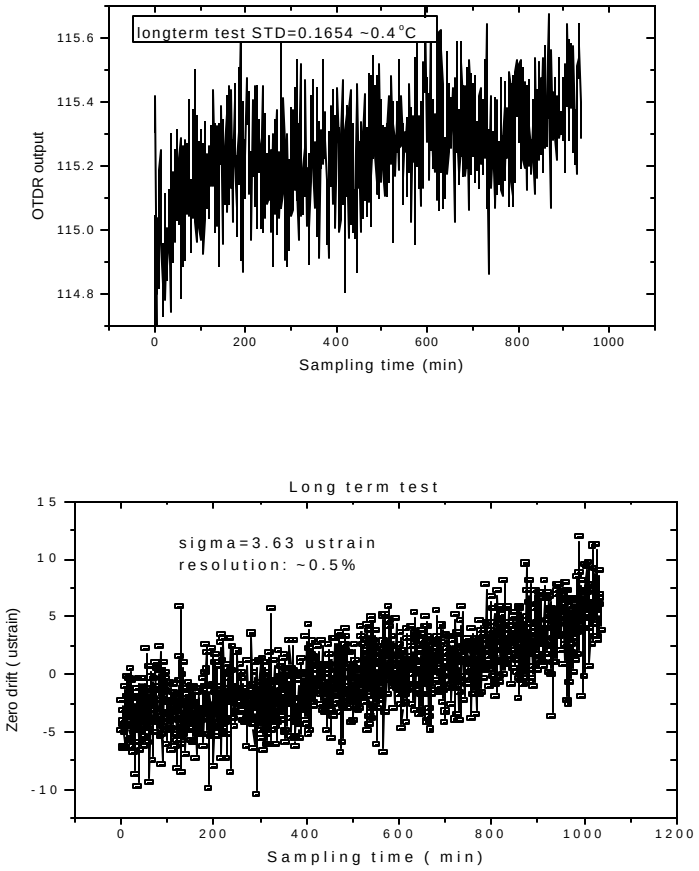

Fig 5.5 a, b. long-term measurement of grating sensor system

5.5. OTDR strain test

The sensor calibration for the strain is also quite important for evaluating the sensor performance. The basic setup shown in Fig 5.6 can help to provide quantitative measurement of fiber Bragg grating tensile properties. Weight as a tension was applied to a sensor in increments of 1/8 of the total weight for the estimating linear range of the Bragg sensor. The OTDR system sampled data into the computer and

stored it in a data file. To ensure the accuracy of the calibration process, the system was held

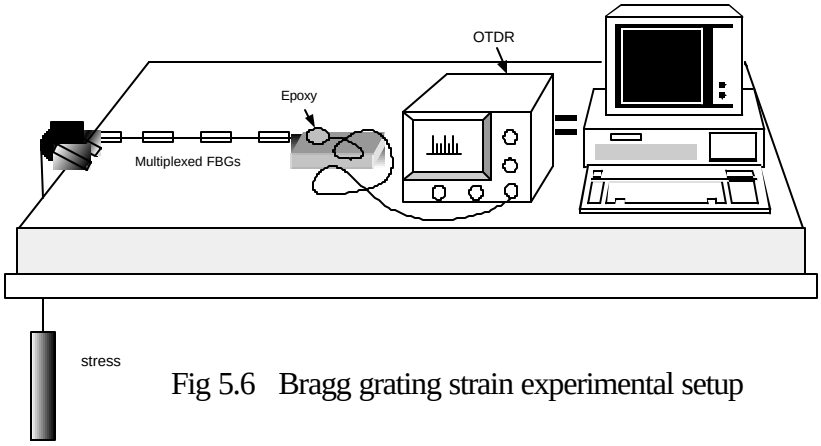

Fig 5.6 Bragg grating strain experimental setup

with the strain for about two minutes to obtain enough data before moving to the next step. By taking the average within the stress ho lding period, the system noise can be drastically reduced.

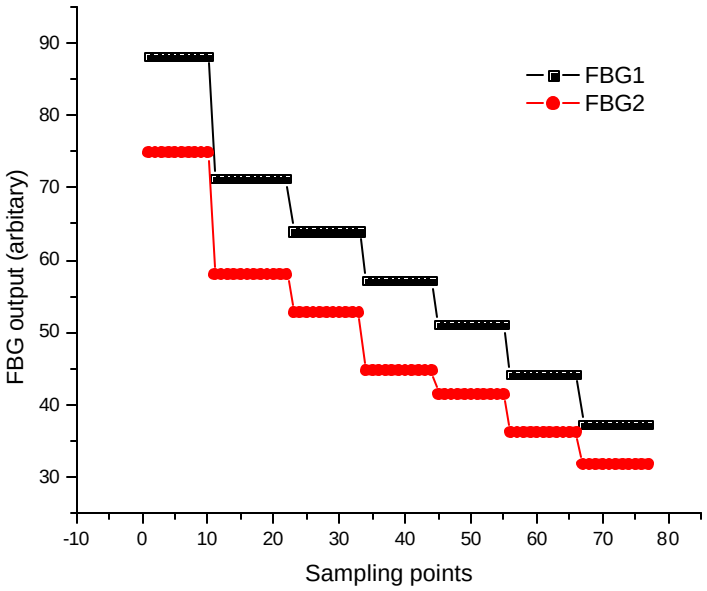

Fig 5.7 FBG strain calibration examples applied a step tensile increment

Figure 5.7 is an example of the pc-OTDR output data during tensile tests.

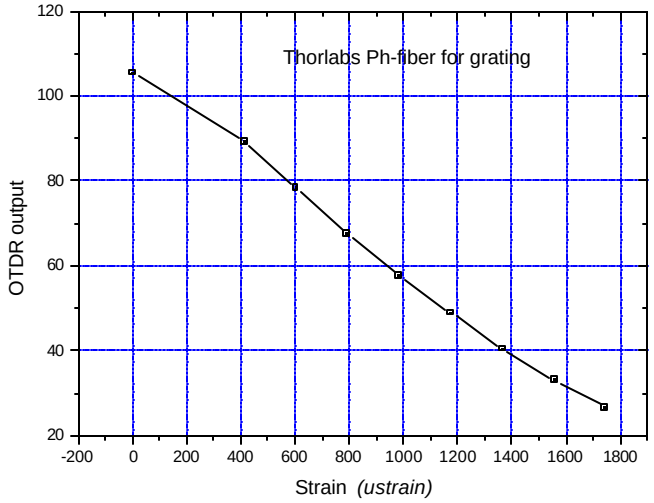

Fig 5.8 typical results of Fiber Bragg grating strain tested by pc-OTDR

Figure 5.8 shows a calibration curve of the pc-OTDR output versus the applied strain. A grating with wavelength 1311.44 nm has total 6.3 dB variations for a large dynamic range up to 1750 micro-strain.

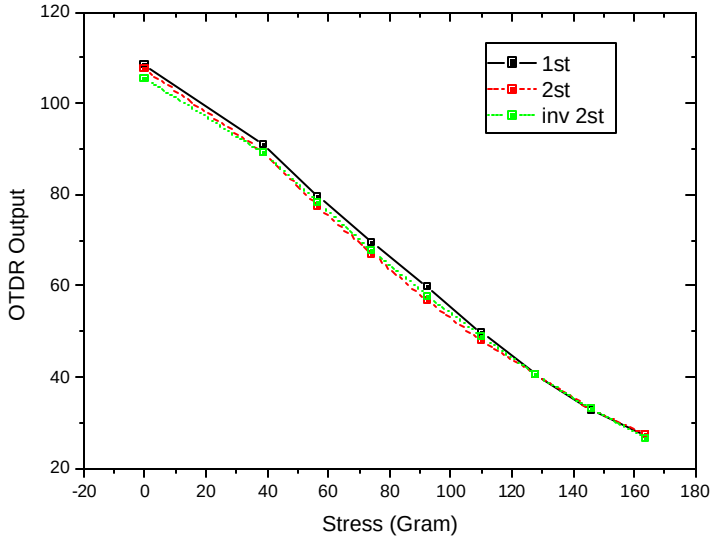

Fig 5.9 Bragg grating repeatability test and hysteresis effect measurement

It indicates better linear features due to a Bragg wavelength located in the most sensitive region in the source spectrum. Figure 5.9 shows the Bragg grating sensor repeatability and hysteresis effect with strain measurement. The normalized repeatability of the sensor system with respect to its dynamic range is about 1.07%.

The strain calibration curve is slightly dependent on the distance of adjacent FBGs close to 10 cm less than OTDR spatial resolution. Under these circumstances, the pigtail trace of one Fresnel reflection curve would overlap the adjacent one, resulting in signal confusions. The left diagram in Fig 10 represents the effect as two sensors become close, and right diagram is a calibration curve with a small shift.

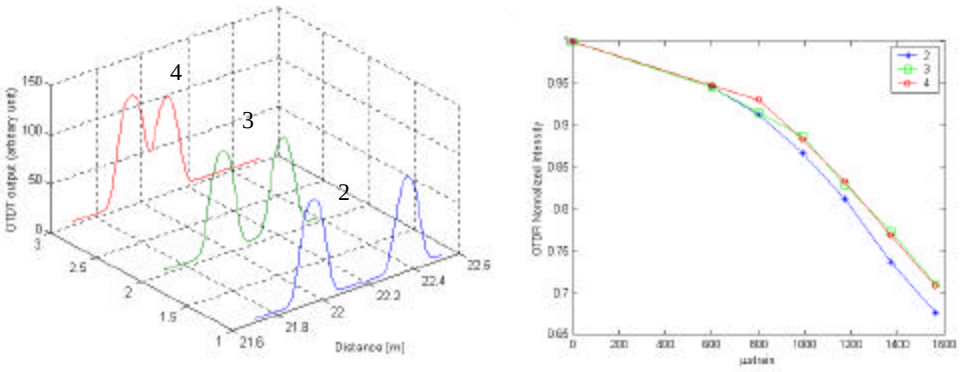

Fig.5.10 Calibration curve affected by adjacent FBGs close to OTDR spatial resolution

5.6. Analysis of pc-OTDR based multiplexed Bragg gratings

5.6.1. Experimental multiplexing results

A typical OTDR signal from a FBG is shown in Fig. 5.10. The pulse shape data can be saved into the computer, which can trace the pulse peak value change so that the reflected intensity variation can be tracked. The pc-OTDR system is a high sensitivity optoelectronic product that can resolve grating signals with a minimum spacing of

approximately 10 cm. Therefore, in terms of high spatial resolution with a 1 km length of a silica fiber, we could theoretically multiplex about 5000 Bragg grating

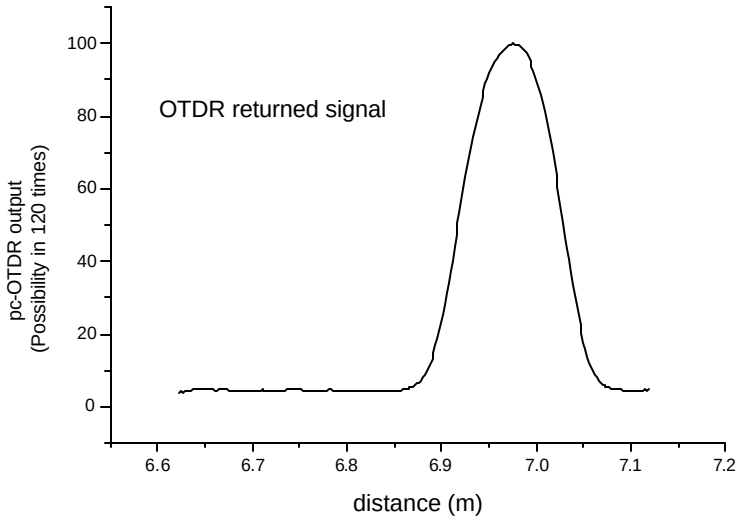

Fig 5.11 Bragg grating reflected signal in the OTDR detection

sensors if we ignore the reflecting attenuation, ghost reflections and excess loss for each FBG sensor. But in practical sensor system, two factors limit the total multiplexing number to less than a thousand: the source pulse-repetition-rate (described in Chapter 3) and the FBG-related loss. The FBG loss includes fiber spliced loss in the range of 0.02 dB~0.1 dB with low reflectance of about 0.01 %~0.5 %. This will greatly reduce the multiplexed number. Figure 5.12 shows twenty-two multiplexed signals along a piece of fiber. All gratings were written by the UV laser through a phase-mask system one by one, and monitored by pc-OTDR to achieve approximately identical reflective power. Some reflective powers are lower than the others due to two reasons: non-uniform photosensitivity section of the fiber, and FBG

writing system misalignment. The multiplexed grating signals were measured at a sensitivity of –36.6 dB.

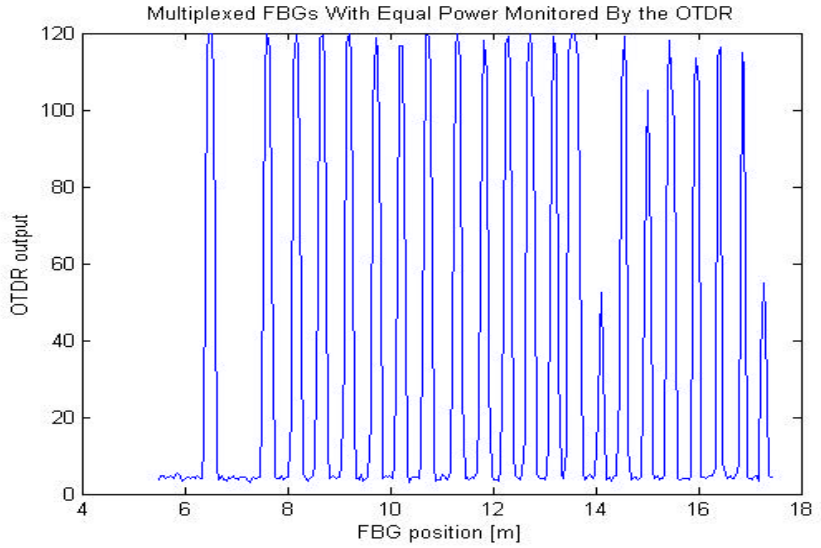

Fig 5.12 Multiplexed gratings with about 45 cm spacing for equal power budget

Note that the pc-OTDR system can provide as high as –60 dB sensitivity in the measurement for a sensor multiplexing system with about 8 dB resolution, Figure 5.13 shows multiplexed sensor signals in the data acquisition system window based on LabWindow software. The left part of Figure 5.13 window shows the measurement parameters settings and data save keys. The right window represents densely multiplexed FBG reflection peaks. There are two multiplexed measurement approaches based on the sensor system. For a small amount of sensors, we can adopt a method to scan each sensor reflection peak one by one according to preset peak positions. The measurement is only focused on a single sensor then transfers to the next one. The operation can be implemented more precisely to detect each intensity change, but it appears to be very slow when monitoring a large number of sensors. Thus the other method, scanning a whole group of sensor peaks at the same time and then moving to the next group to carry

on the same operation, was chosen. As soon as a signal change occurs, we could transfer to the previous measurement mode to accurately trace signal variations. Each group may consist of 20~50 sensors based on the required measurement resolution. In fact, a hybrid of the sensor monitoring approaches can be used to evaluate overall multiplexed FBG signals quickly. After sampling all the peak signals at the same time, we can obtain a profile of Bragg grating intensity variations versus time change. Figure 5.14 shows the profile of seventeen grating reflection intensities responding to a strain pulse distribution randomly applied in real time. Each signal curve represents the sensor output with time and each signal dip denotes the strain response after applying pulsed strains to the corresponding to FBG sensors.

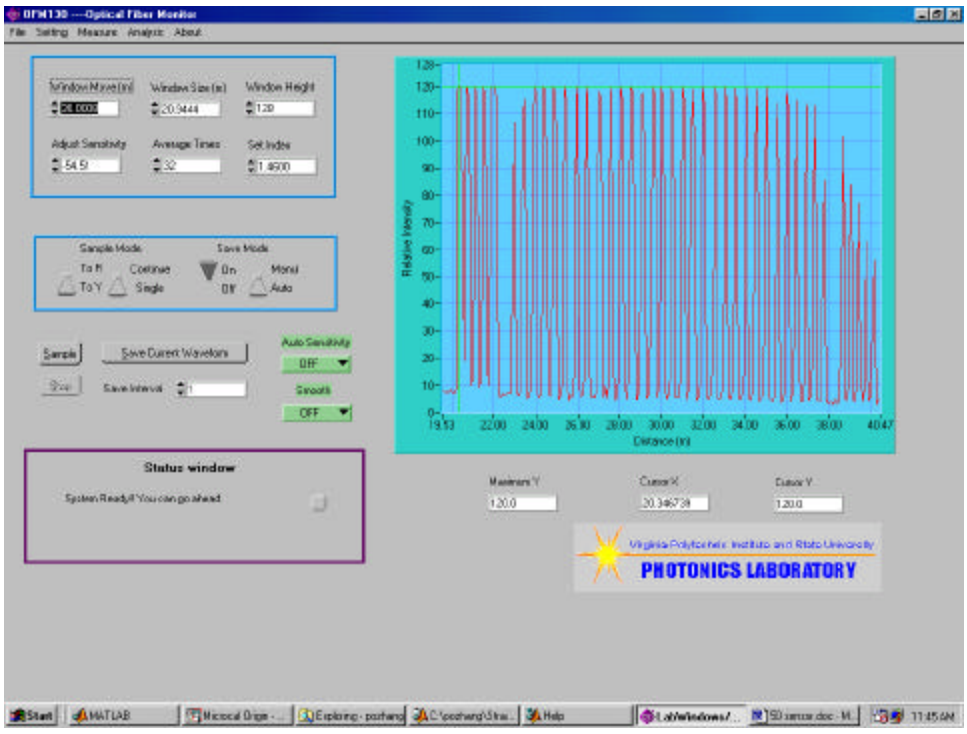

Fig. 5.13 45 sensors in the multiplexing on the LABVIEW window

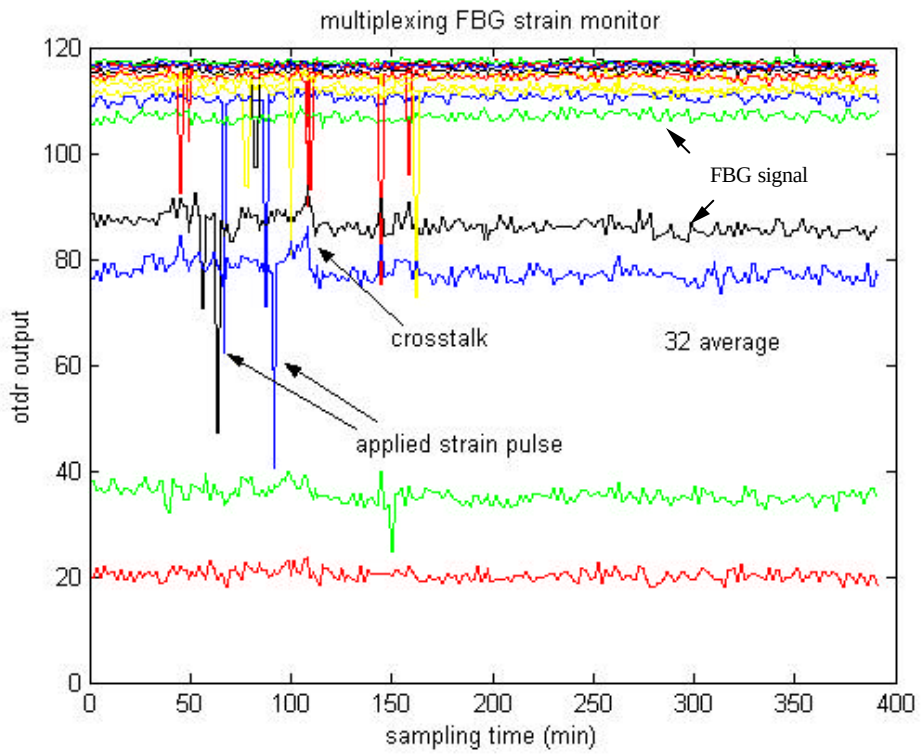

Fig. 5.14 Diagram of the strain distribution in real time monitoring with FBG sensors

5.6.2 Multiplexing FBG reflectance distribution in a practical multiplexing array

One multiplexing array had been implemented by the low-reflectance FBG fabrication system and short piece of fibers with FBGs were spliced one by one with normal single mode fibers to construct multiplexing. Total 68 sensors are monitored by the OTDR for an equal reflection power scheme shown in Figure5.15. All multiplexed sensors have the same Bragg wavelength at about 1312 nm that is determined by the FBG fabrication system and phase mask parameters. Thus this is actually a single wavelength system. It is known that an incident optical power at FBG wavelength is a function of a fraction factor ? over the overall spectral power at this wavelength and the OTDR operating sensitivity parameter S.

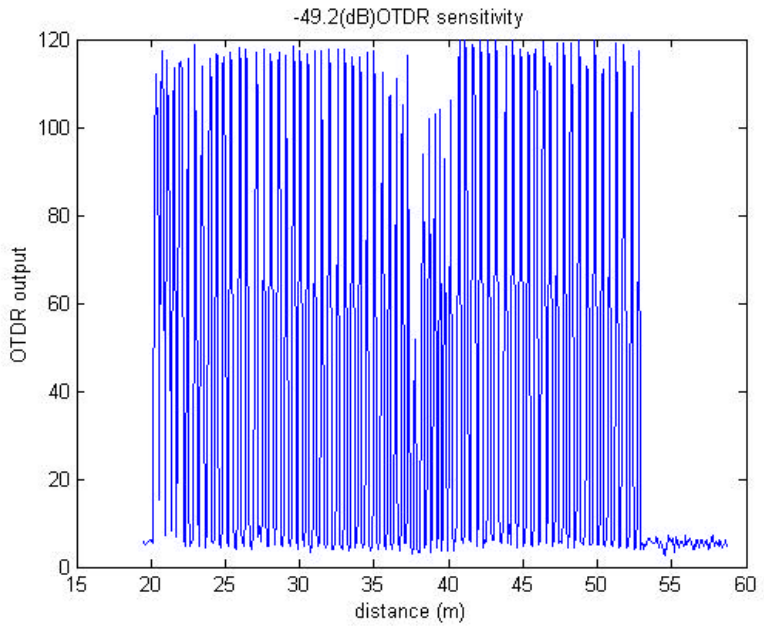

Fig.5.15 one 68-sensors multiplexing array for reflectance distribution measurement

r can be calculated by the OTDR source reflection spectrum, which is approximately –17.3 dB. The incident power I_{in} versus the OTDR sensitivity S and the fraction factor ?, illustrated in Chapter 3, can be written as,

I_{in} (dB)= -0.958× S -69.62+ r (dB). Hence, the first FBG sensor reflectance can be measured by the relation of $R_1 = I_1/I_{in,}$ where the output I_1 =-78.88 dBm is calculated by using Equation (5.8.1) for each observable OTDR equal reflection peak. When the OTDR sensitivity S is set at –49.2 dB for output –78.88 dBm, the first sensor R_1 can be obtained as 0.01252%. Each FBG in upstream can be orderly selected out of the multiplexing array for its reflectance measurement (separating with the multiplexing) in the same way as above. For an OTDR test, the 68th FBG is first chosen for independent test and its reflectance is 0.012 as the OTDR sensitivity is –29.32dB corresponding reflected power –78 dBm. After then, the other FBG sensors are cut out of its main array and the reflectance is separately measured in the similar approach. Therefore, a series reflectance

can be obtained to compare with theoretical curve as shown in Fig 5.16. Theoretical calculation is eventually based on the total loss and the first reflectance value in the multiplexing array as describing in Chapter 3, with the model of $R_n = R_{n-1}/a^2(1-R_{n-1})^2$. The total insertion loss of 8.008dB for this 68-sensor multiplexing was measured by using fiber free-end reflection in the OTDR detector, thus average insertion loss for each FBG section could be evaluated as 0.1178dB. That is a little larger than average fiber spliced loss 2× 0.034 dB when fabricating this multiplexing array. This is because the loss measurement may include all FBG optical reflection losses. For theoretical calculation in Figure 5.16, a is reasonably chosen as 0.078dB. The theoretical curve shows a good match with the measured results. The oscillation of reflectance generates from uneven radiating UV power in writing FBG processing, reflectance measuring error and the OTDR instability in room temperature.

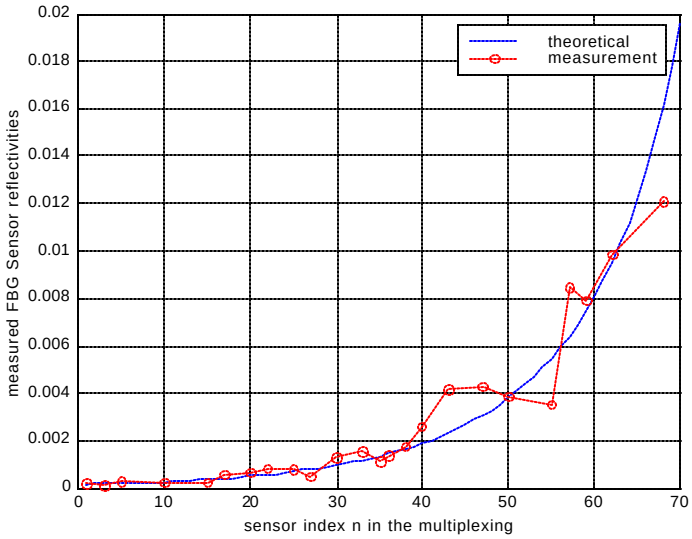

Fig.5.16 Reflectance distribution in implementation of the equal reflection power scheme

5.6.3 Simulating a configuration for a large number multiplexing FBGs

The pc-OTDR based multiplexing approach demonstrates the ability to interrogate a large number of FBGs, according to the theoretical calculation in Chapter 3. Obviously, a thousand sensors can be multiplexed as long as the intrinsic FBG loss and other

excess losses are low (<0.003dB) enough. The OTDR can provide sufficiently high dynamic range (~40 dB in practical case). A variable attenuator can be employed to serve as a simulator of a multiplexed sensor based on their excess and reflection losses. Figure 5.17 indicates two groups of sensors in multiplexing. The first group (0.745dB loss) with 21 FBGs is close to the OTDR side with an approximate similar FBG *R* 0.0344%, and each of their peaks can be clearly observed, while the other group (16) is far from the OTDR, right behind a connected attenuator serving as a simulator for a group of multiplexed sensors. Which, simply say, a multiplexing FBGs is eventually an attenuator for downstream FBG sensors that are exhibited very weak reflection at the OTDR sensitivity of -39.8 dB (the group reflectance from 0.021%-0.095%).

Reflectivity (%)	L (dB)
0.01	0.00043
0.02	0.00087
0.03	0.00133
0.04	0.00174
0.05	0.00217
0.06	0.0026
0.1	0.00436

Table 2: Reflective Loss ($L=10\log_{10}(1-R)$). The table at the left lists FBG reflection loss and each multiplexed FBG excess loss (splicing) is approximately 0.034 dB. Thus for one 500 multiplexed FBGs with the average reflectance of 0.0344% (0.0015dB) each, it corresponds to a total excess loss of –17.746 dB. Figure 5.17 presents the detection for multiplexed FBG signals by adjusting the OTDR sensitivity

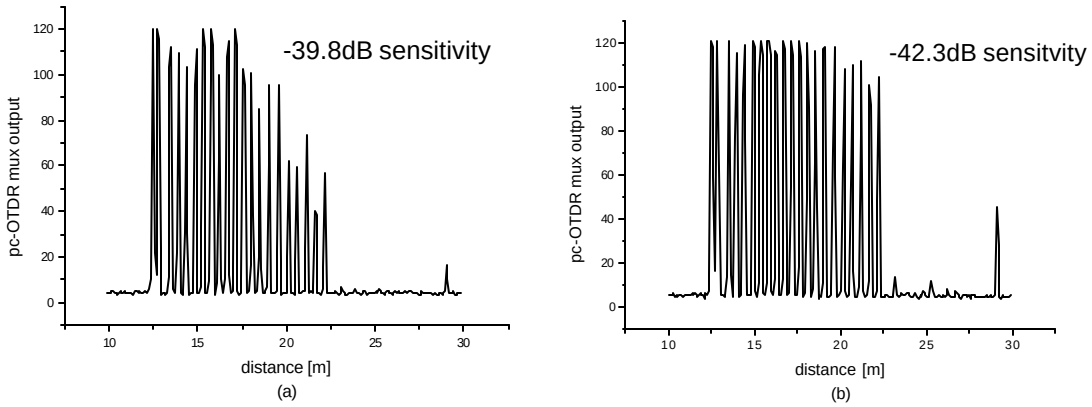

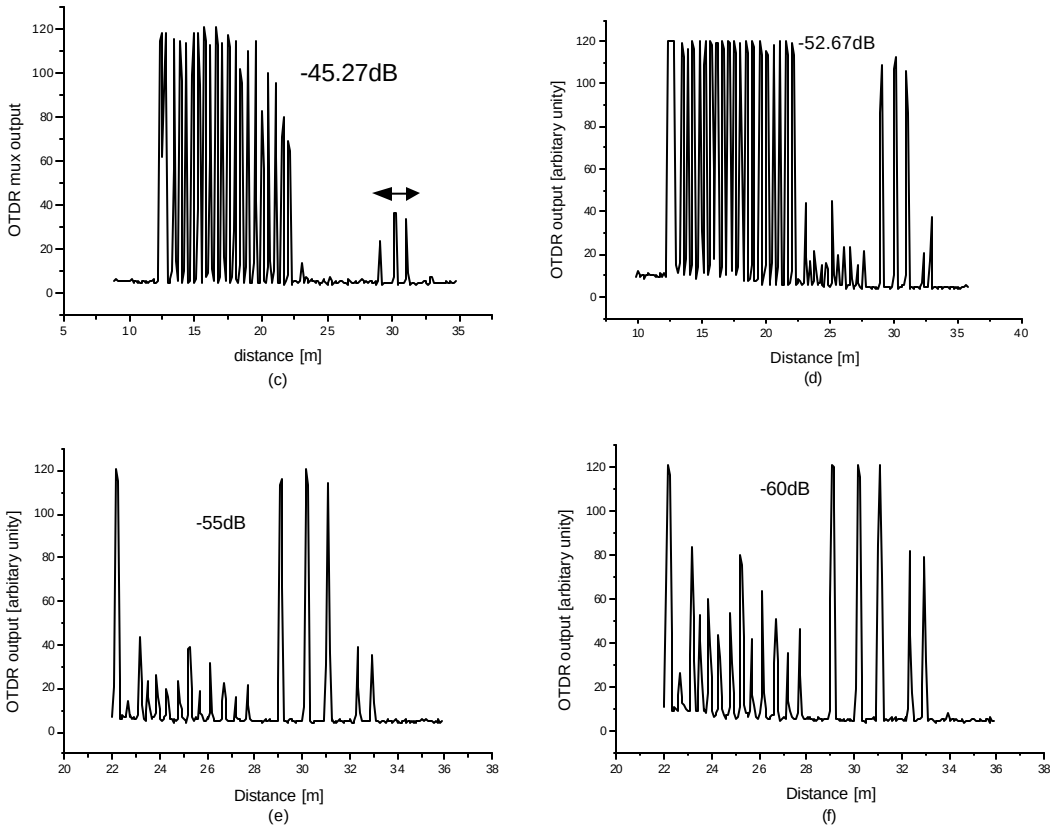

Fig.5.17 the pc-OTDR simulation result (19.96m window width) by adding a 20dB attenuator between FBG groups to validate 560 multiplexing ability

from -40 dB to -60dB. A 20-dB variable attenuator placed in between the FBG groups can be considered as multiplexed 560 FBGs by the attenuation amount. Reflected peaks on the right appear with an increase in the OTDR sensitivity (c,d,e,f). After the OTDR sensitivity reaches –60 dB, a maximum OTDR sensitivity, multiplexed FBGs appear at distance ranges between 23m and 33m. The latter group of sensors in Figure 5.17 (d) and (e) indicates that multiplexed FBGs intensity increases to maximum as the OTDR sensitivity to -60dB (max input power). From theoretical analysis (equal *R*), for 0.0344%

and 0.0355dB loss system it can multiplex 430 sensors (Eq (3.7)), which is rather close to simulation amount of 500 FBGs.

Figure 5.18 shows an overall map of a simulating result based on the attenuation of the grating series for dense multiplexing of several hundred gratings deployed in an array. Basically, one hundred multiplexed gratings correspond to an average 3.55dB excess loss with neglected crosstalk between the gratings due to the low reflectance of each grating.

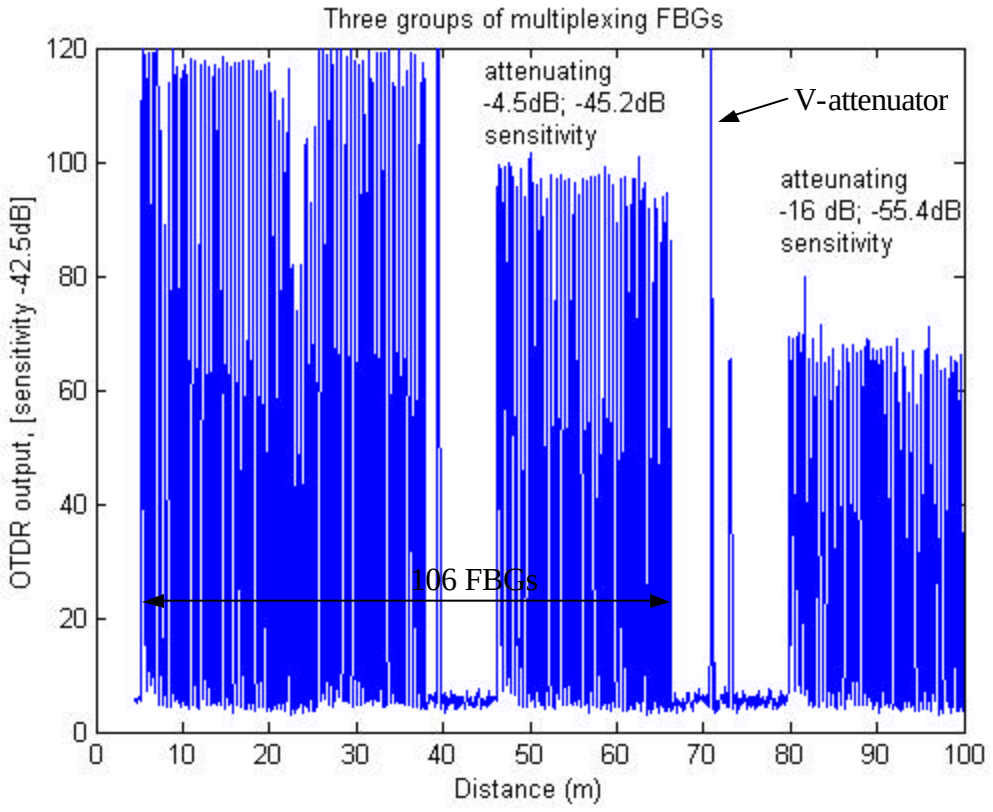

Fig 5.18 simulating several hundred multiplexed gratings in the array

Three groups of sensor amounts were, 60, 46, and 48 respectively, which are multiplexed in a series topology at different spatial positions along a fiber. A variable attenuator was placed between the groups to simulate the behavior of multiplexed gratings. The 3rd group of FBGs at –55.4dB OTDR sensitivity (unloaded state sensitivity -37.5dB and the

1st reflectance 0.19%) was measured under –16 dB attenuation applied ahead, which corresponds to 450 multiplexed FBGs. In this configuration, there are more than 650 FBGs able to be multiplexed with one nominal wavelength. If the combined attenuation coefficient of insertion and transmission of the FBG are improved to be no larger than 0.01dB for the reflectance of 0.02%, a 1000-sensor multiplexed system can be realized.

5.6.3 Evaluation of the crosstalk

To investigate the crosstalk between fiber Bragg gratings with approximate reflectance of 0.5%, four sensors were multiplexed in a serial array and stress is applied to the two upstream sensors, S_1 and S_2, to observe the spectral shadowing effect that may occur on downstream sensors S_3 and S_4 output. All four sensors have a very similar Bragg wavelength. When the output magnitude of the stressed sensor was decreased from 117 to 70 (pc-OTDR probability amplitude, 40% change) after applying the strain experimentally, the corresponding crosstalk contributed from S_1 and S_2 to S_3 and S_4 will be approximately –18 dB and –24 dB respectively from the output change. Obviously, the magnitude of the crosstalk is dependent on the spectral overlap, but low FBG reflectivity definitely benefits the reduction of the crosstalk. Typical crosstalk occurring between the four sensors is shown in Figure 5.19. Stress was applied to the two upstream sensors S_1 and S_2 three times and we could observe a grating signal change of –18 dB based on the signal level. In addition, a three-multiplexed grating trace with separated wavelengths will have little crosstalk as shown in Fig 5.20. Temperature up to 124^{o}C was applied to upstream G_2 sensors, and the other two sensors were remained at room temperature. The temperature applied to the G_2 sensor was increased and decreased for about three hours.

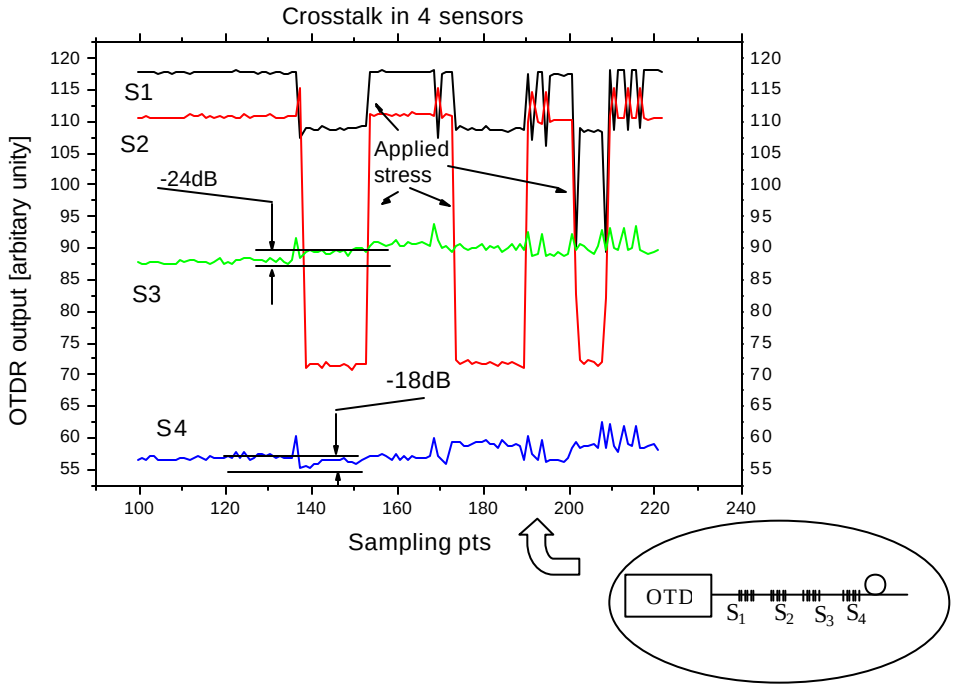

Fig.5.19 Stress applied upstream S_1 and S_2, S_3 and S_4 have crosstalk outputs of about –18db and –24dB,

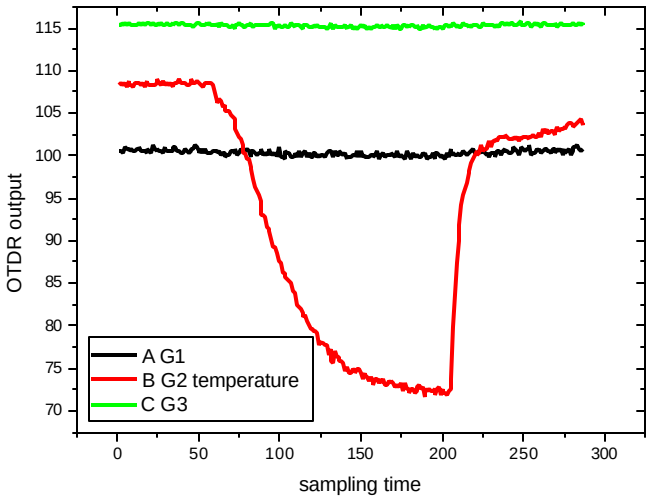

Fig 5.20 traces of multiplexed three sensors, red line (middle) undergoing increases with temperature variations.

It is evident that the G2 sensor has an obvious change while the other two sensors remain unchanged. Due to the low reflectance of the Bragg gratings used, the other two sensors have no crosstalk with the G2 sensor during the temperature variation. Thus, the different wavelength sensors have a small probability to experience spectral-shadowing crosstalk. In addition, low reflectance can greatly reduce the effect of multiple reflections (ghost line) among Bragg gratings that always occur in the other multiplexed system.

5.7 Combined wavelength- and time-domain multiplexing

The use of the pc-OTDR for simultaneous wavelength and time domain multiplexing FBGs is a rather efficient methodology to interrogate more FBG sensors along a single fiber. In fact, from previous simulations FBG sensors can be multiplexed in several hundreds with the same nominal wavelength, but if sensors are designed with several wavelengths over the OTDR source spectrum, we could obtain more efficient multiplexing within the OTDR limitations, such as much less multiple reflections, high incident power utilization, and low crosstalk between FBGs.

One WDM/OTDR multiplexing configuration was measured using an array of 30 FBGs, consisting of similar groups of 5 FBGs each with different wavelengths. The spatial intervals between FBGs or groups were approximately 45 cm, and the 5 FBGs of each group had a separate spectral position based on the spectral slope-position of the source, such as 1283 nm, 1287nm, 1308, 1314nm and 1320nm, as shown in Fig 5.21.

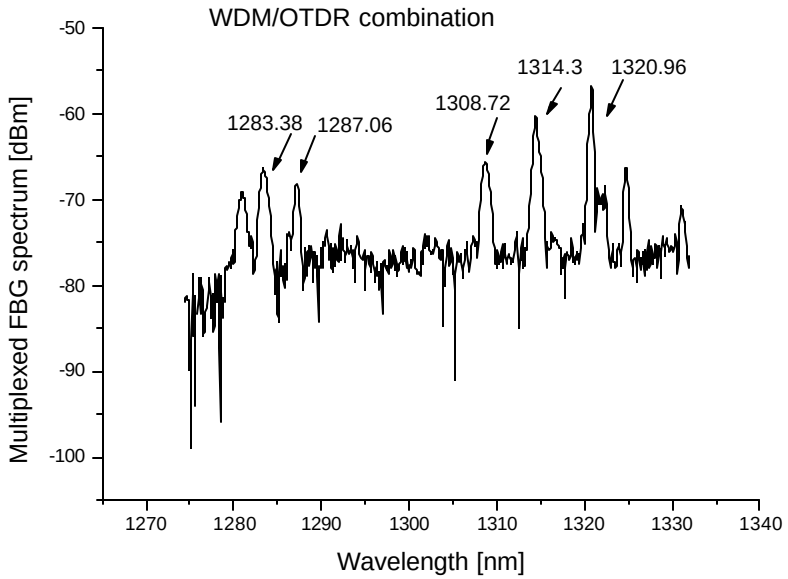

Fig 5.21 Wavelength distribution (WDM) in the OTDR-based multiplexed FBGs

All FBGs were fabricated to have about 1.2-nm FWHM to smoothen the oscillation induced by the multimode laser spacing.

Figure 5.21 shows the results of these multiplexed FBGs separated into 6 groups each with a nominal wavelength. One special difficulty for this combined multiplexing scheme is that each sensor must be clearly marked to differentiate it from the others. Near 1283 nm wavelength, the sensor calibration slope-rates (positive) are different from that of 1314 nm-sensor (negative). Though the WDM/OTDR scheme can multiplex more sensors, it leads to a more complicated situation of the multiplexing system.

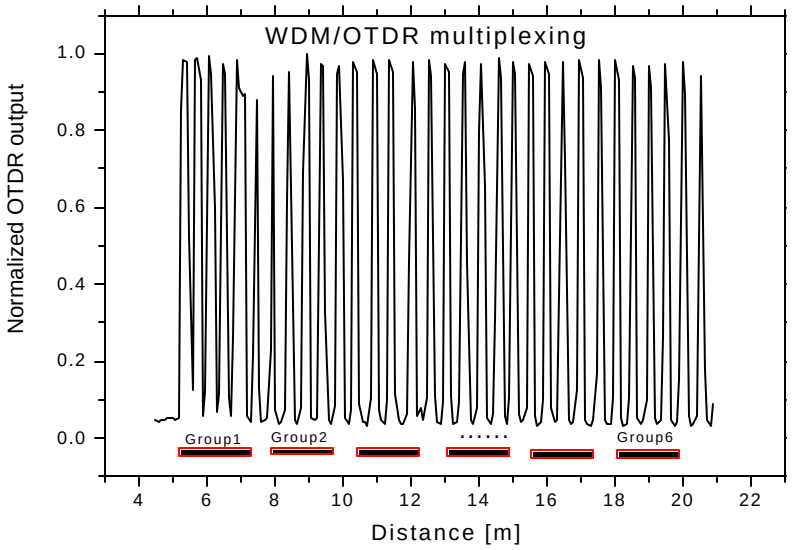

Fig. 5.22 OTDR trace for 6 groups of WDM/OTDR multiplexed sensors with various ?

Tensile loading used for strain calibration during the spectral measurements was applied to a selected FBG at Bragg wavelength of 1314.7 nm. The normalized output is shown in Fig 5.23. Strain measurements repeated two times indicated a repeatability of 1.7 % over the full range.

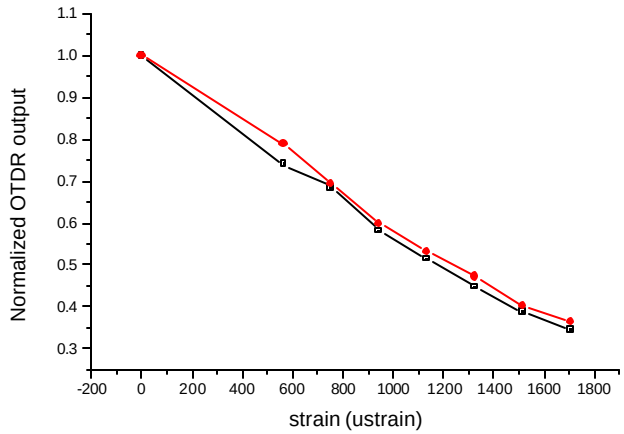

Fig 5.23 Experimental strain results of sensor at a wavelength of 1314 nm in Group 4

In summary, the pc-OTDR system can actually provide real-time measurements for dense multiplexing of a large number of Bragg gratings in a fiber. Based on the OTDR limitation for the ratio of optical pulse repetition rate and duration, a maximum of approximately 1200 sensors can be multiplexed. If the reflection wavelengths of FBG sensors were slotted by separated wavelengths, the system signal-to-noise ratio could be great enhanced through decrease of the crosstalk and multiplexing spectral overlaps. Thus we could practically trace a few hundred sensors in a short fiber (< 100 meter) using a variety of wavelengths of FBG sensors and the high-resolution photon counting OTDR technology.

Chapter 6 Multiplexing System Noise Analysis

The potential application capability of the pc-OTDR technique of multiplexing FBGs has been demonstrated. Its commercial value can be enhanced if the number of sensors within a unit length of fiber can be increased. But densely multiplexed FBGs will result in multiple reflections between the sensors and spectral shadowing due to the FBG similar spectral feature. They will downgrade multiplexing system performance. This chapter provides a detailed analysis of crosstalk effects, multiple reflections, and dark noise, in order to evaluate multiplexing system performance.

6.1 Optically induced noise associated with multi-reflection light

In the pc-OTDR based FBG system we are focusing on, serial pulses travel along the primary path through FBG sensors in the array and then return as a result of the reflection. The signal carries the time and strength information of the sensor. On the other hand, the light passing through all up-stream FBGs is affected by the multiple reflections between them, changing its propagation direction many times. Hence, part of the noisy light

arrives to the detector and mixes with the light coming from the measured FBG to decrease signal to noise ratio.

There are two major types of multiple reflections that will be analyzed in the system:

One is adjacent FBG reflection forming additional reflective ghosts at the measured sensor, which can be described as a mathematical process through the use of a time and space discrete numerical model. The other multiple reflection is the effect of distant FBG multiple reflections on the sensor under test. We can omit previous pulse ghosts since the OTDR is operating at the repetition rate of 1MHz and the fiber length connected is less than 100 meters. If the fiber length were longer than 100 meters, there would be an additional ghost source in the detection, which is a type of real light but it is not arrive from the expected sensor position.

6.1.1 Reflection calculation between adjacent FBGs

The multiplexed FBG system contains *n* number of FBGs, which are arranged from 1 to *n* and are separated by an identical optical path length L, or the observation time interval T_s, where T_s is Ln_{eff}/c. The backscattered light energy fraction *b(m,j)* and transmitted light energy fraction *f(m,j)* at the *m*th FBG and at the j time as indicated in Fig 6.1 are defined by the following expressions:

$$\begin{aligned} b(m, j) &= f(m-1, j-1)\times R_m + b(m+1, j-1)\times T_m \\ f(m, j) &= f(m-1, j-1)\times T_m + b(m+1, j-1)\times R_m \end{aligned}, \tag{6.1}$$

where T_m and R_m are the transmission and reflection coefficients of the *m*th sensor, $f(m-1, j-1)$ and $b(m+1, j-1)$ are the energy fractions transmitted by the m-1 sensor and reflected from the m+1 sensor, respectively, both at the j-1 time.

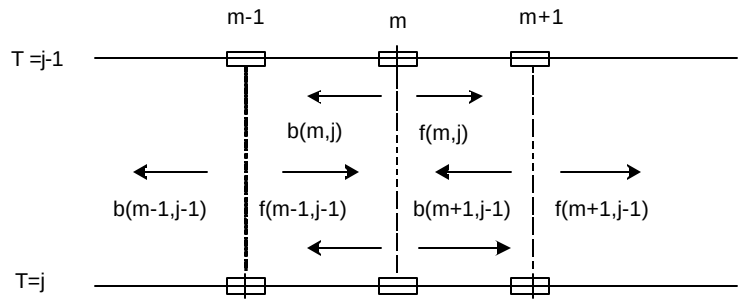

Fig.6.1 Model of reflected and transmitted light at the FBG sensor

Obviously, the *m*th sensor will receive two light sources from its adjacent sensors at the j time to form a possible power enhancement. Coherence [58] in the light is not considered in this model due to the separation of two sensors being longer than the source coherence length. Let us do some simple calculations according to this model to describe the *n*th FBG reflected strength considering adjacent FBG-reflections.

The last sensor backscattering *b(n)* and forward-scattering *f* (n) can thus be written by

$$b(n) = f(n-1, j-1)R_n, \text{ and } f(n) = f(n-1, j-1)\times(1-R_n) . \tag{6.2}$$

where R_n is the nth FBG reflectance. According to Equation. (6.1), the signal of the *n*-1 sensor can be given by

$$\begin{aligned} b(n-1, j) &= f(n-2, j-1)\times R_{n-1} + b(n, j-1)\times T_{n-1} \\ f(n-1, j) &= f(n-2, j-1)\times T_{n-1} + b(n, j-1)\times R_{n-1} \end{aligned} . \tag{6.3}$$

Substituting Equation (6.2) into Equation (6.3), and noting that $R_n = 1-T_n$, we obtain

$$f(n-1) = \frac{1-R_{n-1}}{1-R_n R_{n-1}} f(n-2) = M_{n-1} f(n-2) , \tag{6.4}$$

where $M_{n-1} = \frac{1-R_{n-1}}{1-R_n R_{n-1}}$ is a transmission coefficient for adjacent sensors. Here we ignore time footnote j. Meanwhile, the backscattering energy of the *n*-1sensor is given by

$$b(n-1) = f(n-2)\times(R_{n-1} + \frac{R_n(1-R_{n-1})^2}{1-R_nR_{n-1}}) = K_{n-2}f(n-2) \quad . \tag{6.5}$$

Similarly, a recursive expression for M_i and K_i coefficients can be obtained as

$$K_{n-i} = R_{n-i} + M_{n-i}K_{n-i+1}(1-R_{n-i}),\ \ K_n = R_n \ , \tag{6.6-1}$$

where i = 1,2,3..,n-1, and

$$M_{n-i} = \frac{1-R_{n-i}}{1-K_{n-i+1}R_{n-i}} . \tag{6.6-2}$$

Thus, the reflection energy of the nth sensor can be represented by the first sensor energy and its recursive factor as,

$$b(n) = R_n\prod_{i=1}^{n-2}M_{n-i}\times f(1) . \tag{6.7}$$

It has been shown that the reflected power of the nth FBG will be a little larger than the standard model described in Chapter 3 due to additional adjacent FBG reflections. The $M_{n\text{-}i}$ factor depicts the influences associated with adjacent reflections. The increase in reflected power for multiplexed sensors in comparison with the standard model that does not consider adjacent reflections, as shown in Fig. 6.2, actually corresponds to the multi-reflection noise of the output that decreases signal-to-noise ratio. For the case of 0.05% FBG reflectance, the unwanted reflection results in about a 0.3 dB power enhancements at the 500th FBG. The adjacent reflections can be further decreased through setting random sensor spacing between sensors since the power increase is based on the theoretical calculation of identical spacing in the FBG sensor array.

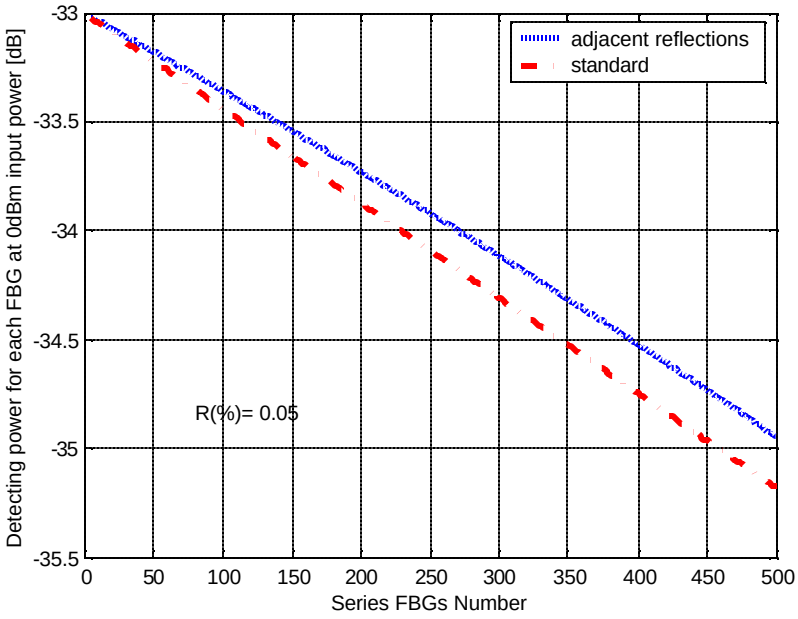

Fig.6.2. Calculation result of the adjacent -reflection power increase

6.1.2 The first-order FBG multiple reflections

Another source of crosstalk in the pc-OTDR based serial multiplexed FBG arises from multiple reflections between an arbitrary two FBGs in the array [59]. This can result in pulses arriving simultaneously at the detector having undergone a direct reflection from a sensor element and also having experienced a number of multiple reflection paths within the sensor array. In other words, the intrinsic optical crosstalk between FBG sensors can be assessed by determining the number of interfering pulses generated at the FBG array due to multiple-reflection paths, which are time-slot coincident with each pulse produced by a single principal reflection, shown in Fig 6.3. Obviously, we only consider the first-order crosstalk pulses that are a total of three reflections between the sensors and are the strongest stray pulses generated. According to compounding theory of choice 2 in N

events, the number of the first-order multi-reflected pulses in the *n*th time slot at the array output other than the reflection from the *N*th FBG is written as

$$m = C_N^2 - N + 1 \tag{6.8}$$

where *N* is the total multiplexed number. This result is similar to the literature[60][61]. The basis of this formula can also be evaluated from the schematic of the first-order multiple reflections shown in Fig.6.3. Here, we depict an optical path through all FBGs to the *N*th FBG and reflections to the detector.

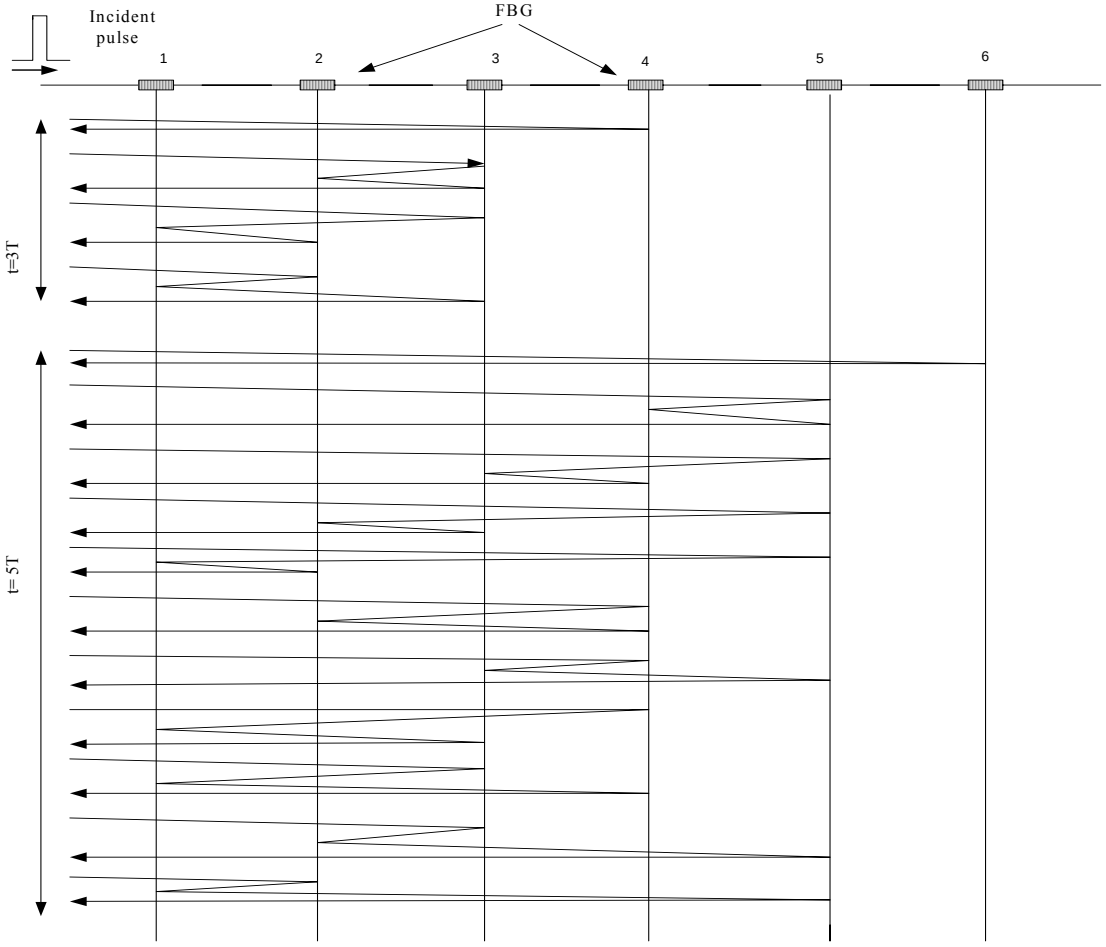

Fig.6.3 FBG principal reflection and their first-order (the three reflections) light path leading to output pulses in the third and fifth time slots

It generates all the possible first-order crosstalk pulses in a FBG array for t = 3t and t = 5t, obviously, the total number is thus given by the sum N-1+N-2+…+1, as described by Equation (6.8). Therefore, an approximate intensity expression for total crosstalk can be indicated as $c \approx -10\log_{10}((C_N^2 - N+1)R^2)$, where R is the FBG reflectance. For example, for 100 multiplexed FBGs there are 4900 possible paths for the first-order reflections, contributing crosstalk of -23.14 dB, possibly increasing to –3 dB for 1000 sensors.

Let's analyze general total multiple-reflection effects in the FBG array. From Figure 6.3, the multiple reflections include numerous interfering signals for the multiplexed number n given. A basic equation for the sum of these first-order multi-reflections can be given as

$$I_{mltp\_R} = R_{n-1}\prod_{j=1}^{n-2}(1-R_j)^2\left[R_{n-2}R_{n-1} + 2\sum_{j=1}^{n-3}R_jR_{j+1}\right] + \sum_{j=3}^{\frac{i}{2}(even)or\frac{i+1}{2}(odd\,i)} R_{n-(j-1)}\left[\prod_{m=1}^{n-j}(1-R_m)^2\right] \times\left\{R_{n-2(j-1)}R_{n-(j-1)}\prod_{k=i-[2(j-1)-1]}^{n-[(j-1)+1]}(1-R_c)^2 + 2\sum_{k=1}^{n-(2j-1)}R_kR_{j-1+k}\prod_{b=1}^{j-2}(1-R_{(j-1-b+k)})^2\right\} \quad 6.9$$

If all FBGs are aligned to a similar Bragg wavelength and the reflected power from them is balanced, the signal-to-noise ratio (s/n) for the distal FBG due to multiple-reflections (MR) from ten to several hundred multiplexing sensors is shown in Fig 6.4. With the increase in multiplexing number, the s/n generated by MR will go down to about 5 dB, as shown in Fig.6.4 (a), which indicates various curves with different reflectance of the last multiplexed FBG to see the MR effects of high-reflectance sensors. However, the change in s/n would become smaller or flatter due to the FBG reflectance being smaller and the decrease in multi-reflection intensity as the multiplexing number increases.

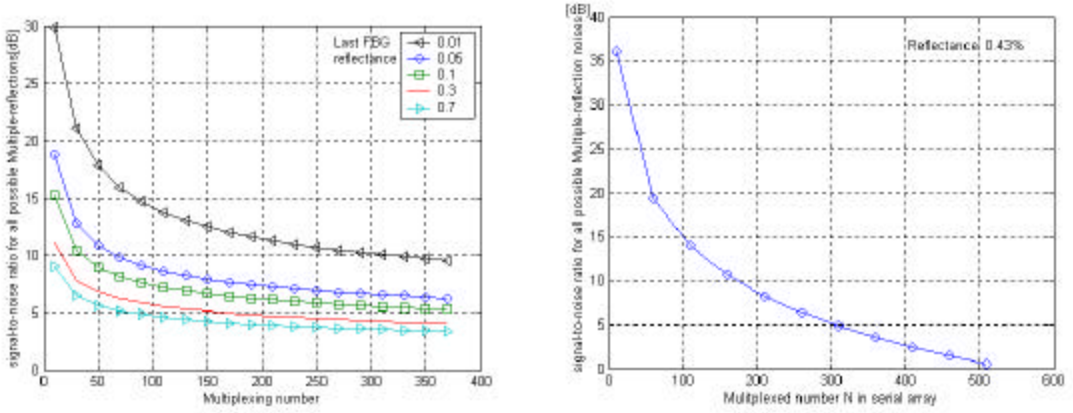

(a) (b)

Fig 6.4 Intensity s/n detection in FBGs' multiplexing with (a) identical power and (b) identical reflectance scheme

The s/n of Fig.6.4 (b) has a larger change, almost to zero dB (equal reflectance), which is dependent on multiplexed FBG reflectance *R*. If *R* is chosen to be a smaller than 0.1%, the entire curve will move up. Here, we ignore the coherent interference between the primary signal and the multiple reflected lights.

6.2 Discussion of the spectral overlap—spectral shadowing

Consider a group of sensors in a multiplexed system that has a similar Bragg wavelength, which is a basic condition of the pc-OTDR based multiplexing, any FBG's spectrum in the downstream is easily distorted by those of the upstream FBGs due to light having to pass through them twice like the spectral filtering effect. Assuming up-stream sensor wavelengths are being randomly shifted by applying strain or temperature, the downstream sensor intensity will vary with the previous sensor slight spectral offsets since its output is eventually related to the convolution of sensor spectra that the light wave passes through. The worst case of distortion, for the FBG being equal in bandwidth

and reflectivity, occurs approximately as if they are spectrally offset by their FWHMs. In fact, it is convenient to simplify the analysis of the peak reflectance R_i change for a FBG sensor instead of analyzing FBG central wavelength shift because the FBG spectrum with a Gaussian-distributed feature is approximately linear in the relationship between wavelength and intensity (R). According to Equation (3.3) in Chapter 3, the basic nth sensor output can be given in decibel form as

$$I_n[dBm] = I_0 + 10\log_{10} R_n(l) + \sum_{k=1}^{n-1} 20\log_{10}[(1 - R_k(l))a_k] , \qquad (6.9.1)$$

where I_0 is the OTDR incident light power, R_k (k=1,2…,n) and a_k are the Bragg grating reflectance and coupling coefficient at the kth index, respectively. It can be directly seen that the output of the nth sensor is dependent on the series of previous sensor reflectances associated with the identical wavelength. Obviously, if wavelengths become mismatched in the multiplexing system, it would imply that the reflectances of other sensors corresponding to the operating wavelength tend to be smaller, so that the output power for the last sensor would increase with the number of mismatched wavelengths.

From a two FBG multiplexed system example, the relationship between wavelength mismatch and power increase can be clearly understood. Assuming FBG_2 (reflectance: $R(l - l_2)$) is the sensor under test connected with FBG_1 ($R(l - l_1)$) located at its upstream, the basic reflected power for the FBG_2 can be written as

$$I_2 = \int_{-\infty}^{\infty} (1 - R(l - l_1, \Delta l))^2 S(l - l_c) R(l - l_2, \Delta l) dl \quad . \qquad (6.9.2)$$

Since $\Delta l << \Delta l_c$ (source bandwidth), thus, $R(l - l_i, \Delta l) \approx R_i d(l - l_i)$. For the case of wavelength match, $l_2 \approx l_1$, (6.9.2) will become

$$I_{2\_match} = \int_{-\infty}^{\infty} (1 - R_1 d(l - l_1))^2 S(l - l_c) R_2 d(l - l_2) dl = (1 - R_1 d(l_2 - l_1))^2 S(l_2 - l_c) R_2 \quad . \tag{6.9.3}$$

If the mismatch occurs, $l_2 \neq l_1$ and probably $|l_2 - l_1| >> \Delta l$, so that the mismatch intensity is given by

$$I_{2\_mismatch} \approx S(l_2 - l_c) R_2, \text{ since } R_1 d(l_2 - l_1) \to 0 \tag{6.9.4}$$

Obviously, $I_{2\_mismatch} > I_{2\_match}$ due to the $R_1(l_2 - l_1)|_{\text{mismatch}} < R_1(l_2 - l_1)|_{\text{match}}$

Based on Equation (6.9.1) and previous analysis, assuming the reflectance variation causing the power enhancement after the wavelength mismatch, the difference in power due to the spectral shadowing effect can be simply written as

$$\Delta I_n[dB] = 20 \sum_{k=1}^{n-1} \log_{10}(1 + \frac{rand(1,k) \times \Delta e_k}{1 - R_k}), \tag{6.9.5}$$

where $\Delta R_k = rand(1,k) \times \Delta e_k$ is a random function describing the degradation of reflectance coefficient ahead of the kth FBG. Since the pc-OTDR only measures the probability of emitted photoelectrons to valuate reflected intensity, the power change will transfer the increase of photon-detecting probability. Hence, according to the illustrated Equation (4.1) in Chapter 4, in which the *nth* FBG detected probability of photons, could be expressed as,

$$P_r(n) = 1 - \exp(-h \times ph \times 10^{2 \sum_{k}^{n-1} \log_{10}[(1 - R_k + \Delta R_k)a]}), \tag{6.9.6}$$

where n is the multiplexing FBG number, h the quantum efficient and ph the reflected photon arriving at the photodetector. Consequently, Figure 6.5 can illustrate the output of sensor changes with mismatching rate.

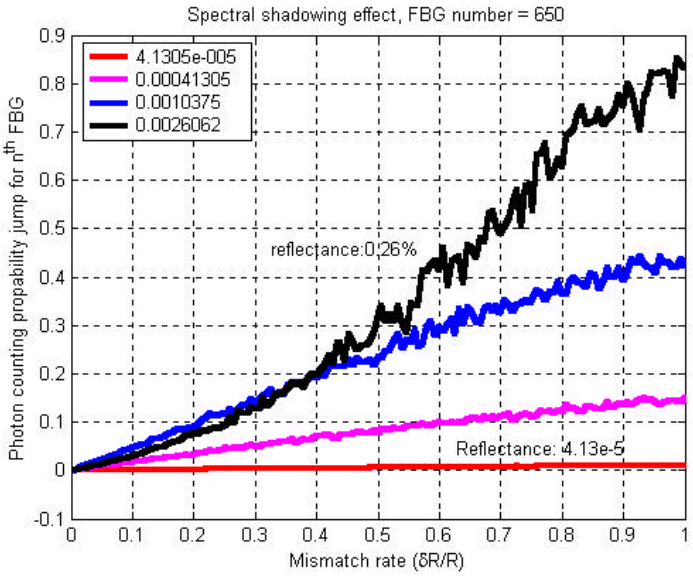

Fig. 6.5. Simulating result of spectral shadowing effect for probability output for different reflectance systems and horizon axis represents the average relative deviation of reflectance R

It shows that for the last FBG the maximum probability jump caused by wavelength mismatch can reach up to 80% if all wavelengths randomly mismatch (reflectance 0.26%). In general, the odds for 80% probability increase are much smaller due to the central wavelengths of FBG sensors being distributed around a certain wavelength within the certain range. In practice, we could not ensure exactly the same wavelength for the whole multiplexed FBG series. The wavelengths fabricated will depend upon the fabrication processing of the sensors as the geometric size of the FBG writing system has mini-changes, but it has some advantages to avoid the further spectral overlaps.

6.3 Fiber bending induced source spectrum distortion

If bending is applied on the fiber in front of the multiplexed FBGs, not only will the optical source intensity vary with the bending radius, but also the spectrum of the light wave transmitted in the fiber will experience a large distortion, the strength of which is also dependent on the bending radius.

Since the transmitted spectrum, especially in high slope-rate region, is vital to the interrogation of the FBG reflection signals, the spectral distortion directly produces FBG signal variations. The greater spectral distortion, the lower the sensor output dynamic range and amplitude to test physical measurands. The fiber bending induced spectrum change is, theoretically, rather complicated, but from

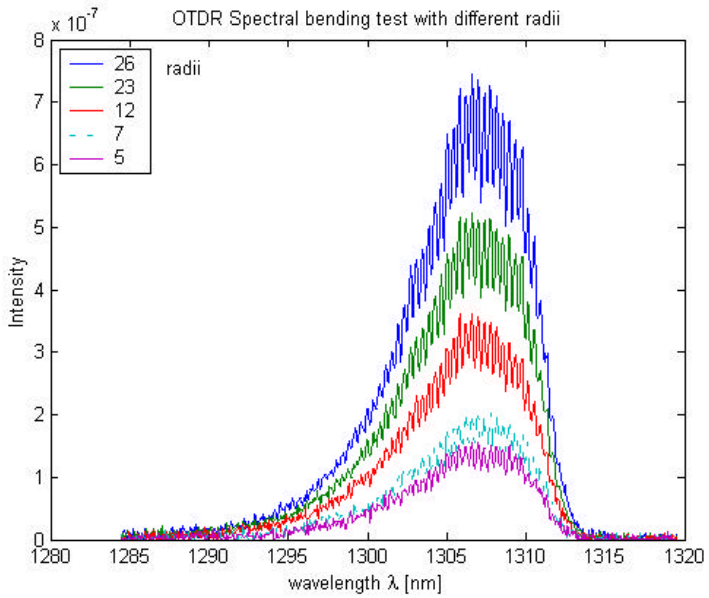

Fig 6.6.1 Bending induced spectrum and intensity change

experiment, we can clearly observe the spectral change for a bent fiber. The typical spectra of pc-OTDR semiconductor laser light transmitted in the original and the bent fiber are plotted in Figure 6.6.1, for a series of reducing radii. As we see, the spectral intensity changes a lot for a small bend radius. Therefore FBG signal interrogation would not be appropriate after bend radius is decreased to 5 cm.

The larger spectral distortion in regular fiber is primarily due to the large mode field diameter of the optical fiber. The larger the mode field diameter, the higher the

propagation loss as the fiber bends. Meanwhile, light with a longer wavelength will suffer more loss since it has a larger mode field diameter as transmitted in the fiber, based on the mode field equation, given by

$$w(l) = a(0.65 + \frac{1.619}{V^{3/2}} + \frac{2.88}{V^{6}}) \tag{6.10}$$

where the electrical field of the guided mode is assumed to have a Gaussian profile, and V is the normalized frequency of the fiber, which is inversely proportional to the wavelength l. In practice, we may not usually see such a big bending status, but an accumulation of bending effects consisting of many small bends in a length of fiber could also result in larger spectrum variations.

The other significant source influence is variation of the source due to the environment temperature. Since the pc-OTDR source is a type of multi-longitudinal mode semiconductor laser that has a temperature dependency, the sensor reflected intensity variation caused by the source input change couldn't be avoided, as shown in Fig 6.6.2.

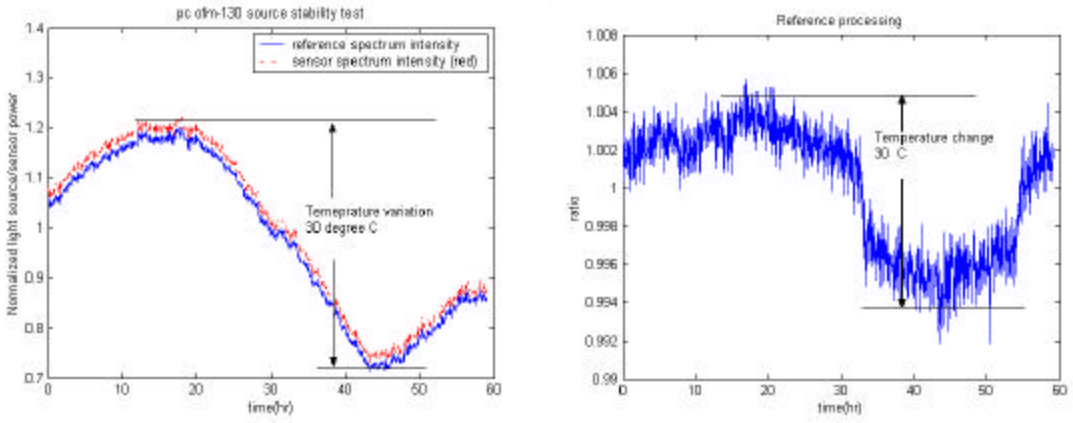

(a) (b)

Fig.6.6.2 OTDR source intensity change with environmental temperature

It was shown that OTDR incident intensity changes about 46% with an environment temperature variation of 30℃ in a long-term drift. A reference approach is essential to interrogate FBG sensors to decrease the source fluctuation effect to 0.6% variation, as shown in Figure 6.6.2(b).

6.4 pc-OTDR SAPD (single photon avalanche photodetector) noise analysis

6.4.1 Single photons to macroscopic current pulse in OTDR

A special semiconductor device called single photon avalanche diode (SPAD) functions as the optical detector heart in our high-resolution photon counting OTDR. Silica SPADs that consist of an avalanche photodiode have very good performance: quantum efficiencies for detecting single photon are around 20%; dark counts in the absence of light below 100 counts per second; and a sub-nanosecond timing resolution.

An avalanche photodiode is basically a p-i-n diode specifically designed to provide an internal current gain, making it much more sensitive to small light fluxes. The physical phenomenon behind the current gain is known as impact ionization. When reverse-biased, the APD is designed to be able to sustain a large electric field across the intrinsic i-region between the p-type and the n-type layer. An incoming photon is absorbed to create an electron-hole pair in the narrow bandgap InGaAs i-layer. The generated hole crosses to the wider bandgap InP multiplication region, where the hole is accelerated to gain enough energy generated secondary electron-hole pairs by impact ionization. These pairs, in turn, can generate new electron-hole pairs and so forth.

To achieve single-photon sensitivity in the detection, the SADP are biased to operate in a so-called “Geiger mode” with an excess bias voltage to reverse bias the ADP above

breakdown voltage for a very short time after a precision delay from the pulsed laser trigger to result in avalanche process. Under such conditions, a primary charge created in the junction causes its entire breakdown and triggers a macroscopic avalanche current pulse, which can readily be detected by the ensuing electrical circuitry. The circuitry must also suppress the avalanche process before it actually destroys the device. Sometime, bias well above breakdown can be achieved without breakdown if the bias time is very short. This procedure makes the diode so sensitive to light that it responds to only one photon. The precision delay permits the light round trip to be measured, and thus the length calculated. The value of the breakdown voltage is structure, material, and temperature dependent and may range from 10-500V. Raising the bias voltage increases the quantum efficiency, but it also increases the dark count noise.

6.4.2 Gated passive quenching

When an avalanche is trigged either by the photon or a noise event, a current starts to flow in the device that rapidly reaches the milliampere regime. One must quench the avalanche in the detector in order to avoid the destruction of the device. In our OTDR application, the arrival time of the photon at the junction is known, making it possible to use a gated mode of operation. In this approach, the APD bias voltage is brought above T_g during which avalanche occurs. The order of magnitude of T_g is typically around a sub-nanosecond. These periods are separated by a longer hold off time when the bias voltage is leveled below the breakdown voltage. A basic circuit diagram of a gated mode quenching process is shown in Figure 6.7.

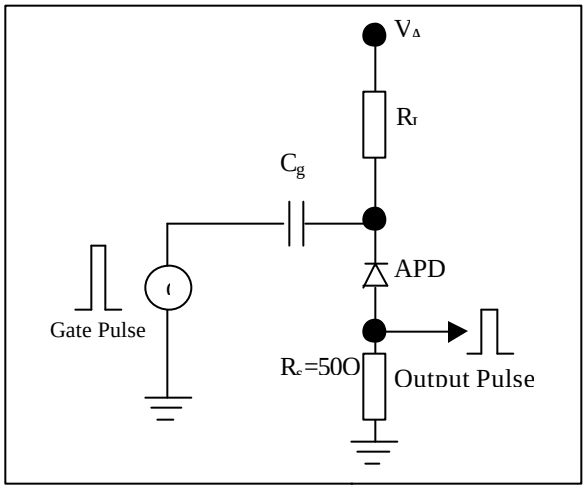

Fig.6.7 Schematic circuit diagram of a gate passive quenching circuit breakdown for short time periods

6.4.3 Quantum efficiency and dark count

The quantum efficiency ? in the Geiger mode results from three factors

1) The probability that a photon will be absorbed in the InGaAs layer (absorption efficiency)
2) The probability that photon-generated carriers will trigger the avalanche crossing the junction (trigger probability)
3) The optical coupling efficiency of the light to the device

The avalanche rate in ADP is due not only to signal photons, but may also be randomly triggered by bulk carriers generated in the thermal, tunneling, or trapping processes inside the semiconductor. These processes cause a self-triggering rate of the detector that is named the dark rate. Simply put, the dark count is made by turning the laser source off, but counting events as though it were on. Events thus counted are not due to the laser

light source but to stray light, spontaneous avalanching of the detector diode or other things. In the pc-OTDR the expected dark count is 2 to 4 percent.

Typically, dark rate in silicon ADP are about 10 to 100 dark counts per second, whereas for InGaAs/InP APD have more random bulk carriers, dark-count rates are in the order of hundreds of thousands of pulses per second.

6.4.4 Photon counting receiver model and *NEP* expression

The main elements of a photon counting receiver in an OTDR are shown Figure 6.8. The avalanche photodiode is suitably biased to operate in the photon counting mode. The comparator eliminates amplifier thermal noise and electrical front-end crosstalk noise. The principal remaining noise components are

I Signal dependent quantum noise

II Dark-count noise

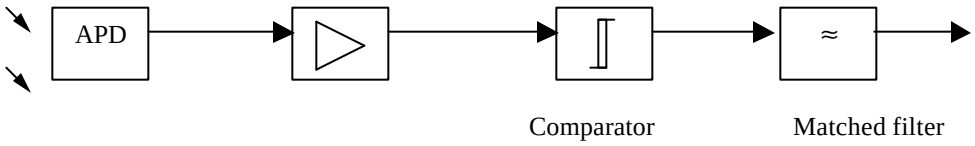

Fig. 6.8 photon counting received model

Trapping effects are negligible.

The matched filter has a rectangular impulse response in the time domain, equal in duration to the launch pulse width *w*, and therefore a (*sin*(x)/x) response in the frequency domain i.e.

$$F(f) = \left(\frac{\sin 2\pi fw}{2\pi fw}\right) e^{-j2\pi fw} \tag{6.11}$$

The individual count pulse and diode recovery time are narrowing compared to *w* and a flat noise spectrum is able to be assumed. The matched filter attenuates the noise power by the factor $|F(f)|^2$. Hence, the effective noise bandwidth is

$$B_N = \int_0^\infty |F(f)|^2 \, df = 1/2w \tag{6.12}$$

The matched filter is simply a digital integrator that counts the number of detector pulse in a given time *w*. It is assumed that detection events correspond to a non-homogeneous Poisson process. In any interval the number of events is distributed according to the Poisson distribution. Let the optical power incident on the detector be P_r. The resulting average detector-counting rate is $l(t)$ and given by

$$l(t) = l_r(t) + l_0 \tag{6.13.1}$$

where $l_r(t) = hP_r / hn$, h is photon detection probability, hn is the photon energy and l_0 is the dark count rate. In any interval W centered on time, the mean count $\bar{n}(t_o)$ is given by the sum of signal and dark counts i.e.

$$\bar{n}(t_o) = \overline{n_r}(t_o) + \bar{n}_{dark} = \int_{t_o+(\frac{w}{2})}^{t_o+(\frac{w}{2})} l_r(t)dt + T\,l_o \tag{6.13.2}$$

In practice, $w << 1/av_g$ and the mean count can be approximately written

$$\bar{n}(t_o) \approx w(l_r(t_o) + l_o) \tag{6.13.3}$$

The above equation corresponds to the noise variance at time t_o, denoted by s_n^2, as we have assumed a Poisson distribution of events. The signal to noise power ratio is thus,

$$\frac{s}{n(t_o)} = \frac{\overline{n_r}(t_o)}{s_n^2(t_o)} \approx w\frac{l_r^2(t_o)}{l_r(t_o)+l_0} \tag{6.13.4}$$

Since both the quantum efficiency and dark count rate l_0 contribute to the detector sensitivity, one would need a figure of the merit that takes both into account. The benchmark used is the noise equivalent power *NEP*, which defined as the pre-averaged signal power in a $1Hz$ bandwidth and results in unity of s/n. It may be derived from above Equation (6.13.4) by setting $s_n^2(t_o) = wl_o$. Therefore

$$NEP_{pc} = hn(2l_o)^{1/2} w/h \quad (\sqrt{Hz}) \tag{6.14.1}$$

If we perform signal averaging by summing the results of N independent measurements an output can be achieved S/n=Ns/n, and the minimum detectable power $P_{\min}$, given when S/N=1, may be found from $P_r(t_o)=P_{min}$

$$l(t_o) \approx [1+\sqrt{(1+4Nwl_o)}]/2Nw \tag{6.14.2}$$

and

$$P_m = B_N hn[1+\sqrt{(1+4Nwl_o)}]/hN \tag{6.14.3}$$

A simple form is calculated as,

$P_m = NEP\sqrt{B_N/N} = \frac{hu}{h}\sqrt{2n_{dark}/(Nt)}$ where $NEP = \frac{hu}{h}\sqrt{2n_{dark}}$ (6.14.4), and hu is a photon energy, and n_{dark} (300/s) is dark count rate of photon counting detector. For our 1.3μm-photon within the clock time period of 1μ s, the *NEP* of SAPD is about $3.733*10^{-15}$ $w/Hz^{1/2}$.

6.5 *K*-scale factor in the OTDR detection

A scale factor *K*, which represents the wavelength-to-intensity conversion, is dependent on the operating point on the spectral region. Obviously, at the top of the source spectrum there is a minimum scale factor. In practice, *K* of single sensor in pc-OTDR detection equals to the first derivative of $I(dl)$ that can be given by

$$K = \frac{dI}{d(dl)} = \frac{dI}{d(dl_{norm})}\frac{ddl_{norm}}{d(dl)}$$

$$where\ \ dl_{norm} = \frac{2\sqrt{\ln 2}}{\sqrt{\Delta l_o^{\ 2} + \Delta l_B^{\ 2}}} dl,\ dl = l_B - l_0 + \Delta l_B \qquad (6.15)$$

where $dl = l_B - l_o + \Delta l_B$, FBG wavelength l_B is variable with measurand parameters, *I* is the Gaussian based reflection intensity

Similarly, *K* factor as a function of multiplexed number *n* can be obtained from derivative of Equation (4.7) in Chapter 4, i.e.

$$I_{mux\_n^{th}} = \frac{P_o \Delta l_B}{\Delta l_o} \exp\left[-4\ln 2 \frac{(l_B - l_o)^2}{\Delta l_o^2}\right] \sum_{k=0}^{2(n-1)} C_{2(n-1)}^k (-1)^k R_o^{\ k+1} / \sqrt{k+1} \qquad (6.16)$$

$$K(n) = 2P_o \frac{\Delta l_B}{\Delta l_o} \exp(-dl_{norm}^2) dl_{norm} \sum_{k=0}^{2(n-1)} C_{2(n-1)}^k (-1)^k R_o^{\ k+1} / \sqrt{k+1} \qquad (6.17)$$

The normalized scale factor K_{nor} as a function of dl_{norm} is shown in Figure 6.9. *K*(n) will decrease with an increased number of multiplexed sensors

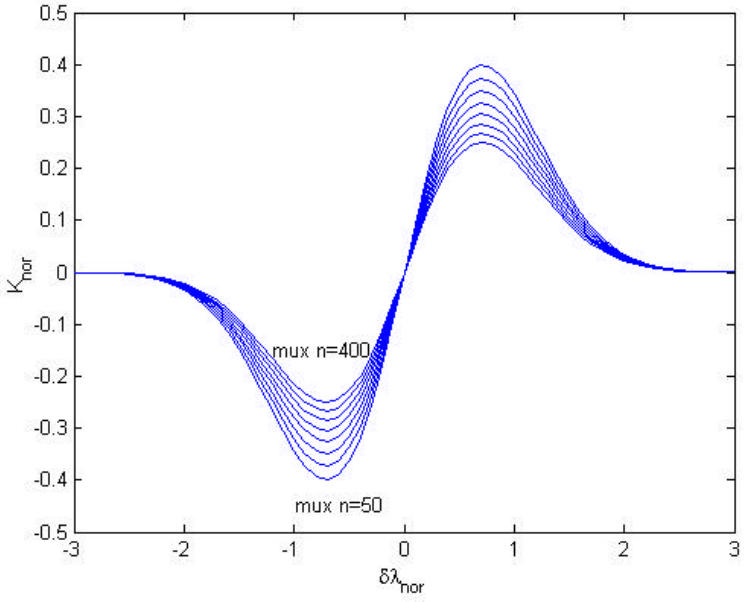

Fig. 6.9 Dependence of the normalized scale factor on the normalized wavelength mismatch $d\,l_{norm}$

6.6 Wavelength sensitivity analysis in pc-OTDR

In this section, considering the principal noise source (shot noise, and dark noise), the minimum Bragg wavelength shift in a sensing grating detected by the OTDR system is evaluated. A variation of $d\,l_B$ in the wavelength of the FBG sensor will produce some changes in the optical power arriving at the photon detector (APD) in the OTDR, ($d\,I_{Ph}$) so that

$$d\,l_B = \frac{1}{dI_{ph}/d\,l_B} d\,I_{ph} \tag{6.18}$$

where $dI_{ph}/d\,l_B$ is the derivative in the following (6.19) in terms of the FBG wavelength l_B. Based on the previous descriptions of the interrogation of the FBG reflection power,

after solving the convolution integral, the received optical power for a *single* FBG is given by

$$I_{ph}(l_B) = S_o \frac{R_B\sqrt{p}}{\sqrt{4\ln 2}} \left\{ \frac{\Delta l_B \Delta l_o}{(\Delta l_B^{\,2} + \Delta l_o^{\,2})^{1/2}} \exp\left[-4\ln 2 \frac{(l_B - l_o)^2}{\Delta l_B^{\,2} + \Delta l_o^{\,2}} \right] \right\} \quad , \tag{6.19}$$

where S_o is the peak power injected into the fiber by the OTDR source. For multiplexed sensors, the senor intensity change rate with FBG wavelength is written by

$$\frac{dI_{mux\_n^{th}}}{d\,l_B} = F(P_o, R_o, \Delta l_B) \frac{dg}{d\,l_B},$$

$$\text{where } g = \exp\left[-4\ln 2 \frac{(l_B - l_o)^2}{\Delta l_o^{\,2}} \right], \quad \text{and } F_n(P_o, R_o, \Delta l_B) = \frac{P_o \Delta l_B}{\Delta l_o} \sum_{k=0}^{2(n-1)} C_{2(n-1)}^{k} (-1)^k R_o^{\,k+1} / \sqrt{k+1} \tag{6.20}$$

Equation (6.20) is obtained based on Equation (4.7) of Chapter 4. Hence, for a signal-to-noise ratio of one, the minimum detectable Bragg wavelength shift in the presence of a particular noise source (j) can be written by

$$d\,l_{Bn}\Big|_j = \frac{1}{F_n(P_o, R_o, \Delta l_B) \dfrac{dg}{d\,l_B}} \sqrt{BH_j} \tag{6.21}$$

where, for a particular noise source, H_j is the equivalent one-sided spectral density of the squared equivalent optical noise and B is the detection bandwidth. Assuming that all noise sources are independent, the minimum detectable Bragg wavelength shift is the sum of the variance for different noise sources:

$$dl_B\big|_{\min} = \left[\sum_j dl_B\big|_j^2\right]^{1/2} \tag{6.22}$$

According to the *NEP* expression (6.14.4), the Bragg wavelength (or corresponding pc-OTDR central wavelength) shift caused by the dark count is given by

$$\begin{aligned}\frac{dl_{Bn}\big|_{darkcount}}{\sqrt{B}} &= \frac{1}{F_n(S_o, R_o, \Delta l_B)\dfrac{dg}{dl_B}} P_{\min} \\ &= \frac{\Delta l_o^2}{8\ln 2\left|l_B - l_o\right| I_{mux\_n^{th}}} \times \frac{hu}{h}\sqrt{\frac{n_{dark}}{Nt}}\end{aligned} \tag{6.23}$$

where B is the detection bandwidth for the case of N repeated measurements, and n_{dark} =300/s is a typical dark count rate. t =1μs and h =10% are the time resolution and quantum efficiency, respectively. In the pc-OTDR-based multiplexing system usually $I_{mux\_n^{th}}$ = -75 dBm for sensors far from OTDR with 0.001 reflectance, u =2.2901× 10^{14} / l (1/s.), and using the following values: The OTDR source spectral width Δl_o^2 =68.89 nm^2, $\left|l_B - l_o\right|$ = 2 *nm*, and *N*=120 (OTDR measured times of each OTDR screen painting). The sensitivity of the sensor limited by the photon counting can be calculated by Equation (6.23), therefore, resulting in $dl_{Bn}\big|_{darkcount}/\sqrt{B}$ = 4.734e-5 $nm/Hz^{1/2}$. It is shown that if the OTDR system sends out an optical pulse at a 1MHz repetition rate and then forms 33 Hz sampling rate in the OTDR measurement, the minimum detectable wavelength limited by the dark noise would be 0.021793 *nm*.

Chapter 7 Conclusions and Future Works

This thesis describes the detailed research work on the modeling, implementation, analysis, and evaluation of a novel pc-OTDR based FBG multiplexing system. This chapter summarizes major conclusions for the dissertation research work, and suggests results future work for further improvement of the multiplexing FBG sensors

7.1 Conclusion

This is the first time that pc-OTDR Fresnel reflection is used to spectrum based interrogate densely multiplexed fiber Bragg gratings. Individual grating signals were precisely located, amplified and evaluated by the pc-OTDR system. For the measurement of a large number of multiplexed sensors, fiber Bragg gratings seem to be a unique option for dense stress detection and distributed temperature measurement because of its very low insertion loss and stable optical spectral properties. Owing to the pc-OTDR detection of the photon arrival probability with high photon-timing resolution, it can also sense a rather low Fresnel-reflection (10^{-5}) for very weak refractive index variations in the fiber core within a high spatial resolution. However, the OTDR source is a multi-longitudinal mode semiconductor laser easily affected by environmental temperature variations. The experimental results show that the OTDR output from optical reflection of a fiber endface can have variations as high as 20% as the environmental temperature around the OTDR

changes by 20℃. Meanwhile, the pc-OTDR interrogation is actually intensity-based detection in nature, which may be subject to intrinsic source intensity fluctuation, fiber bending influence, and crosstalk between FBGs. Thus, the fluctuation of transmitted power in the optical fiber will result in a severe problem for sensor interrogation, and it is thus important to have a self-referencing approach for the cancellation of unwanted power fluctuation in the single fiber channel through the use of referencing gratings or fiber intrinsic reflectors, which are not sensitive to the measurands only dependent on the OTDR power. A self-referencing methodology using dual gratings, one that is sensitive to and the other insensitive to the measurands, has been applied to improve system performance. This can effectively eliminate perturbation duo to those two influences. Two advancements in the multiplexing pc-OTDR based technology were made in the thesis work.

a. The OTDR offers a potential interrogation approach to measure Bragg grating sensors for strain and temperature measurement. Theoretical calculation and practical measurement indicate that the output amplitude of sensors can reach about 7.5 dB and yields a smooth calibration curve even with the OTDR source longitudinal mode effect. A few hundred FBG sensors can be implemented on a short length of fiber (100 meter long). Theoretically, if we improve each grating reflectance to 0.05% or less and reduce insertion loss of each grating to 0.01 dB, the number of the maximum multiplexed sensors can increase to more than 1000 for a 40 dB-OTDR dynamic range (power adjustable range).

b. An innovative FBG writing system was developed using the phase mask technique so that the Bragg resonated wavelength and the grating spectral bandwidth can be easily adjusted by varying experimental setup parameters. This provides the potential for multiplexing FBG arrays in which their variations of intensity could have a better linearity in relation to the measurands, and generates sufficient bandwidths for the gratings to smooth severe spectral ripples

c. A self-referencing multiplexed Bragg grating system based on a referencing grating with different Bragg wavelength from the sensing grating was developed to reduce noise induced by fiber bending and source power fluctuation.

d. A multiplexed system with a large number of gratings was implemented, and demonstrated modeled for its crosstalk problems. The mathematical models of the grating sensor response to strain and temperature were further studied to offer a guideline for optimal design of the Bragg grating sensor. The model can also determine how the initial Bragg wavelength and bandwidth determines the sensor linear range and calibration precision.

The source spectrum random drift and the fiber bending-induced spectral shift are significant disturbance factors for the system performance. A two-day spectrum measurement demonstrated a random spectral shift of s=0.025 nm, which will induce a corresponding intensity variation of 0.02 dB. However severe a fiber bending results in much stronger spectrum deformation described in Chapter 6. Hence, it is important to balance the balance budget of detection accuracy and the sensor multiplexing number in sensor system design.

In the preparation of a Bragg grating sample, a small piece of photosensitive fiber (2 cm) was cut from the big fiber spool and then spliced separately to two pieces of regular fibers at both its ends so a series FBGs can be made on a single fiber. The process contributes additional insertion loss for each FBG in multiplexing configuration up to 0.02dB~0.04dB due to the slightly high splicing loss between the regular and photosensitive fibers. Therefore, to multiplex a thousand-FBGs, the dynamic range of the system at least needs to be in the range of 20~40 dB to cover overall FBG measurements.

7.2 The improvements

Based on the previous work done, some future improvements to the Bragg grating performance are suggested here, including the reliability and robustness required to implement a large of number of FBGs in the measurement. A H_2 loading system is an appropriate option to realize photosensitive fiber from a piece of single-mode fiber at very low cost, so that a multiplexed Bragg grating array can be directly formed in a single length of fiber without splices. This would save splicing losses in the sensor system to increase the number of multiplexed FBG sensors. Additional opportunities for future improvement are discussed in the rest of this section

7.2.1 Solving the temperature and strain measurement ambiguity

In Bragg grating tensile tests, grating temperature effects usually add to the strain variation to resulting in an ambiguous measurand. The temperature coefficient of regular Bragg gratings is about 0.01 *nm*/ºC. From the intensity measurement in Figure 5.4.1, 1ºC variation will result in an OTDR intensity change of 0.343 (arbitrary unit), which may correspond to a misleading strain change of about 7.5 μstrain according to the strain sensor calibration curve. For a single FBG measurement, this has been resolved through the use of

a double FBG system with different temperature and strain coefficients [64]. A suppressed temperature sensitive FBG can be obtained by controlling the doping concentration of GeO_2 and B_2O_3 in the fiber. A difficult challenge is to reduce the cross-sensitivity between temperature and strain in the multiplexing operation. The problem could be partly solved by employing a *K*–matrix approach that is a twin-grating scheme with a small Bragg wavelength separation, and then using the coefficients of strain and temperature to realize a 2^{nd}-order inverse matrix to interrogate the strain change. In our sensor system, dual-wavelength FBG could be used to make up grating multiplexed sensors, one of which is a strain sensor for only measuring strain distribution but still has small temperature coefficient. The other one would be only a temperature sensor with a strain-free coefficient. Purely temperature grating sensor is actually regular FBG that could be placed in a strain-free status in the structural strain measurement. The temperature sensor data can compensate the strain sensor variation through the *K*-matrix method.

7.2.2 Increasing FBG multiplexing capacity and reducing FBG crosstalk

Achieving a greater number multiplexing ability in the pc-OTDR system is potentially important for many practical applications. From the theoretical simulation in Chapter 3, the maximum multiplexed number of sensors in a serial topology scheme will be limited by the source optical power, the coupling coefficients and the system SNR requirement, However, if sensor wavelengths can spread several spectral regions based on the OTDR source spectrum, the multiplexed sensors can be classified into several sections according to their wavelengths as described in Chapter 5. In principle, one avenue to improving multiplexing capacity is the combination of wavelength division multiplexing (WDM) and time division multiplexing to dissolve the multiplexing number in different wavelengths. This approach

may improve system resolution and decrease the workload on one wavelength channel. Figure 7.1 shows a four-wavelength multiplexed FBG spectrum with several tens of sensors. The light transmission coefficients are apparently enhanced because each grating group has a specific wavelength and low spectral-shadowing crosstalk occurs between the groups. Thus, this multiplexing scheme may increase the sensor multiplexing capacity. By selecting a tunable optical filter corresponding to the multiplexed wavelengths close to the OTDR connector, the number of sensors for each wavelength channel can be distinguished.

The other approach is to adopt a hybrid parallel and serial topology scheme. Instead of using a single fiber channel, multiplexed FBGs can be divided into several channels and

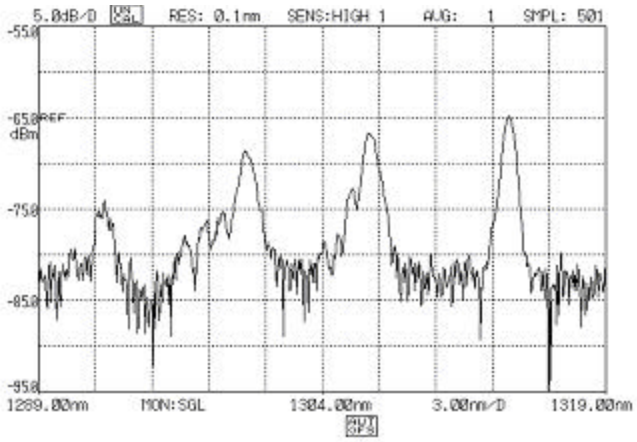

Fig 7.1 FBG spectrum in WDM/OTDR

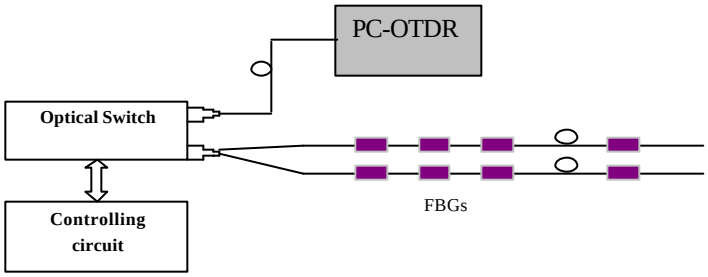

Fig 7.2 optical switch used in multiplexing system

the multiplexing crosstalk can be further reduced. An optical switch can be employed in a dual-channel multiplexing system, as schematically shown in Fig 7.2. Serial reflected signals in the two channels would be alternatively presented on the OTDR window as the optical switch operates in the slow mode (10s).

7.2.3 Improving real-time data processing

Since a large number of multiplexed sensors need to be traced to evaluate the distributed change in measurands within a short time in the pc-OTDR measurement, each sensor is individually sampled in turn and then the computer can save the signal data in almost real-time to obtain each grating information. If the sampled rate from the GBIP of the OTDR is too slow, it will affect the real-time test rate. Currently, the OTDR system can pick up FBG- peak values sampled at the rate of 10 points/min or 10 sensors/min since it scans an one FBG each time, which implies that only one sensor signal is shown in the OTDR measurement window. The measurement rate is totally limited by the communication speed between the computer and the GBIP interface. Meanwhile, the OTDR averaging process used to increase the signal-to-noise ratio may also slow down the sampling rate. Therefore, there are two ways to improve the data transmission between the computer and the OTDR interface. One is that the interface program is directly modified to satisfy high-speed measurement and the other is sampling multiple peaks at the same time in one window, so that we could obtain more than 10 peaks sensor information each time within a short time at the price of resolution reduction in each sensor,

Appendix

Derivation of the equation (5.6) measured fiber optical grating peak reflectance R

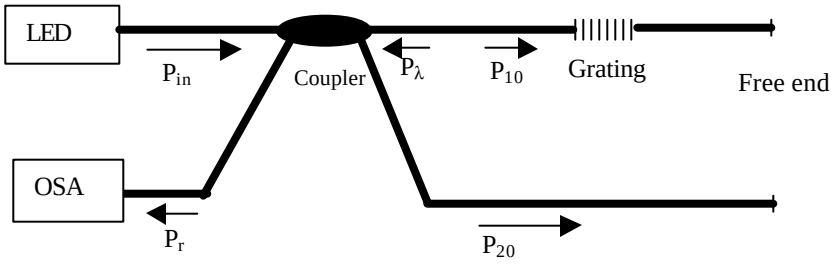

Solution:

Input power: $P_{in} = P_{10} + P_{20}$; where P_{10} is power at Bragg grating wavelength

if coupling coefficient is 0.5

then, $P_{10} = P_{20} = 0.5P_{in;}$ free end reflectance is 4%

OSA *R*eflected power at Bragg wavelength received from coupler

$$P_r = \frac{1}{2}(P_l + (P_{10} - P_l)(1-R)4\% + P_{20}4\%).....(1)$$

noted $P_l = RP_{10}(l)$

Hence, $P_r = \frac{P_o}{2}[R + (1-R)^2 4\% + 4\%]$

Bragg grating reflection power ΔG can be written

$$10^{\Delta G/10} = [1 + (1-R)^2 + \frac{R}{4\%}]/2$$

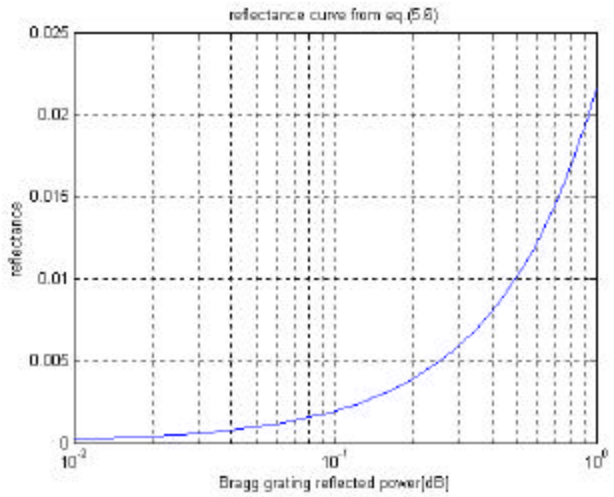

Reference

[1] K. O. Hill, Y. Fujii, D. C. Johnson, and B. S. Kawasaki, "Photo-sensitivity in optical fiber waveguides: Application to reflection filter fabrication," *Appl. Phys. Lett.*, vol. 32, p 647, 1978.

[2] J. Stone, "Photorefractivity in GeO2 -doped silica fibers," *J. Appl. Phys.*,vol. 62, p. 4371, 1987.

[3] F. P. Payne, "Photorefractive gratings in single-mode optical fibers," *Electron. Lett.*, vol. 25, p. 498, 1989.

[4] D. P. Hand and R. St. J. Russell, "Photoinduced refractive-index changes in germanosilicate fibers," *Opt. Lett.*, vol. 15, p. 102, 1990.

[5] G. Meltz, W. W. Morey, and W. H. Glenn, "Formation of Bragg gratings in optical fibers by a transverse holographic method," *Opt. Lett.*, vol. 14, p. 823, 1989.

[6] R. Kashyap, "Photosensitive optical fibers: Devices and applications," *Optic. Fiber Technol.*, vol. 1, p. 17, 1994.

[7] W. W. Morey, G. Meltz, and W. H. Glenn, "Fiber Bragg grating sensors," in *Proc. SPIE Fiber Optic & Laser Sensors VII*, 1989, vol. 1169, p. 98.

[8] W. W. Morey *et al.*, "Bragg-grating temperature and strain sensors," in *Proc. OFS'89.* Paris, France, 1989, p. 526.

[9] W. W. Morey, J. R. Dunphy, and G. Meltz, "Multiplexing fiber Bragg grating sensors," in *Proc. SPIE Distributed and Multiplexed Fiber Optical Sensors,* Boston, MA, Sept. 1991, vol. 1586, p. 216.

[10] S. M. Melle, K. Liu, and R. M. Measures, "A passive wavelength demodulation system for guided-wave Bragg grating sensors," *IEEE Photon. Technol. Lett.*, vol. 4, p. 516, 1992.

[11] E.J. Frebele, C. G.Askins, M.A.Putnam etc. " distribution strain sensing with fiber Bragg grating arrays embedded in CRTM composite" *Electron Lett*., 30 (21, 1994, pp1783-4

[12] D.A.Jackson, A. B Lobo Riberio, etc. "Simple Multiplexing scheme for a fiber – optic grating sensor network" *Opt. Lett*., **18**(7) 1993, pp1192

[13] M.A.Davis and A.D. Kersey " Matched filter interrogation technique for fiber Bragg grating arrays", *Electronics Lett*., 31(10), 1995, pp822~3.

[14] A.D kersey, T.A Berkoff and W.W. Morey, " Multiplexed fiber Bragg grating strain sensor", *Electronics Letters*, 29(11), 1996, 1522-4

[15] T.A. Berkoff and A.D Kersey , " fiber Bragg grating array sensor system using a band-pass wavelength division multiplexer and interferometric detection", IEEE photonics technology Letters, 8(11),1996, pp1522

[16] A.D kersey, T.A Berkoff and W.W. Morey, " Multiplexed fiber Bragg grating strain sensor system with a fiber Fabry-Perot wavelength filter", *Optical Letters*, 18(16), 1993, 1370-2

[17] Weis,R.S. A.D. Kersey, and T.A. Berkoff, " A four-element fiber grating sensors array with phase sensitive detection", *IEEE Photonics Technology Letter*, V6, 1994, pp1469~1472.

[18] W.W. Morey, J. R. Dunphy and G. Meltz, " Multiplexing fiber Bragg grating sensor", SPIE 1586 Distributed and multiplexing fiber optical sensors, 1991, pp216-24

[19] Y.J. Rao, " In-fiber Bragg grating sensors," *Meas. Sci. Tehnol*. Vol.8 p355~375,1997

[20] R.L. Idriss, M. B. Kodindouma, A.D. Kersey, and M.A. Davis, " Multiplexing Bragg Grating optical fiber sensors for damage evaluation in high way bridges, *Smart Material* structure, V7 pp209~216,1998

[21] M.A. Davis, D. G. Bellmore, M.A. Putna, and A.D. Kersey, " A 60 element fiber grating semsor system ," in *Proc. OFS 12th* , 1997, pp 100-103

[22] K.I. Mallalieu, R.Youngquist, and D.E.N.Davis, " FMCW of optical source envelop modulation for passive multiplexing of frequency-based fiber –optical sensor", *Electronics Lett.*, vol. 22, pp809-810 1986

[23] A.D. Kersey and W.w. Morey, " Multiplexed Bragg grating fiber-laser strain sensor system with mode-locked interrogation", *Electronics Lett. 29(1), 1993 pp123-124*

[24] Peter K.C. Chen, Wei Jin, S. Demokan, " FMCW Multiplexing of fiber Bragg Grating sensors", *IEEE Journal of selected topic in quantum electronics*, vol.6 No. 5 2000

[25] I.Sakai, Multiplexing of optic al fiber sensor using a frequency-modulated source and gated output", *J. Lightwave technology*., vol. LT-5, pp932-40 1987

[26] Peter K.C. Chen, Wei Jin, J.M. Gong, S. Demokan, "Multiplexing of fiber Bragg Grating sensors using an FMCW technology", Photon. Technol. Lett. Vol.11 pp1470-2 1999

[27] Y.J. Rao, K.Kalli, G. Brady, D.J.Webb, A.D. Jackson,L. Zhang and I. Bennion, " Spatially-multiplexed fiber optic Bragg grating strain and temperature sensor system

based on interferometric wavelength-shift detection," *Electronics Lett.* **31**(12) 1995, 1009-10

[28] Y.J.Rao, *et al.* " Simultaneous spatial, time and wavelength division multiplexed in fiber grating sensor network," *Optical Communication* vol.125, 1996, pp53-58

[29] Kalli,K, et al. " Wavelength division and spatial multiplexing using tandem interferometers for Bragg grating sensor networks," *Optics Letter,* v20 1995, pp2544-6

[30] Kalli,K, et al. " wavelength division and spatial multiplexing of Bragg grating sensor networks using concatenated interferometers," *Proceedings of the Optical fiber sensor conference (OFS11)* Sapporo japan,1996pp522-525.

[31] Lobo Ribeiro, A. B., et al. " Time-and spatial multiplexing tree topology for fiber optic Bragg grating sensors with interferometric wavelength-shift detection," A*pplied Optics,* Vol 35,1996, pp2267-73

[32] K.P.Koo, A.B. Tveten, and S.T. Vohra, " dense wavelength division multiplexing of fiber Bragg grating sensors using CDMA," Electron Lett., vol 35 pp165 –7 1999

[33] Dakin, J.P. et al. " new multiplexing scheme for monitoring fiber optic Bragg grating sensors in coherence domain," *Proceedings of the Optical fiber sensor conference (OFS12),* Williamsburg, VA, USA 1997 pp31-4.

[34] A.D. Kersey et al. " fiber Grating sensors," *IEEE Journal of Lightwave Technology* v15, 1997 001442-1463

[35] I.P. Giles, D>Uttam, B. Culshaw, and D.E. Divies, " coherent optical fiber sensors with modulated laser sources", Electronics Letter, v19 n1 pp14-5,1983

[36] B.R. Mahafza, *Introduction to radar Analysis*. 1998

[37] Kashyap, R: ‘ Assessment of tune the wavelength of chirped and unchirped fiber Bragg grating with single phase-mask’, *Electronics Letters*, 1998, V34, N21, pp2025

[38] Kashyap, R., McKe, P.F. “ Novel method of produced all fiber photoinduced chirped gratings”. Electronics Letter, 9th 1994, v30,N 12 pp996

[39] A. othonos and Xavier Lee “ Novcel and Improved Methods of Writing Bragg Gratings with Phase Masks”, IEEE Photonics Technology Letters, v7, No. 10 1995

[40] Kenneth O. Hill and Gerald Meltz, “Fiber Bragg Grating Technology fundamental and Overview”, *JOURNAL OF LIGHTWAVE TECHNOLOGY, VOL. 15, NO. 8, AUGUST 1997 1263*

[41] K. O. Hill, Y. Fujii, D. C. Johnson, and B. S. Kawasaki, “Photosensitivity in optical fiber waveguides: Application to reflection filter fabrication,” *Appl. Phys. Lett.*, vol. 32, pp. 647–649, 1978.

[42] B. Poumellec, P. Niay, D. M., and J. F. Bayon, “The UV-induced refractive index grating in Ge:SiO2 preforms: Additional CW experiments and the macroscopic origin of the change in index,” *J. Phys. D, Appl. Phys.*, vol. 29, pp. 1842–1856, 1996.

[43] K. O. Hill, B. Malo, F. Bilodeau, D. C. Johnson, and J. Albert, “Bragg gratings fabricated in monomode photosensitive optical fiber by UV exposure through a phase mask,” *Appl. Phys. Lett.*, vol. 62, pp. 1035–1037, 1993.

[44] D. Z. Anderson, V. Mizrahi, T. Erdogan, and A. E. White, “Production of in-fiber gratings using a diffractive optical element,” *Electron. Lett.*,vol. 29, pp. 566–568, 1993.

[45] N. Katcharov,U J. Rioublanc, J. L. Auguste, J. M. Blondy, and P. Di Bin, “Characterization of Low-Reflectance Bragg Gratings Using Optical Time Domain Reflectometry”, *OPTICAL FIBER TECHNOLOGY* **3,** 168-172 1997

[46] P. Lambelet, P. Y. Fonjallaz, H. G. Limberger, R. P. Salathe, C. H. Zimmer, and H. H. Gilgen, ‘‘Bragg-grating characterization by optical low-coherence reflectometry,’’ *IEEE Photon. Lett. Technol.*, vol. 5, 565 1993.

[47] F. P. Kapron, B. P. Adams, E. A. Thomas, and J. W. Peters, ‘‘Fiber-optic reflection measurements using OCWR and OTDR techniques,’’ *J. Lightwa*ve *Technol.*, vol. 7, pp1234 1989.

[48] Blanchard, P. H. Zongo, and P. Facq, ‘‘Accurate reflectance and optical fiber backscatter parameter measurements using an OTDR,’’ *Electron. Lett.*, vol. 26, pp2060 1990.

[49] Anbo Wang, H.Xiao et al “ Self-calibrated Interferometric-Intensity-Based optical fiber sensors”, *J. of Lightwave technology* vol.19 n10, 2001. pp 1495

[50] A. Othonos, K. Kalli, “ Fiber Bragg Gratings”, Artech House, London

[51] M. K. Barnoski and S. M. Jensen, “Fiber waveguides: A novel technique for investigating attenuation characteristic,” *Appl. Opt.* vol 15, No. 9, pp2112-2115, 1976

[52] S.D. Personick, “ Photon probe – An optical fiber time domain reflectometer,” *Bell Syst. Tech.* J., vol 56, no.3, pp355-366, 1977

[53] P. Healy, “ Multichannel photon-counting backscatter measurements on mono-mode fiber,” *Electron lett.*, vol 17 no. 20 pp 751-852 1981

[54] P. Healy, P. Hensel, “Optical time domain reflectometry by photon counting,” *Electron. Lett.*, vol 16, no 16, pp631-633, 1980

[55] P. Healy, “Optical time domain reflectometry –A performance comparison of the analog and photon counting techniques,” *Opt. Quantum Electron.*, vol 16, pp267-276, 1984

[56] C.G. Bethea, B.F. Levine, etc., "High-resolution and sensitivity optical time domain reflectometer," *Opt Lett*., vol.13, no.3, pp, 133-135, 1988

[57] B.F. Levine, C. G. Bethea and J. C. Campbell "1.52-μ m room temperature photon-counting optical time-domain reflectometer," *Electron. Lett*., vol. 21, no. 5, pp194-196 1985

[58] A. Karlsson, M. Bourennane, Gregoire Ribordy, Hugo Zbinden, John Ratity, and Paul tapster, " A Single-Photon Counter for Long-Haul Telecom," *Circuits & Devices*, 1999IEEE, pp34-40, Nov. 1999

[59] Valeria Gusmeroli, "High-Performance Serial Array of Coherence Multiplexed Interferometric Fiber-optic Sensor," *J. Lightwave Technol*., vol.11, No.10, pp 1681-1686, O*ct*. 1993

[60] A. D. Kersey, K. L. Dorsey and A. Dandridge, " Crosstalk in a Fiber Optic Fabry-Perot Sensor array with ring reflectors," *Opt. Lett.*, vol 14, No.1, pp93-95, *Jan* 1989

[61] A. D. Kersey, A. Dandridge, and K. L. Dorsey, " Transmissive Series Interferometer Fiber Sensor," *J.Lightwave Technol*., vol.7, No.5, pp 846-854, *May* 1989

[62] J. L. Brooks, B. Moslehi, B.Y.Kim and H.J. Shaw, " Time-domain Addressing of Remote Fiber-Optic Interferometer Sensor Arrays," *J. Lightwave Technol.*, vol. LT-5, No.7, pp1014-1022, *July* 1987

Vita

Po Zhang was born on November 16,1962 in Beijing, China. He graduated from Wuhan University of Space Physics in 1984 with a Bachelor of Science in Microwave and Propagation. He entered Shanghai Optics and Fine Mechanical Institute, Academia Sinica, in 1988 and obtained his Master of Science in the Material Science in 1990. From 1994 to 1999 he was with the national key R&D center worked on the precision instrument and fiber sensor technologies as a senior research engineer, in Shanghai Fiber Optic R&D Center, where his research scope covered optical fiber sensor, laser technology, integrated optics, photonics components, and digital signal processing. He then joined the Center for Photonics Technology of the Department of Electrical and Computer Engineering at Virginia Polytechnic Institute and State University as a research assistant in January 1999, and since then he has been working with Dr. Anbo Wang towards his Ph.D. degree in Electrical Engineering.